Study on Cellular Interaction of Single-Walled Carbon Nanotubes and Their Biomedical Applications

Hongli Mao

Doctoral Program in Materials Science and Engineering

Submitted to the Graduate School of

Pure and Applied Sciences

in Partial Fulfillment of the Requirements

for the Degree of Doctor of Philosophy in

Engineering

at the

University of Tsukuba

Content

List of abbreviations

1D	One-dimensional
2D	Two-dimensional
3D	Three-dimensional
AFM	Atomic force microscope
ANOVA	Analysis of variance
BACs	Bovine articular chondrocytes
BSA	Bovine serum albumin
calcein-AM	Calcein-acetoxymethyl
CNTs	Carbon nanotubes
Col	Collagen
DAB	Diaminobenzidine
DMEM	Dulbecco's modified Eagle medium
DNA	Deoxyribonucleic acid
ECM	Extracellular matrix
EDTA	Ethylenediaminetetraacetic acid
EMEM	Eagle’s Minimum Essential Medium
EPR	Enhanced permeability and retention
FBS	Fetal bovine serum
FVH	Force-volume height
HEPES	4-(2-hydroxyethyl)-1-piperazineethanesulfonic acid
hMSCs	Human mesenchymal stem cells
HWHH	Half width taken at the half height
MRI	Magnetic resonance imaging
MWCNTs	Multi-walled carbon nanotubes
PBS	Phosphate buffer saline
PDT	Population doubling time
PI	Propidium iodide
QDs	Quantum dots
RBM	Radial breath mode
RNA	Ribonucleic acid
SD	Standard deviation
SEM	Scanning electron microscope
sGAG	Sulfated glycosaminoglycans
SWCNTs	Single-walled carbon nanotubes
TEM	Transmission electron microscope
UV-vis-NIR	Ultraviolet-visible-near-infrared

Chapter 1

General introduction

1.1 Nanomaterials

Nanomaterials are considered to be materials which are sized between 1 and 100 nm in at least one dimension[1–3]. The properties of material at nanoscale are often quite different from those of the bulk materials. The differences are commonly believed to be caused by two primary size-dependent factors: surface effects and quantum effects[4]. In general, nanomaterials can be generated by nature and conventional industrial processes as well as nanomanufacturing technologies[2].

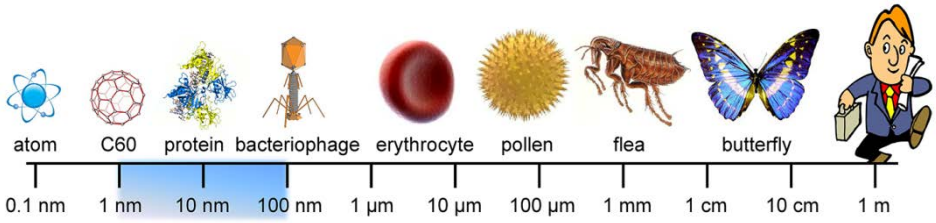

Fig. 1.1 Scale diagram: objects at different scales. Nanomaterials are typically 1-100 nm in at least one dimension.

1.1.1 Nature nanomaterals

Nanomaterials exist in nature universally in the forms of nanodots, nanowires, nanotubes, nanosheets and even nanomachines. They can be produced through a lot of natural processes, such as dust storms, wildfires, weatherings, erosions and physiological activities of some plants and animals.

Dust storms are believed to be one of the major sources of natural nanoparticles[5]. The particles produced through dust storms usually sized in a range from nanometers to micrometers. Small particulates (including nanoparticles) are also present in the smoke of wildfires (such as forest fires and grass fires) that may be caused by lightnings, volcanic eruptions, sparks from rockfalls as well as human activities[6]. Nanomaterials in nature can also be produced through weatherings and erosions processes. In addition to inorganic nanomaterials, a vast array of organic nanomaterials exists in nature as well. Actually, many organisms, such some bacteria[7,8] and viruses (20-300 nm), are in nanoscale in size. Some viruses can be

regarded as organic nanoparticles or used as templates to synthesize materials on the nanoscale[9–11]. Meanwhile, many organisms produce nanomaterials through intracellular and extracellular processes. For example, magnetotactic bacteria can synthesize magnetite nanoparticles which are used for navigation relative to the earth's magnetic field[12,13]. Another example is nanobacterium that can synthesize a shell of calcium phosphate in nanoscale to cover itself and this process might have a potential role in forming kidney stones[7,8,14].

1.1.2 Synthetic nanomaterials

Nanomaterials can be fabricated by numerous procedures[15–20]. Generally speaking, there are three basic approaches to making nanomaterials: top-down, bottom-up and mixed methods. Top-down preparation is a subtractive method to fabricate nanomaterials starting from bulk materials by using some external radiation and/or chemical while bottom-up preparation is an additive method to fabricate nanomaterials starting from precursor molecules or atoms. A critical fact to consider with engineered nanomaterials is that they can be synthesized in almost any shape and size by materials scientists. Followings are some typical synthetic nanomaterials used in biomedicine or biotechnology (Fig. 1.2).

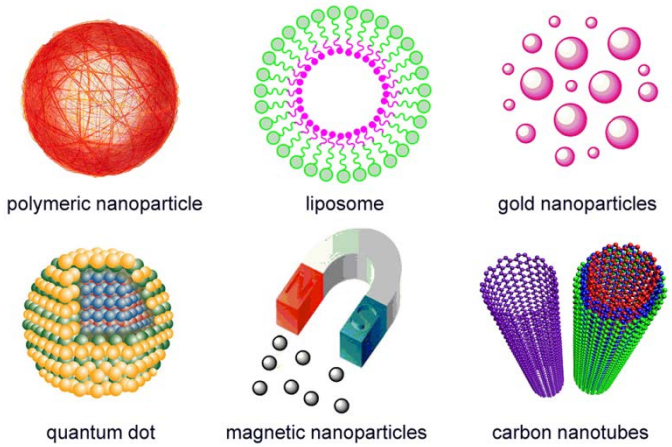

Fig. 1.2 Examples of synthetic nanomaterials used in biomedicine or biotechnology.

Polymeric Nanoparticles[21–25]**:** Polymeric nanomaterials can be prepared either from natural polymers, including collagen, alginate, albumin and gelatin, or synthetic polymers, such as polycarprolactone (PCL), polyethylene glycol (PEG) and poly(D,L-lactide-co-glycolide) (PLGA) by the polymerization of the prefabricated polymer or the monomers. The polymerization of monomer units may be accomplished using the emulsion or interfacial methods. For biomedicine use, many polymeric nanomaterials consist of a cargos-containing (such as drugs) hydrophobic core that and a hydrophilic surface layer to stabilize the nanomaterials in aqueous solution. According to the structure, polymeric nanomaterials can be further divided into nanocapsules and nanospheres. Nanocapsules are comprised of an aqueous or oil core and a shell while nanospheres are comprised of a solid mass.

Liposomes[26–28]**:** Liposomes are artificially-prepared spherical vesicles composed of one or more phospholipids bilayers. Liposomes are widely used as delivery vehicles due to their good biocompatibility and closed sphere structure which can shield the hydrophobic parts from the water. Cargos with different

hydrophilicities can be carried either encapsulated in the aqueous volume or within the bilayers of liposomes. Many methods have been developed for the preparation of liposomes, including mechanical dispersion methods, solvent dispersion methods and detergent removal method. The correct method for liposome preparation is determined by many parameters, such as the optimum size of liposome for the intended applications, the properties of the dispersing medium, the physicochemical characteristics of the liposomal ingredients and those of the materials to be carried and the possibility of the preparation on a large scale.

Gold Nanoparticles[15,29–31]**:** Because of their unique optical, electronic and surface properties, gold nanoparticles (AuNPs) are receiving great attention. Besides spherical shape, gold nanoparticles are also engineered with the shape of rods, cages, stars and shells used to coat other nanoparticles. The intrinsic properties and the relevant applications of AuNPs largely rely on the size, shape, surface chemistry and aggregation state. Numerous approaches exist for fabrication of AuNPs, such as Turkevich method, Brust-Schiffrin method, Perrault-Chan method and others. Generally speaking, AuNPs are produced by the simple reduction of metal salt precursors with reducing agents under certain conditions in a liquid environment. This initiates the formation of neutral gold atoms from gold ions and thus forming nanoparticles. To prevent the aggregation of the formed nanoparticles, some sort of stabilizing agent is usually required during the preparation processes.

Quantum Dots[32–34]**:** Quantum dots (QDs) are first discovered by Alexei Ekimov in 1981[35] while the term "quantum dot" is first reported by Mark Reed in 1988[36]. QDs are semiconductor nanocrystals that are small enough (typically sized from 1 to 10 nm) to exhibit quantum mechanical properties. They have been widely studied in the field of transistors, solar cells, LEDs, diode lasers as well as biological imaging. Additional attractive advantages of QDs for imaging are their higher stability than conventional organic fluorophores and lack of photobleaching and chemical degradation. However, QDs are typically comprised of heavy metals such as cadmium, mercury and lead which are usually toxic. Several different methods have been developed to produce quantum dots, including top-down preparation methods (such as molecular beam epitaxy, ion implantation and X-ray lithography) and bottom-up methods (self-assembly of the precursor compounds dissolved in solutions). Recently, many researches have been focused on the developing of heavy-metal-free QDs using “green” procedures, which means that QDs do not contain any heavy metal composition and the synthetic procedure for them does not use the non eco-friendly reagents.

Magnetic Nanoparticles[37–41]**:** Magnetic nanoparticles (MNPs) are usually composed of magnetic elements such as iron, nickel, cobalt and their chemical compounds that allow them to be manipulated under magnetic field. They have attracted intense interest and show great potential in a variety of applications, such as nanomaterial-based catalysts, data storage, environmental remediation, sensors, bioseparations, magnetic resonance imaging (MRI) for medical diagnosis and therapeutics. Currently, three major types of MNPs are being produced and used: ferrite nanoparticles, metallic nanoparticles and metallic core with a shell. Ferrite MNPs are the most extensively studied MNPs up to date. Just like other nanoparticles, the surface of MNPs is also need to be modified to improve their stability in medium. Magnetic nanoparticles can be synthesized by many methods, such as the co-precipitation method, thermal decomposition method and microemulsion and flame spray synthesis method. For biomedical applications, the protection, stabilization and functionalization of MNPs by precious metals, such as gold, and biomoleculars are important and necessary.

Carbon Nanotubes[42–45]: A carbon nanotube (CNT) can be considered as a sheet of graphene that is rolled into a cylindrical tube[46–48]. According to the number of graphene layers, carbon nanotubes can be further classified as single-walled carbon nanotubes (SWCNTs, a single graphite sheet that is seamlessly rolled into a cylindrical tube) and multi-walled carbon nanotubes (MWCNTs, more than one layer of graphene that are concentrically rolled into cylindrical tubes like the growth rings of a tree). Two models are developed to represent the structures of MWCNTs. In one model, MWCNTs are described as a Russian doll that the sheets of graphene are arranged in concentric cylinders. In another model, MWCNTs are described to be a parchment that a single sheet of graphene is rolled around itself just like a scroll of parchment. MWCNTs are more commonly existed with the Russian Doll structure and the individual layers can be described as a SWCNT. Due to their unique inherent physical and chemical properties, CNTs showed great promise and widely used industrial, biology, biomedicine, and so on [43,44]. Since they were first discovered in 1991 (MWCNTs)[48] and 1993 (SWCNTs)[46,47], CNTs and their derivatives have been produced by many approaches on the industrial scale, including arc discharge, laser ablation, plasma torch, chemical vapor deposition (CVD) and high-pressure carbon monoxide disproportionation.

1.2 Nanomaterials in nanomedicine

Nanomedicine is defined as the application of nanoscience and nanotechnology in medicine for treatment, diagnosis, monitoring and controlling of biological systems[49]. Due to the small size, vast surface area and diverse surface chemistry, nanomaterials play an important and direct role in nanomedicine[50–55]. The main applications of nanoparticles in medicine include drug delivery, molecular imaging, biological isolation, stem cell research, cancer therapy and so on. It's believed that next generation nanomedicine will dependent on the development of novel nanomaterials.

1.2.1 Cargo delivery

The use of nanomaterials in delivery of drugs, genes, proteins or other biomolecules for treating various diseases is widespread[41,56–62]. Compared with the traditional delivery system, the major advantage that nanomaterials-based delivery system can provide is that they can easily cross the cell plasma membranes and other biological barriers[63–65]. Meanwhile, the therapeutic effect can be enhanced by prolonging half-life and circulation time of drugs *in vivo*, reducing the administration frequency and the negative side effects of drugs and regulating the release of drugs in a sustained and controllable manner. What's more, drugs-carrying nanomaterials can be passively accumulated in a particular location, such as the cancerous place, through the enhanced permeability and retention (EPR) effect[66,67].

Among various of nanomaterials, CNTs are developed as promising delivery carriers for disease treatment due to their unique physical and chemical properties[68]. For example, MWCNTs were used as nanocarriers for the delivery of anti-inflammatory drugs in one report[69]. MWCNTs were treated with acid sonication to improve the hydrophilicity of the outer and inner surfaces and the anti-inflammatory drug dexamethasone were loaded in the nanotubes. The open ends of the drug-carrying nanotubes were sealed with polypyrrole (PPy) films to prevent the unwanted release of drugs. The results showed that the prepared

drug-carrying system can effectively load drugs and release them in a controllable manner by electrical stimulation. In another very recent report, SWCNTs were used for the delivery of siRNA which can specifically regulate gene expression. SWCNTs were functionalized with succinated polyethyleimine to improve the dispersibility in water. The authors found a significant uptake of Cy3-labeled siRNA specific to Braf (siBraf) and gene silencing in the tumor tissue and resulted in attenuation of tumor growth in a mice melanoma model by using this delivery system[62].

1.2.2 Biological imaging

With the brilliant progress in biomedical technology, biomedical researchers recognized that the disease and patients are heterogeneous, and each patient needs optimized therapy based on the differences in genetic factors, physical conditions and the disease characteristics. In this regard, *in vivo* imaging approaches are fascinate tools to visualize the abnormal state of the body and monitor biological circumstance at the targeted site[70,71]. In general, imaging modalities in the clinic include optical imaging, photoacoustic imaging, ultrasound (US), computed tomography (CT) and magnetic resonance imaging (MRI) and so on. Each imaging modality has its own advantages and intrinsic limitations[72,73].

Nanomaterials have been widely used in different imaging methods, such as iron oxide nanoparticles for MRI, gold nanoparticles for CT, CNTs and quantum dots for optical imaging. They can also be combined with each other by co-encapsulation or conjugation to develop multimodal imaging platforms[74]. What's more, by using traditional organic nanoparticles (*e.g.*, liposomes, micelles and polymeric nanoparticles) as a carrier, more than two imaging agents can be integrate together. For example, tri-modal imaging probes for PET/optical/MRI have also been designed by combining radiometal chelates, such as ^{64}Cu-DOTA and ^{111}In-DOTA[75]. In another report, gold-coated iron oxide nanoroses with multiple functions, including aptamer-mediated targeting, optical/magnetic resonance dual imaging and photothermal/chemotherapy dual therapy were demonstrated[76]. In particular, CNTs have also been widely used in imaging of living subjects. For example, SWCNTs modified with cyclic Arg-Gly-Asp (RGD) peptides were prepared and used as contrast agents for photoacoustic imaging of tumours[77]. To image live cells, tissues and animals by using CNTs, techniques include Raman, photoacoustic and near-infrared photoluminescence can be used[78].

1.2.3 Targeted cancer therapy

Cancer has become a leading cause of death worldwide. In 2012 alone, cancer caused up to 8.2 million deaths and 14.1 million new cancer cases, according to the World Health Organization. With the development of nanoscience and nanotechnology, nanomedicine shows the potential to enable novel approaches to treat cancers and nanomaterials play an important and direct role in nanomedicine-based cancer treatment. So far, a wide range of nanomaterials, such as polymeric nanomaterials, liposomes, MNPs, AuNPs, QDs and CNTs, were used in cancer diagnosis or therapy. In addition to the delivery of dugs for cancer treatment, the fascinating and unique properties of nanomaterials made themselves to be good candidate for cancer therapy, such as AuNPs or CNTs-mediated photo-hyperthermia therapy and magnetic nanoparticles-mediated magnetic-hyperthermia therapy[79]. For example, H. Moon *et al* demonstrated that the photothermal effect of SWCNTs upon irradiation by near-infrared (NIR) light, which is in the tissue

transparency regions, was able to induce the destruction of solid malignant tumors *in vivo* in a noninvasive manner[80]. To improve the tumor imaging and photothermal effect of SWNTs, researchers modified SWCNTs with noble metal, such as gold, to get the SWCNTs-metal nanocomposites. They found that SWCNTs-Au composite nanomaterials dramatically improved the photothermal killing efficacy of cancer cells due to the strong surface plasmon resonance absorption by the Au shell[81]. Meanwhile, MWCNTs were also applied in cancer therapy research. J. W. Fisher *et al*. demonstrated the capability of MWNTs to increase tumor injury upon laser irradiation through the improved and controlled thermal deposition and the down-regulated heat shock protein (HSP) expression[82].

To achieve targeted cancer therapy, nanomaterials are usually functionalized with targeting ligands, such as antibodies, peptides or aptamers. For example, SWCNTs were functionalized with the F3 peptide which can be used to target nucleolin, a protein that was found on the surface of endothelial cells in the vasculature of solid tumors, to achieve targeted cancer cell killing[83].

1.2.4 Stem cell research

Stem cells have shown great potential in the field of medicine because of their ability to self-renew and generate multiple cell lineages through differentiation, and stem cell implantation has been considered as a promising therapeutic strategy for various diseases and defects[84–86]. Two major aspects in stem cell study are to keep the stemness when cells undergoing proliferation and to control the directional differentiation to a desired cell lineage. It is known that stem cell proliferation or differentiation can be regulated by the properties of the cell culture substrata, revealing a possible approach to manipulate the behavior of stem cells with nanomaterials.

Due to the unique mechanical, optical, electrical and surface properties, CNTs, showed great potential in stem cell research. Actually, CNTs have been used to promote neural differentiation of stem cells. For example, Y. -S. Chen *et al* found that the neural differentiation of human bone marrow mesenchymal stem cells (hBMMSCs) can be induced and maintained by carboxylated MWCNTs without any exogenous induction factors through the up regulation of the expression of neural growth factors and trapping them to create a proper microenvironment for long-term neural differentiation[87]. In another study, the length-dependent effects of the MWCNTs on the behavior of PC12 cells were studied[88]. The researches found that short MWCNTs showed higher cellular internalization and greater capacity to improve PC12 cell differentiation. The underlying mechanism was explained by the up-regulated expression of neurotrophin signaling pathway associated TrkA/p75 receptors and Pincher/Gap43/TH proteins. Namgung *et al* reported that the growth direction and differentiation of human mesenchymal stem cells (hMSCs) could be controlled by culture them on different CNT networks[89]. Cells cultured on the aligned CNT networks showed directional growth and improved proliferation and osteogenic differentiation compared to those cultured on randomly oriented CNT networks.

Besides CNTs, other nanomaterials, such as gold nanoparticles (AuNPs) have also been used in the stem cell research. In one report, cellular effects of AuNPs on the differentiation of MSCs and the associated mechanism were investigated[90]. The researchers found that AuNPs improved the osteogenic differentiation of MSCs higher than adipogenic differentiation through activating p38 MAPK signaling pathway, which can

regulate the expression of relevant genes to induce osteogenic differentiation and inhibit adipogenic differentiation.

1.3 Nanomaterials in tissue engineering

Tissue engineering has been developed as a promising approach to improve or replace biological functions by the combination of cells, scaffolds and growth factors[91,92]. Among these three key factors, the scaffolds play a crucial role by furnishing a biomimetic microenvironment to control cell functions and guiding new tissue formation[93–96]. So, a scaffold with appropriate properties, such as good biocompatibility, high mechanical property and feasible inner structure is highly demanded for tissue engineering by furnishing a biomimetic microenvironment to control cell functions and to guide new tissue formation. Since cells in biological systems create and directly interact with nanostructured extracellular matrices (ECM), nanomaterials with excellent biomimetic features and physiochemical properties show great potential in the fabrication of novel biomaterials and scaffolds for tissue engineering[97,98].

1.3.1 Nanomaterials for bone tissue engineering

Bone is a type of dense connective tissue that plays a critical role as the protective and supportive framework for the body. What's more, bone also serves as a vital place to store nutrients, minerals and produce red and white blood cells. Nowadays, a variety of bone fractures and bone diseases represent universal and serious clinical problems. Currently, bone defects are often treated with surgical procedures which are usually restricted by the limited supply, poor biocompatibility and the risks of immune rejection and diseases transmission. Bone tissue engineering provides a encouraging alternative approach to treat bone defects[99]. An adapted scaffold that serves as a temporary support is one of the most critical factors in tissue engineering.

From the composition aspect, bone are rich in unique nano scale components, including the hydroxyapatite nanocrystallites and the organic matrix that is mainly composed of collagen[100]. The crystals are often 20-80 nm in length and 2-5 nm in thickness[101], and the protein constituents of bone matrix are also in nanometer scale in dimension. Accordingly, compositing with nanomaterials should be a promising approach to construct novel scaffolds for bone tissue engineering. Indeed, scaffolds containing various nanomaterials have been fabricated and used for bone tissue engineering in the past year. For example, researchers found that primary human osteoblasts cultured in the needle-like HA nanoparticles coated biphasic calcium phosphate scaffolds showed upregulated osteogenic gene expression and improved alkaline phosphatase activity compared to control groups[102]. Another example is that researchers found that MWCNTs/PCL composite scaffolds can promote the proliferation and differentiation of rat bone-marrow-derived stroma cells (BMSCs) than that of pure PCL control group and the effects were dependent on the concentration of MWCNTs[103]. X. Li *et al* demonstrated that MWCNTs might regulate inducible cells in the soft tissues to form inductive bone by the adsorption of proteins which might improve the cell attachment, proliferation and differentiation[104].

1.3.2 Nanomaterials for cartilage tissue engineering

Cartilage is a type of connective tissue comprised of cells called chondrocytes that secrete a great deal of nanostructured extracellular matrix (ECM) that is rich in fibers of collagen and sometimes elastin. Cartilage is stiffer and less flexible than muscle but is not as hard as bone and widely exists in the joints between bones, ears, nose, ribcage and other parts of the bodies of human and animals. Unlike other tissues, cartilage is a type of avascular tissue. The nutrients for chondrocytes are supplied by diffusion through the matrix under the help of the pumping effect produced by compression. In addition, the mobility of chondrocyte in the dense ECM is limited and the presence of progenitor cells is lacking. Therefore, compared to other tissues, cartilage is a low growth and regenerative tissue[105].

Cartilage tissue engineering has also benefited from the development of nanoscience and nanotechnology. Nanomaterials, such as nanoceramics and CNTs, have been used to improve the mechanical or biological properties of the scaffolds used in cartilage tissue engineering. In one report, the authors developed a nanocomposite photopolymerized hydrogel[106]. Mechanical strength of the hydrogels was notably improved through the in situ mineralization with calcium phosphate nanocrystals and the mineralized co-polymer firmly adhered to the nearby cartilage that could help to restore physical force loaded in the defected areas. In another study, rosette nanotubes (RNTs) fabricated by the self-assembly of DNA base pairs were introduced into a 3D scaffold by electrospinning technique for cartilage defect treatment[107]. The results showed that this nanostructured scaffold improved the cell adhesion, viability and subsequent functions compared to that of the control scaffold without RNTs.

1.3.3 Nanomaterials for vascular tissue engineering

Due to the increasing prevalence of vascular diseases, vascular implants with improved efficiency to replace the damaged blood vessels are demanded. Since vascular tissue is a kind of layered structure possessing numerous nanostructured features, nanomaterials have exhibited a great potential in the vascular tissue engineering. For example, a heparin-nanomodified acellular bovine jugular vein scaffold was created in one report[108]. Heparin was securely binded to the scaffold and nanoscale coatings were formed around the fibers. The modification of scaffolds markedly enhanced the biomechanical stability, reduced the adhesion of platelet and induced the proliferation of endothelial cells *in vitro,* and decreased the calcification *in vivo* in a rat model.

In vascular tissue engineering, an important requirement about the ideal vascular scaffold should restrain the proliferation of vascular smooth muscle cells (VSMCs) and stimulate the proliferation of endothelial cells (ECs). The response of VSMCs and ECs to TiO_2 nanotube arrays was studied in one study[109]. The results showed that nanotubes improved the proliferation and motility of ECs, reduced the proliferation of VSMCs, and down-regulated the expression of inflammation and coagulation associated molecules in both cell types.

1.3.4 Nanomaterials for neural tissue engineering

The nervous system is consists of two major subparts: the central nervous system (CNS) and the

peripheral nervous system (PNS). The CNS consists of the brain and the spinal cord, while the PNS consists of nerves that originate from the brain and spinal cord and innervate the rest of the body[110]. The nervous system injuries can be caused by stroke, neurodegenerative disorders, trauma or encephalopathy. Generally, there are two different repair procedures for these two systems after injury[111,112]. The damaged PNS usually regenerate through the proliferation of Schwann cells, phagocytosing myelin, forming bands of Bünger and sprouting axons in the distal segment[113]. However, CNS injuries are much more difficult to repair than PNS injuries because of the lack of Schwann cells and the easy formation of thick glial scar tissue around the neural therapy materials which will prevent proximal axon growth and inhibit neuron regeneration.

The need for neural tissue engineering arises from the difficulty of the nerve cells and neural tissues to regenerate on their own after neural damage has occurred. The development of nanomaterials provides a promising approach to fabricate novel materials for neural tissue engineering. For example, Ketul C. Popat *et al* fabricated PCL nanowire surfaces to culture and maintain the differentiation of neuronal cells[114]. Key neuronal markers were expressed by cells cultured on nanowire surfaces and the neuronal phenotypic behavior of the cells was detected compared to that of the cells cultured on the control surfaces. Ging-Ho Hsiue *et al* found that neural differentiation of human bone marrow mesenchymal stem cells (hBMMSCs) can be induced and maintained by carboxylated MWCNTs without any exogenous induction factors[87].

1.3.5 Nanomaterials for other tissue engineering

Nanomaterials have also been used in other soft tissues, such as the skin and bladder. In one paper, the preparation of sandwich-type scaffolds composing of nanofiber membranes with nanoscale cues for skin tissue engineering was reported[115]. The nanostructured fibers of this scaffold presented nanotopographic factor to the cultured NIH 3T3 fibroblasts and primary rat skin cells, stimulating their migration *in vitro* and enhanced the re-epithelialization of wound *in vivo*. In another report, an asymmetric CGC membrane was fabricated by the injection of collagen I nanoparticles into the prefabricated porous chitosan-genipin (CG) membrane[116]. Fibroblasts cultured on the CGC membrane showed higher efficient in wounds healing than both gauze and the commercial wound dressing, Suile. The application of nanomaterials in bladder tissue engineering was summarized in a review report[117].

1.4 Potential risks of nanomaterials

As described, nanomaterial applications are being developed increasingly and achieved tremendous progresses in different fields. However, it is important to note that there is still much remaining to be elucidated concerning their potential adverse health.

In medical applications, the ability to be internalized by cells is being considered to be the precondition for a success of nanomaterials-based applications in disease diagnosis and therapy. However, the internalized nanomaterials may produce some negative effects on cells. For example, when nanomaterials enter the biological system and accumulate within cells, they may disrupt the organelle integrity, alter gene expression and lead to other intracellular changes. In addition, they may translocate between different cells that finally poses risks to the health. In the past few years, research data on the acute and chronic toxicity of

nanomaterials are expanding but are not yet complete. Meanwhile, research reports related to the genotoxicity of nanomaterials are still limited.

The assessment of safety of nanomaterials are complicated because of a great variety in nanomaterial types, stabilizing coating agents, physicochemical properties of the nanomaterials, cellular incubation conditions, cell types and the investigation methods. Furthermore, regardless of all these differences mentioned above, the ‘‘nano’’ factor itself can induce many negative effects. As the size of nanomaterials approaches to that of the natural proteins, nanomaterials can easily penetrate the biological barriers and enter the places where the particles with larger size can not reach, such as the cell nucleus[118,119]. The high specific surface area of nanomaterials endow they with high surface energy and reactivity, resulting in strong interaction with cell components[120]. What’s more, the enhanced retention of nanomaterials in subcellular organelles can cause a high local concentration that free ions can not reach and induce more severe adverse cellular effects[121].

Therefore, with the increasing applications of nanomaterials in medicine, further systematic and well-designed toxicological studies are needed. Due to intravenous and subcutaneous injections, nanomaterial carriers for drug-delivery application need to undergo biosafety evaluation. Evaluation of the toxicology of nanomaterials by extrapolation from data with parent fine (or bulk) particles may not be appropriate, considering the unique physicochemical properties of selected nanoparticles. Therefore, specific, no-observed-effect level (NOEL) need to be determined from toxicological studies with nanomaterials, especially for those nanomaterials designed for use in nanomedicine. A battery of tests for evaluation of the toxicity of nanomaterials is also essential in future studies because individual tests each cover only one aspect of toxicity.

1.5 Motivation and objectives

Because of their small size, large specific surface area and high surface atomic slot insufficiency, nanomaterials exhibit fascinating and novel properties that are often vastly different from their bulk counterparts. Nanomaterials usually have low weight, high plasticity and high electrical/thermal conductivity as well as unique optical properties. The unique properties of nanomaterials offer excellent platforms for their applications to the diagnosis and therapy of diseases. Meanwhile, since cells in biological systems create and directly interact with nanostructured extracellular matrices (ECM), nanomaterials with excellent biomimetic features and physiochemical properties show great potential in the fabrication of novel biomaterials and scaffolds for tissue engineering. Among various nanomaterials, carbon nanotubes (CNTs), especially single-walled carbon nanotubes (SWCNTs) have attracted intense interest and shown promising applications in the realm of targeted drug/gene delivery, diagnostics, cancer research and tissue engineering.

For biomedical usage, the interaction of nanomaterials with biological systems, especially with cells is the focus of current investigations. The success of nanomaterials-based applications in disease diagnosis and therapy largely depends on whether the designed nanomaterials can be easily internalized by cells. However, the internalized nanomaterials may produce some negative effects on cells. For example, when nanomaterials enter the biological system and accumulate within cells, they may disrupt the organelle integrity, alter gene

expression and lead to other intracellular changes. Therefore, one of the crucial issues regarding nanomaterials-based applications that have to be addressed is to understand how nanomaterials interact with cells and to uncover their potential risks. Meanwhile, feasible techniques are needed to detect the subtle changes of cells when they are exposed to nanomaterials.

Therefore, the objectives of this study are to investigate the biosafety and interactions of SWCNTs with cells and to explore the potential of SWCNTs-based applications in stem cell research and tissue engineering, and to develop novel method for the investigation of interactions of nanomaterials with cells. All of these researches are expected to facilitate the nanomaterials-based biomedical applications. On the other hand, the investigation of the effects of nanomaterials on cells will contribute to a deeper understanding of the interactions of nanomaterials with biological system and help to design more reasonable and effective nanomaterials for clinical trials.

1.6 References

1. Rao, C. & Cheetham, A. Science and technology of nanomaterials: current status and future prospects. *J. Mater. Chem.* **11,** 2887–2894 (2001).
2. Buzea, C. *et al*. Nanomaterials and nanoparticles: sources and toxicity. *Biointerphases* **2,** MR17–71 (2007).
3. Arivalagan, K. Nanomaterials and its Potential Applications. *Int. J. ChemTech Res.* **3,** 534–538 (2011).
4. Roduner, E. Size matters: why nanomaterials are different. *Chem. Soc. Rev.* **35,** 583–92 (2006).
5. D'Almeida, G. & Schütz, L. Number, mass and volume distributions of mineral aerosol and soils of the Sahara. *J. Clim. Appl. Meteorol.* **22,** (1983).
6. Sapkota, A. *et al.* Impact of the 2002 Canadian forest fires on particulate matter air quality in Baltimore city. *Environ. Sci. Technol.* **39,** 24–32 (2005).
7. Kajander, E. O. & Ciftçioglu, N. Nanobacteria: an alternative mechanism for pathogenic intra- and extracellular calcification and stone formation. *Proc. Natl. Acad. Sci. USA* **95,** 8274–9 (1998).
8. Ciftcioglu, N. *et al*. Nanobacteria: fact or fiction? Characteristics, detection, and medical importance of novel self-replicating, calcifying nanoparticles. *J. Investig. Med.* **54,** 385–94 (2006).
9. Shenton, W., Douglas, T., Young, M., Stubbs, G. & Mann, S. Inorganic-Organic Nanotube Composites from Template Mineralization of Tobacco Mosaic Virus. *Adv. Mater.* **11,** 253–256 (1999).
10. Blum, A. S. *et al.* An engineered virus as a scaffold for three-dimensional self-assembly on the nanoscale. *Small* **1,** 702–6 (2005).
11. Nam, K. T. *et al.* Virus-enabled synthesis and assembly of nanowires for lithium ion battery electrodes. *Science.* **312,** 885–8 (2006).
12. Blakemore, R. Magnetotactic bacteria. *Science.* **190,** 377–379 (1975).
13. Yan, L. *et al.* Magnetotactic bacteria, magnetosomes and their application. *Microbiol. Res.* **167,** 507–19 (2012).
14. ÇIFTÇIOĞLU, N. & Haddad, R. A potential cause for kidney stone formation during space flights: enhanced growth of nanobacteria in microgravity. *Kidney Int.* **67,** 483–491 (2005).
15. Patra, C. R., Bhattacharya, R., Mukhopadhyay, D. & Mukherjee, P. Fabrication of gold nanoparticles for

targeted therapy in pancreatic cancer. *Adv. Drug Deliv. Rev.* **62,** 346–361 (2010).

16. Wang, X., Liu, Y., Hu, P. & Yu, G. Controllable fabrication of aligned carbon nanotubes: Selective position and different lengths. *Adv. Mater.* **14,** 1557–1560 (2002).
17. Hulteen, J. A general template-based method for the preparation of nanomaterials. *J. Mater. Chem.* **7,** 1075–1087 (1997).
18. Nikoobakht, B. & El-Sayed, M. Preparation and growth mechanism of gold nanorods (NRs) using seed-mediated growth method. *Chem. Mater.* **15,** 1957–1962 (2003).
19. Li, Q. *et al.* Fabrication of ZnO Nanorods and Nanotubes in Aqueous Solutions. *Chem. Mater.* **17,** 1001–1006 (2005).
20. Lazzari, M. *et al*. Block Copolymers as a tool for nanomaterial fabrication. *Adv. Mater.* **15,** 1583–94 (2003).
21. Hu, C.-M. J. *et al.* Erythrocyte membrane-camouflaged polymeric nanoparticles as a biomimetic delivery platform. *Proc. Natl. Acad. Sci. USA* **108,** 10980–5 (2011).
22. Kamaly, N. *et al.* Targeted polymeric therapeutic nanoparticles: design, development and clinical translation. *Chem. Soc. Rev.* **41,** 2971–3010 (2012).
23. Santos, T. *et al.* Polymeric nanoparticles to control the differentiation of neural stem cells in the subventricular zone of the brain. *ACS Nano* **6,** 10463–74 (2012).
24. Hu, C.-M. J. *et al.* Erythrocyte membrane-camouflaged polymeric nanoparticles as a biomimetic delivery platform. *Proc. Natl. Acad. Sci. USA* **108,** 10980–5 (2011).
25. Alexis, F., Pridgen, E. & Molnar, L. Factors affecting the clearance and biodistribution of polymeric nanoparticles. *Molecular* **5,** 505–515 (2008).
26. Bochot, A. & Fattal, E. Liposomes for intravitreal drug delivery: a state of the art. *J. Control. release* **161,** 628–34 (2012).
27. Drummond, D. C., Meyer, O., Hong, K., Kirpotin, D. B. & Papahadjopoulos, D. Optimizing liposomes for delivery of chemotherapeutic agents to solid tumors. *Pharmacol. Rev.* **51,** 691–743 (1999).
28. Sharma, A. *et al*. Liposomes in drug delivery: progress and limitations. *Int. J. Pharm.* **154,** 123–140 (1997).
29. Dreaden, E. C. *et al*. The golden age: gold nanoparticles for biomedicine. *Chem. Soc. Rev.* **41,** 2740–79 (2012).
30. Jans, H. & Huo, Q. Gold nanoparticle-enabled biological and chemical detection and analysis. *Chem. Soc. Rev.* **41,** 2849–66 (2012).
31. Arvizo, R., Bhattacharya, R. & Mukherjee, P. Gold nanoparticles: Opportunities and challenges in nanomedicine. *Expert Opin. Drug Deliv.* **7,** 753–763 (2010).
32. Chen, C. *et al.* Quantum dots-based molecular classification of breast cancer by quantitative spectroanalysis of hormone receptors and HER2. *Biomaterials* **32,** 7592–9 (2011).
33. Shah, B. S. & Mao, J. J. Labeling of mesenchymal stem cells with bioconjugated quantum dots. *Methods Mol. Biol.* **680,** 61–75 (2011).
34. Yukawa, H. *et al.* Quantum dots labeling using octa-arginine peptides for imaging of adipose tissue-derived stem cells. *Biomaterials* **31,** 4094–103 (2010).
35. Ekimov, A. & Onushchenko, A. Quantum size effect in three-dimensional microscopic semiconductor crystals. *JETP Lett.* **34,** 345–349 (1981).

36. Reed, M. & Randall, J. Observation of discrete electronic states in a zero-dimensional semiconductor nanostructure. *Phys. Rev. Lett.* **60,** 535–537 (1988).
37. Berry, C. C. Possible exploitation of magnetic nanoparticle-cell interaction for biomedical applications. *J. Mater. Chem.* **15,** 543 (2005).
38. Pan, Y. *et al*. Magnetic nanoparticles for the manipulation of proteins and cells. *Chem. Soc. Rev.* **41,** 2912–42 (2012).
39. Reddy, L. H., Arias, J. L., Nicolas, J. & Couvreur, P. Magnetic nanoparticles: design and characterization, toxicity and biocompatibility, pharmaceutical and biomedical applications. *Chem. Rev.* **112,** 5818–78 (2012).
40. Prodan, A. M. *et al.* Iron Oxide Magnetic Nanoparticles: Characterization and Toxicity Evaluation by In Vitro and In Vivo Assays. *J. Nanomater.* **2013,** 1–10 (2013).
41. Arruebo, M., Fernández-pacheco, R., Ibarra, M. R. & Santamaría, J. Magnetic nanoparticles for drug delivery. *Nano Today* **2,** 22–32 (2007).
42. Kostarelos, K., Bianco, A. & Prato, M. Promises, facts and challenges for carbon nanotubes in imaging and therapeutics. *Nat. Nanotech.* **4,** 627–633 (2009).
43. Chen, P., Lin, J. & Tan, K. L. Carbon nanotubes: a future material of life. *IUBMB Life* **49,** 105–8 (2000).
44. Schnorr, J. M. *et al*. Emerging Applications of Carbon Nanotubes. *Chem. Mater.* **23,** 646–57 (2011).
45. Baughman, R. H., Zakhidov, A. A. & de Heer, W. A. Carbon nanotubes--the route toward applications. *Science.* **297,** 787–792 (2002).
46. Bethune, D., Klang, C. & Vries, M. De. Cobalt-catalysed growth of carbon nanotubes with single-atomic-layer walls. *Nature* **363,** 605–607 (1993).
47. Iijima, S. & Ichihashi, T. Single-shell carbon nanotubes of 1-nm diameter. *Nature* **363,** 603–605 (1993).
48. Iijima, S. Helical microtubules of graphitic carbon. *Nature* **354,** 56–58 (1991).
49. Zhao, J. & Castranova, V. Toxicology of nanomaterials used in nanomedicine. *J. Toxicol. Environ. Health. B. Crit. Rev.* **14,** 593–632 (2011).
50. Lei, J. & Ju, H. Signal amplification using functional nanomaterials for biosensing. *Chem. Soc. Rev.* **41,** 2122–34 (2012).
51. Marchesan, S. & Prato, M. Nanomaterials for (Nano)medicine. *ACS Med. Chem. Lett.* **4,** 147–149 (2013).
52. Barreto, J. A. *et al.* Nanomaterials: applications in cancer imaging and therapy. *Adv. Mater.* **23,** H18–40 (2011).
53. Cai, X.-J. & Xu, Y.-Y. Nanomaterials in controlled drug release. *Cytotechnology* **63,** 319–23 (2011).
54. Li, X. *et al.* "Smart" nanomaterials for cancer therapy. *Sci. China Chem.* **53,** 2241–2249 (2010).
55. Hubbell, J. A. & Chilkoti, A. Chemistry. Nanomaterials for drug delivery. *Science* **337,** 303–5 (2012).
56. Endres, T. K. *et al*. Self-assembled biodegradable amphiphilic PEG-PCL-lPEI triblock copolymers at the borderline between micelles and nanoparticles designed for drug and gene delivery. *Biomaterials* **32,** 7721–7731 (2011).
57. Wang, F. *et al.* Doxorubicin-tethered responsive gold nanoparticles facilitate intracellular drug delivery for overcoming multidrug resistance in cancer cells. *ACS Nano* **5,** 3679–92 (2011).
58. Guo, J. *et al.* Aptamer-functionalized PEG-PLGA nanoparticles for enhanced anti-glioma drug delivery. *Biomaterials* **32,** 8010–20 (2011).

59. Guo, R. *et al.* Dual-functional alginic acid hybrid nanospheres for cell imaging and drug delivery. *Small* **5,** 709–717 (2009).
60. Di Crescenzo, A., Velluto, D., Hubbell, J. A. & Fontana, A. Biocompatible dispersions of carbon nanotubes: a potential tool for intracellular transport of anticancer drugs. *Nanoscale* **3,** 925–928 (2011).
61. Liu, Z. *et al.* Drug delivery with carbon nanotubes for in vivo cancer treatment. *Cancer Res.* **68,** 6652–60 (2008).
62. Siu, K. S. *et al.* Non-covalently functionalized single-walled carbon nanotube for topical siRNA delivery into melanoma. *Biomaterials* **35,** 3435–42 (2014).
63. Neuwelt, E. *et al.* Strategies to advance translational research into brain barriers. *Lancet Neurol.* **7,** 84–96 (2008).
64. Bhaskar, S. *et al.* Multifunctional Nanocarriers for diagnostics, drug delivery and targeted treatment across blood-brain barrier: perspectives on tracking and neuroimaging. *Part. Fibre Toxicol.* **7,** 3 (2010).
65. Dilnawaz, F. *et al.* The transport of non-surfactant based paclitaxel loaded magnetic nanoparticles across the blood brain barrier in a rat model. *Biomaterials* **33,** 2936–51 (2012).
66. Matsumura, Y. & Maeda, H. A new concept for macromolecular therapeutics in cancer chemotherapy: mechanism of tumoritropic accumulation of proteins and the antitumor agent smancs. *Cancer Res.* **46,** 6387–6392 (1986).
67. Greish, K. Enhanced permeability and retention (EPR) effect for anticancer nanomedicine drug targeting. *Methods Mol. Biol.* **624,** 25–37 (2010).
68. Meng, L., Zhang, X., Lu, Q., Fei, Z. & Dyson, P. J. Single walled carbon nanotubes as drug delivery vehicles: Targeting doxorubicin to tumors. *Biomaterials* **33,** 1689–1698 (2011).
69. Luo, X., Matranga, C., Tan, S., Alba, N. & Cui, X. T. Carbon nanotube nanoreservior for controlled release of anti-inflammatory dexamethasone. *Biomaterials* **32,** 6316–6323 (2011).
70. Parveen, S., Misra, R. & Sahoo, S. K. Nanoparticles: a boon to drug delivery, therapeutics, diagnostics and imaging. *Nanomedicine* **8,** 147–66 (2012).
71. Lee, D.-E. *et al.* Multifunctional nanoparticles for multimodal imaging and theragnosis. *Chem. Soc. Rev.* **41,** 2656–72 (2012).
72. Bardhan, R. *et al.* Nanoshells with Targeted Simultaneous Enhancement of Magnetic and Optical Imaging and Photothermal Therapeutic Response. *Adv. Funct. Mater.* **19,** 3901–3909 (2009).
73. Willmann, J. *et al.* Molecular imaging in drug development. *Nat. Rev. Drug. Discov.* **7,** 591–607 (2008).
74. Louie, A. Multimodality imaging probes: design and challenges. *Chem. Rev.* **110,** 3146–95 (2010).
75. Xie, J. *et al.* PET/NIRF/MRI triple functional iron oxide nanoparticles. *Biomaterials* **31,** 3016–22 (2010).
76. Li, C. *et al.* Gold-Coated Fe3O4 Nanoroses with Five Unique Functions for Cancer Cell Targeting, Imaging, and Therapy. *Adv. Funct. Mater.* **24,** 1772–80 (2014).
77. De la Zerda, A. *et al.* Carbon nanotubes as photoacoustic molecular imaging agents in living mice. *Nat. Nanotech.* **3,** 557–562 (2008).
78. Bergstrom, D. E. & Cheng, J. X. Label-free imaging of semiconducting and metallic carbon nanotubes in cells and mice using transient absorption microscopy. *Nat. Nanotech.* **7,** 56–61 (2012).
79. Singh, R. *et al.* Carbon nanotubes in hyperthermia therapy. *Adv. Drug Deliv. Rev.* **65,** 2045–2060 (2013).

80. Moon, H., Lee, S. & Choi, H. In vivo near-infrared mediated tumor destruction by photothermal effect of carbon nanotubes. *ACS Nano* **3,** 3707–3713 (2009).
81. Wang, X., *et al.* Noble metal coated single-walled carbon nanotubes for applications in surface enhanced Raman scattering imaging and photothermal therapy. *J. Am. Chem. Soc.* **134,** 7414–22 (2012).
82. Fisher, J. W. *et al.* Photothermal response of human and murine cancer cells to multiwalled carbon nanotubes after laser irradiation. *Cancer Res.* **70,** 9855–64 (2010).
83. Prickett, W. M., Van Rite, B. D., Resasco, D. E. & Harrison, R. G. Vascular targeted single-walled carbon nanotubes for near-infrared light therapy of cancer. *Nanotechnology* **22,** 455101 (2011).
84. Pittenger, M. F. Multilineage potential of adult human mesenchymal stem cells. *Science.* **284,** 143–7 (1999).
85. Weissman, I. L. Translating Stem and Progenitor Cell Biology to the Clinic: Barriers and Opportunities. *Science.* **287,** 1442–1446 (2000).
86. Reya, T. *et al.* Stem cells, cancer, and cancer stem cells. *Nature* **414,** 105–11 (2001).
87. Chen, Y.-S. & Hsiue, G.-H. Directing neural differentiation of mesenchymal stem cells by carboxylated multiwalled carbon nanotubes. *Biomaterials* **34,** 4936–4944 (2013).
88. Meng, L. *et al.* Short multiwall carbon nanotubes promote neuronal differentiation of PC12 cells via up-regulation of the neurotrophin signaling pathway. *Small* **9,** 1786–98 (2013).
89. Namgung, S., Baik, K. Y., Park, J. & Hong, S. Controlling the growth and differentiation of human mesenchymal stem cells by the arrangement of individual carbon nanotubes. *ACS Nano* **5,** 7383–90 (2011).
90. Yi, C., Liu, D., Fong, C.-C., Zhang, J. & Yang, M. Gold nanoparticles promote osteogenic differentiation of mesenchymal stem cells through p38 MAPK pathway. *ACS Nano* **4,** 6439–48 (2010).
91. Langer, R. & Vacanti, J. P. Tissue Engineering. *Science.* **260,** 920–926 (1993).
92. Griffith, L. G. & Naughton, G. Tissue engineering--current challenges and expanding opportunities. *Science.* **295,** 1009–14 (2002).
93. Chen, G. *et al.* Scaffold Design for Tissue Engineering. *Macromol. Biosci.* **2,** 67–77 (2002).
94. Hollister, S. J. Porous scaffold design for tissue engineering. *Nat. Mater.* **4,** 518–24 (2005).
95. Teixeira, A. I., Abrams, G. a, Bertics, P. J., Murphy, C. J. & Nealey, P. F. Epithelial contact guidance on well-defined micro- and nanostructured substrates. *J. Cell Sci.* **116,** 1881–92 (2003).
96. Lutolf, M. P. & Hubbell, J. a. Synthetic biomaterials as instructive extracellular microenvironments for morphogenesis in tissue engineering. *Nat. Biotechnol.* **23,** 47–55 (2005).
97. Shi, J., Votruba, A. R., Farokhzad, O. C. & Langer, R. Nanotechnology in drug delivery and tissue engineering: from discovery to applications. *Nano Lett.* **10,** 3223–3230 (2010).
98. Dvir, T., *et al.* Nanotechnological strategies for engineering complex tissues. *Nat. Nanotech.* **6,** 13–22 (2011).
99. Amini, A. R., Laurencin, C. T. & Nukavarapu, S. P. Bone Tissue Engineering: Recent Advances and Challenges. *Crit. Rev. Biomed. Eng.* **40,** 363–408 (2012).
100. Chan, C. K. *et al.* Biomimetic nanocomposites for bone graft applications. *Nanomedicine* **1,** 177–88 (2006).
101. Sachlos, E., Gotora, D. & Czernuszka, J. T. Collagen scaffolds reinforced with biomimetic composite nano-sized carbonate-substituted hydroxyapatite crystals and shaped by rapid prototyping to contain internal microchannels. *Tissue Eng.* **12,** 2479–87 (2006).
102. Roohani-Esfahani, S.-I. *et al.* The influence hydroxyapatite nanoparticle shape and size on the properties of

biphasic calcium phosphate scaffolds coated with hydroxyapatite-PCL composites. *Biomaterials* **31,** 5498–509 (2010).

103. Pan, L., Pei, X., He, R., Wan, Q. & Wang, J. Multiwall carbon nanotubes/polycaprolactone composites for bone tissue engineering application. *Colloids Surf. B. Biointerfaces* **93,** 226–34 (2012).
104. Li, X. *et al.* The use of carbon nanotubes to induce osteogenic differentiation of human adipose-derived MSCs in vitro and ectopic bone formation in vivo. *Biomaterials* **33,** 4818–27 (2012).
105. Vasita, R. & Katti, D. S. Nanofibers and their applications in tissue engineering. *Int. J. Nanomedicine* **1,** 15–30 (2006).
106. Schlichting, K. E. *et al.* Synthesis of a novel photopolymerized nanocomposite hydrogel for treatment of acute mechanical damage to cartilage. *Acta Biomater.* **7,** 3094–100 (2011).
107. Chen, Y., Bilgen, B. & Pareta, R. Self-assembled rosette nanotube/hydrogel composites for cartilage tissue engineering. *Tissue Eng. Part C* **16,** 1233–1243 (2010).
108. Tao, Y. *et al.* Heparin nanomodification improves biocompatibility and biomechanical stability of decellularized vascular scaffolds. *Int. J. Nanomedicine* **7,** 5847–58 (2012).
109. Peng, L. *et al.* Whole genome expression analysis reveals differential effects of TiO2 nanotubes on vascular cells. *Nano Lett.* **10,** 143–8 (2010).
110. Schmidt, C. E. & Leach, J. B. Neural tissue engineering: strategies for repair and regeneration. *Annu. Rev. Biomed. Eng.* **5,** 293–347 (2003).
111. Bähr, M. & Bonhoeffer, F. Perspectives on axonal regeneration in the mammalian CNS. *Trends Neurosci.* **17,** 473–9 (1994).
112. Zhang, N., Yan, H. & Wen, X. Tissue-engineering approaches for axonal guidance. *Brain Res. Brain Res. Rev.* **49,** 48–64 (2005).
113. Evans, G. R. Peripheral nerve injury: a review and approach to tissue engineered constructs. *Anat. Rec.* **263,** 396–404 (2001).
114. Bechara, S. L., Judson, A. & Popat, K. C. Template synthesized poly(epsilon-caprolactone) nanowire surfaces for neural tissue engineering. *Biomaterials* **31,** 3492–501 (2010).
115. Ma, B., Xie, J., Jiang, J. & Wu, J. Sandwich-type fiber scaffolds with square arrayed microwells and nanostructured cues as microskin grafts for skin regeneration. *Biomaterials* **35,** 630–41 (2014).
116. Chen, K.-Y. *et al.* Asymmetric chitosan membrane containing collagen I nanospheres for skin tissue engineering. *Biomacromolecules* **10,** 1642–9 (2009).
117. Harrington, D. *et al*. Bladder tissue engineering through nanotechnology. *World J Urol.* **26,** 2008 (2008).
118. Chu, M. *et al.* Transfer of quantum dots from pregnant mice to pups across the placental barrier. *Small* **6,** 670–8 (2010).
119. Gu, Y. *et al.* Nuclear penetration of surface functionalized gold nanoparticles. *Toxicol. Appl. Pharmacol.* **237,** 196–204 (2009).
120. Pisanic, T. R., Blackwell, J. D., Shubayev, V. I., Fiñones, R. R. & Jin, S. Nanotoxicity of iron oxide nanoparticle internalization in growing neurons. *Biomaterials* **28,** 2572–81 (2007).
121. Adler, A. F. & Leong, K. W. Emerging links between surface nanotechnology and endocytosis: impact on nonviral gene delivery. *Nano Today* **5,** 553–569 (2010).

Chapter 2

Cellular interaction of collagen-functionalized SWCNTs in 2D cell culture system

2.1 Summary

Carbon nanotubes (CNTs) have shown great potential for biological and medical applications because of their intrinsic unique properties. However, applications of CNTs have been severely restricted by their super-hydrophobicity and easy aggregation in aqueous medium, which are related to cytotoxicity and other negative cellular effects. What's more, the interactions of CNTs with cells need to be thoroughly investigated before they can be applied in clinical trials. In this part, single-walled carbon nanotubes (SWCNTs) were functionalized with collagen (Col-SWCNTs). The Col-SWCNTs retained the inherent properties of SWCNTs and the suspension solution was stable for months. The cellular effects, uptake and intracellular distribution of the Col-SWCNTs were investigated by using them for culture of bovine articular chondrocytes (BACs). The Col-SWCNTs showed no obvious negative cellular effects and high amount of SWCNTs were internalized by cells. The internalized Col-SWCNTs were distributed in the perinuclear region and retained in the cells for more than one week. Adsorption of SWCNTs by extracellular matrix (ECM) was shown to be an important step for cellular uptake of SWCNTs. The high stability, easy cellular uptake and long retention in cells of the Col-SWCNTs will facilitate the biomedical and biotechnological applications of SWCNTs.

2.2 Introduction

Among various nanomaterials, carbon nanotubes (CNTs) have attracted intense interest and shown great potential for biomedical and biotechnological applications, including delivery of bioactive molecules such as drugs[1–4], proteins[5–7] and nucleic acids[8,9]; targeted cancer therapy[10–12] and biological imaging[13–16]. The great potential of CNTs results from their small size, large surface area, low density, high stability and other unique inherent mechanical, optical and electrical properties[18–20]. One of the most fascinating benefits of

CNTs is the ability to efficaciously traverse biological barriers and enter even cell nuclei[21–23] in an energy dependent or independent manner[7,24–31]. Nevertheless, the applications of CNTs have been severely restricted by their super-hydrophobicity and easy aggregation in aqueous medium. The features are associated with cytotoxicity and other negative cellular effects[32], whereas well-dispersed CNTs show no apparent cytotoxicity[6,7,33]. Therefore, stable CNT dispersion systems that retain the intrinsic CNT properties and have no or negligible negative cellular effects are desirable. Many previous studies have been devoted to increasing the dispersibility and avoiding aggregation of CNTs in aqueous medium[6,15,29,30,33–37]. One of the most common processes is to introduce hydrophilic carboxylic acid groups at the ends of the tubes and at the site of defects on the sidewalls through multistep acid treatment using oxidizing acid to improve the dispersibility of CNTs in an aqueous medium[6,7,29]. The acid-treated CNTs are necessary precursors for the synthesis of a number of other functionalized CNTs. However, the complicated procedures may randomly cut CNTs and result in a change in the fundamental optical properties. On the other hand, several studies have shown that CNTs can be non-covalently functionalized by surfactants[34], carbohydrates[4,30] and proteins [31,36] as well as nucleic acids[15,27,37] and other biomolecules[12,35] to improve the dispersibility. However, it is quite difficult to obtain a high yield of isolated CNTs via some of these approaches and many of these dispersants usually produce significant negative cellular effects.

Collagen, the most abundant protein in mammals, has a wide variety of applications in tissue engineering and regenerative medicine because of its regular helical structure, excellent biocompatibility and moderate immunogenicity. Previous studies show that collagen/SWCNT composite materials have great utility as scaffolds in tissue engineering[38]. Collagen has also been used to stabilize silver nanoparticles in water[39]. The Col-functionalized silver nanoparticles are stable over one month and show non-toxic effects on human fibroblasts and keratinocytes. However, to the best of our knowledge, there is no report characterizing Col-SWCNT dispersions. Additionally, the interaction between Col-SWCNTs and cells has also barely been investigated, especially cellular effects and uptake over long times.

Meanwhile, regarding the cytotoxicity of CNTs, published data were fiercely debated and extremely inconsistent. Some papers demonstrated that CNTs are toxic to multiple types of cells[40–42], whereas other studies came to completely opposite conclusions if the CNTs were well-dispersed in water[6,7,33]. So the effects of CNTs on cells need to be thoroughly investigated before they can be used in clinical trials.

In this part of study, single-walled carbon nanotubes (SWCNTs) were non-covalently functionalized with type I collagen (Col-SWCNTs) to improve their dispersibility in aqueous solution and used for culture of bovine articular chondrocytes (BACs). The cellular effects were investigated through WST-1 assay, live/dead staining and collagen II staining. The cellular uptake of Col-SWCNTs was quantified through concentration-dependent ultraviolet-visible-near-infrared (UV-vis-NIR) spectroscopy. In addition, the distribution of Col-SWCNTs in cells was investigated using confocal Raman imaging.

2.3 Materials and methods

2.3.1 Preparation of Col-SWCNTs

To improve the dispersibility in water, SWCNTs (purity > 90%, 0.7-1.3 nm in diameter, Sigma-Aldrich, USA) were functionalized with collagen using a simple non-covalent approach. Briefly, 1,000 μg SWCNTs were sterilized using ultraviolet light for 2 hours and put in 10 mL 0.1 wt% collagen solution that was prepared by diluting 1.0 wt% collagen aqueous solution (type I collagen in pH = 3.0 acetic acid aqueous solution, Nippon Meat Packers Inc., Japan) with pH = 3.0 acetic acid aqueous solution. The mixture was sonicated (135 W, Bransonic, Japan) in an ice bath for 2 hours. The dispersion solution was then centrifuged (Tomy MX-301, Japan) at 20,000× g for 30 minutes to remove aggregated and bundled SWCNTs. Finally, the supernatant was collected and underwent an additional centrifugation round.

2.3.2 Characterization of Col-SWCNTs

The morphology of Col-SWCNTs was examined by high-resolution transmission electron microscopy (TEM, JEM-2100F, JEOL, Japan) after being deposited onto a carbon-coated copper grid. AFM images of Col-SWCNTs deposited on a mica substratum were taken in the tapping mode using an MFP-3D-BIO atomic force microscope (Asylum Research, CA). The length of the SWCNTs was measured using an ImageJ software. The final concentrations of Col-SWCNTs in the dispersions were determined via concentration-dependent UV-vis-NIR spectroscopy (V-7200, JASCO, Japan). For each concentration of SWCNT dispersion, the NIR absorbance intensity was obtained at 1032 nm. To investigate the stability of Col-SWCNT dispersions, NIR spectroscopy data were acquired from the supernatant immediately after centrifugation and from the same sample after 63 days of storage at room temperature. To obtain the Raman spectra of Col-SWCNTs, the supernatant was dropped and dried on a glass slide, then placed under the objective of the Raman microscope. After focusing, the Raman spectrum of the dried sample was recorded (laser excitation wavelength = 532 nm, 100 mW power, 3 second collection time).

2.3.3 Cell culture and incubation with Col-SWCNTs

Bovine articular chondrocytes (BACs) were isolated from the articular cartilage derived from a 9-week old female calf. Freshly isolated chondrocytes were defined as P0. BACs that were subcultured twice (P2) were used in this study. The BACs were cultured in 75 cm^2 tissue culture flasks (BD Falcon, USA) with normal cell culture medium at 37 °C in humidified air containing 5% CO_2. The normal cell culture medium was Dulbecco's modified Eagle's medium (DMEM, Sigma, USA) supplemented with 10% fetal bovine serum, 4,500 mg/L glucose, 4 mM glutamine, 100 U/mL penicillin, 100 μg/mL streptomycin, 0.1 mM nonessential amino acids, 0.4 mM proline, 1 mM sodium pyruvate and 50 μg/mL ascorbic acid. P2 cells were seeded into 6-well, 24-well, 96-well plates and 4-chamber culture slides (BD Falcon, USA) at a density of 50,000 cells/cm^2. After 4 hours of pre-culture, the cell culture medium was changed to DMEM containing Col-SWCNTs for the experimental samples. DMEM containing the same amount of collagen as the experimental samples was used as a positive control. To prepare the cell culture medium containing

Col-SWCNTs, the Col-SWCNT dispersion was diluted with DMEM to a designed concentration.

2.3.4 Determination of cellular effects of Col-SWCNTs

To evaluate cell viability, BACs were cultured in 96-well plates with or without Col-SWCNTs for a designated period from 4 hours to 15 days. The medium was changed every 3 days. At each time point, cell viability was evaluated by WST-1 assay. The medium was replaced with 110 μL of WST-1 solution (Roche, Germany, 10 μL of WST-1 stock solution diluted with 100 μL of complete medium) and the cells were cultured for an additional 3 hours. The absorbance of each well of the 96-well plates was measured at 440 nm using a plate reader (Benchmark Plus, USA) to determine cell viability. Live/dead staining with a Cellstain Live-Dead Double Staining kit (Dojindo, Japan) was also used to confirm live and dead cells after cell culture. The staining was conducted according to the manufacturer's instructions. Briefly, cells, after being cultured in 24-well plates with or without Col-SWCNTs for 4 days, were washed with warmed PBS 3 times and incubated in 2 mM calcein-AM and 4 mM propidium iodide (PI) in serum-free DMEM for 15 minutes. The cells were then immersed in serum-free medium after being rinsed with PBS. The live/dead images were observed using an inverted fluorescence microscope (Olympus, Japan). Immunological staining of type II collagen was performed to evaluate cell function. Briefly, cells cultured in 24-well plates in normal DMEM with or without Col-SWCNTs and normal DMEM containing collagen were fixed by 4% paraformaldehyde solution and incubated sequentially with proteinase K for 10 minutes for antigen retrieval, peroxidase blocking solution for 5 minutes and 10% goat serum solution for 30 minutes. The cells were then incubated with the first antibodies (rabbit polyclonal anti-collagen type II, Sanbio B.V., Uden, Netherlands) for 1 hour, followed by incubation with the peroxidase-labeled polymer-conjugated second antibodies (Dakocytomation Envisionþ, Dako, CA) for 30 minutes. The cells were then incubated with 3,3'-diaminobenzidine (DAB) for 5 minutes to visualize the bound antibodies. The nuclei were counterstained with hematoxylin. The stained samples were observed under an optical microscope. All procedures were performed at room temperature (RT).

2.3.5 Cellular uptake of Col-SWCNTs

To determine the amount of Col-SWCNTs internalized in the BACs, the cells were cultured in 6-well plates in normal DMEM with Col-SWCNTs for 3 days. The medium was then changed to normal DMEM without Col-SWCNTs and the cells were cultured for another 6 days. The total culture period was 9 days. As is well known, cells are surrounded by their own ECM after cell culture. To precisely determine the amount of cellular uptake of SWCNTs, cells should be harvested without ECM. In this study, the cell culture medium was removed from the cell culture plates and the cells were washed with PBS three times. Next, the BACs were treated with trypsin/collagenase mixed solutions to separate the BACs from the surrounding ECM. After centrifugation, the supernatant (trypsin/collagenase solution) was collected and the cell pellet was washed with warm PBS through two rounds of washing-centrifugation. The PBS supernatant from each round was also collected and added into the collected trypsin/collagenase supernatant. The amount of SWCNTs in this mixed collection was measured using UV-vis-NIR spectroscopy and considered to be the amount of SWCNTs absorbed in the ECM. The washed cells were ruptured via a papain (Sigma, USA)

buffer solution and the amount of SWCNTs was measured and considered to be the amount of SWCNTs taken up in cells. Before being ruptured, the cells were counted with a cytometer and the population doubling time (PDT) was calculated using the equation $PDT = t \times \log 2 / (\log N - \log N_0)$, where N_0 represents the initial cell number, N represents the final cell number and t represents the time interval between N_0 and N.

2.3.6 Intracellular distribution of Col-SWCNTs

An inverted confocal Raman microscope (AMANplus, Nanophoton, Japan) with a 532 nm laser (500 mW) and phase objectives (Nikon Microsystems, Japan) was used for both Raman and phase-contrast imaging. Briefly, after the BACs were cultured in 4-chamber culture slides in normal DMEM with Col-SWCNTs for 4 hours to 5 days, the cells were washed with warm PBS and fixed with 4% paraformaldehyde solution to prevent morphological and chemical changes during image acquisition. After that, the samples were washed with PBS and the slides were mounted and hermetically sealed using nail lacquer. A phase-contrast image of a cell population was focused, revealing cellular morphologies including the nuclei and extensions. And then, a horizontal confocal Raman image (x-y imaging mode) was acquired to investigate the time course change of SWCNTs distribution in cells. Furthermore, an entire vertical section image (x-z imaging mode) of a single cell and a cell population after being cultured with Col-SWCNTs for 3 days were acquired to show the detailed SWCNTs distribution. The confocal Raman spectra from 779.7 to 1970.0 cm^{-1} were collected and the G-band, indicative of SWCNTs, was used to map the distribution of SWCNTs. Control of imaging parameters and processing and data analysis were performed in a Raman Data Viewer software (Nanophoton, Japan).

2.3.7 Statistical analysis

All data were reported as mean ± standard deviation (SD). One-way analysis of variance was performed to reveal statistical differences followed by Tukey's post hoc test for pairwise comparison. All statistical analyses were executed using Kyplot 2.0 beta 15.

2.4 Results and discussion

2.4.1 Dispersibility and stability of Col-SWCNTs

The main intrinsic drawbacks of SWCNTs are their super-hydrophobicity and easy aggregation in aqueous medium. Although various methods have been introduced to improve the dispersibility of SWCNTs, facile and effective methods for functionalizing SWCNTs are desirable. In this study, we used type I collagen to modify SWCNTs by non-covalent adsorption for good dispersion in an aqueous phase (Fig. 2.1a). Fig. 2.1b shows the high resolution TEM image of the Col-SWCNTs, revealing the lattice spacing of individual carbon layer and surface of the nanotube was coated by collagen. The morphology of Col-SWCNTs was observed using AFM after the Col-SWCNTs were deposited on a mica substratum (Fig. 2.1c). Most of the Col-SWCNTs were individually dispersed on the surface, suggesting the individual dispersion state of Col-SWCNTs in solution. The length of the nanotubes measured from the image was 235 ± 42 nm. The

dispersibility of Col-SWCNTs and their stability in aqueous solutions were evaluated using UV-vis-NIR and Raman spectroscopy. The high absorbance of SWCNTs in the NIR spectrum originates from the electronic transitions between the first or second van Hove singularities of the nanotubes. The data in Fig. 2.1d revealed a highly linear relationship between the concentration of nanotubes and the corresponding NIR absorbance at 1032 nm with $R^2 = 0.9999$. This NIR spectroscopy calibration curve was used to determine the concentration of SWCNTs in the aqueous solutions. It was confirmed that SWCNTs with the same concentration were found to exhibit similar NIR intensities in water, PBS buffer, cell culture medium, trypsin/collagenase solution and papain solution. The full range UV-vis-NIR spectra of the same Col-SWCNTs dispersion solution immediately after preparation and after storage for 63 days were exactly the same (Fig. 2.1e), indicating that the Col-SWCNTs solution was highly stable during storage. The concentration of SWCNTs in this supernatant was up to ≈ 30 μg/mL. Therefore, highly stable nanotube solutions consisting of individually dispersed SWCNTs could be obtained after functionalization with collagen.

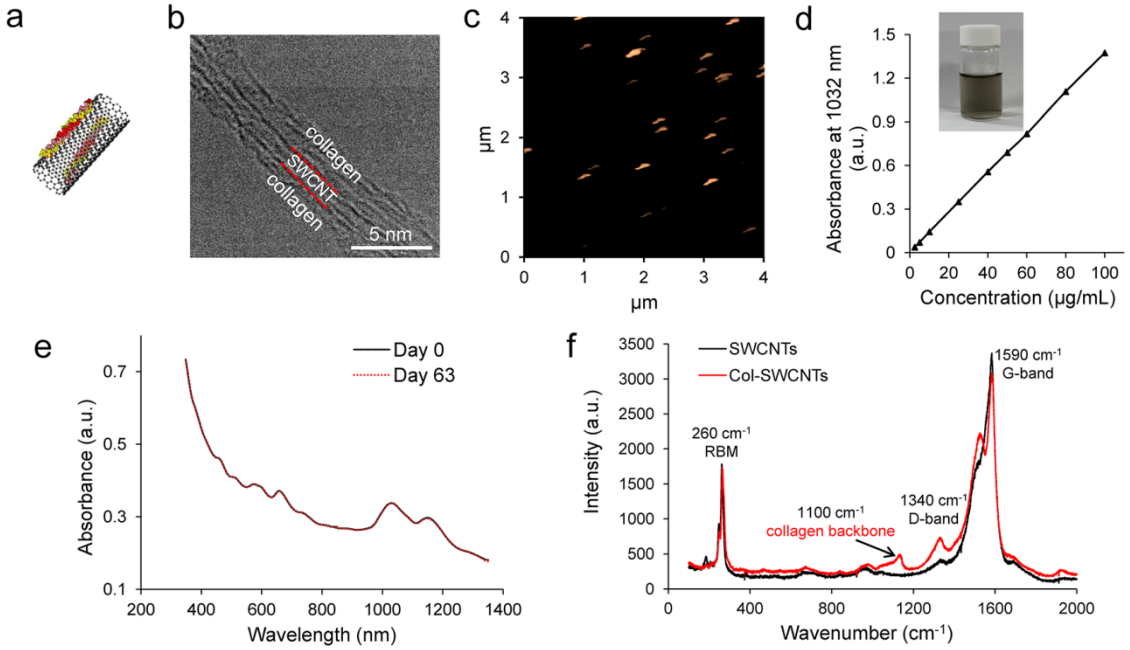

Fig. 2.1 (a) Schematic of a collagen-functionalized SWCNT (Col-SWCNT). The color parts indicate collagen molecules. (b) High resolution TEM image of Col-SWCNTs. (c) AFM image of Col-SWCNTs deposited on a mica substratum. (d) Correlation between the NIR absorbance at 1032 nm and the corresponding SWCNT concentration. The inset shows a photo of the Col-SWCNT solution. (e) Full range UV-vis-NIR spectra of Col-SWCNTs obtained from the same samples immediately after preparation (time = 0 day) and after 63 days of storage. (f) Raman spectrum of pristine and Col-functionalized SWCNTs.

In a typical SWCNT Raman spectrum, the following intense bands can be observed: 120-300 cm^{-1} for the radial breath mode (RBM) that is caused by uniaxial vibrations of SWCNTs, 1580-1600 cm^{-1} for the tangential G band that is caused by stretching along the C-C bonds in the graphitic plane and 1330-1360 cm^{-1} for the disorder-induced D band that provides information regarding amorphous impurities and carbon nanotube wall disorders. The Raman spectra of the pristine SWCNTs and dried Col-SWCNTs on the glass slides showed these characteristic peaks and were similar except for the peak at 1100 cm^{-1} (Fig. 2.1f). The

new peak at 1100 cm^{-1} resulted from the collagen backbone, confirming the modification of SWCNTs by collagen.

All these results indicated that functionalization of SWCNTs with collagen did not affect the optical properties of SWCNTs and that the Col-SWCNTs were individually dispersed in the aqueous solution, highly stable and suitable for further biological research.

2.4.2 Cellular effects of Col-SWCNTs

Fig. 2.2a shows the results of WST-1 assays on the metabolic activity (cell viability) of cell populations upon exposure to Col-SWCNTs at a concentration of ≈ 15 μg/mL over time. No obvious differences were observed among the cells cultured with normal culture medium, medium supplemented with collagen or medium supplemented with Col-SWCNTs during the 15 days of culture. The results indicated that Col-SWCNTs at a concentration of ≈ 15 μg/mL did not affect cell viability. The viability of the cells was further confirmed by live/dead staining (Fig. 2.2b). Few red-stained cells were detected. Most of the cells were alive in all of the three culture conditions with or with Col-SWCNTs.

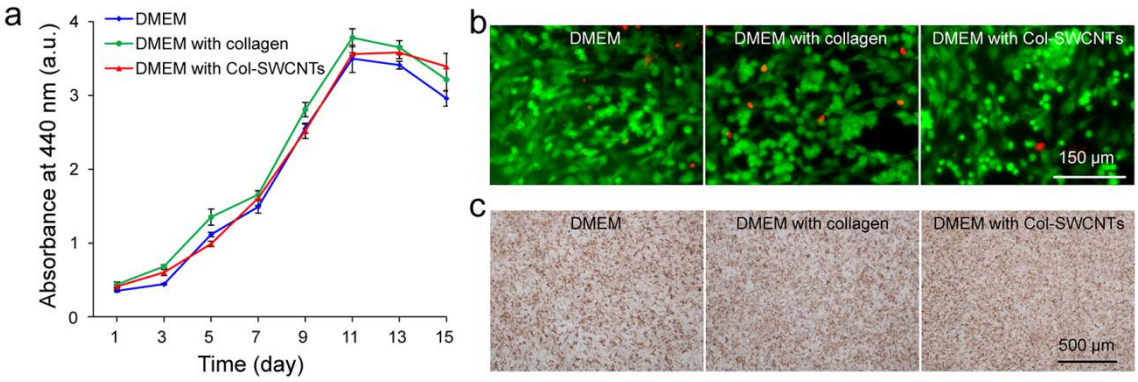

Fig. 2.2 (a) WST-1 assay of BACs cultured for 1 to 15 days with normal medium, medium with collagen and medium with Col-SWCNTs. (b) Live/dead staining of BACs after being cultured with normal medium, medium with collagen and medium with Col-SWCNTs for 4 days. (c) Collagen II staining of BACs after being cultured with normal medium, medium with collagen and medium with Col-SWCNTs for 2 weeks.

Type II collagen is a specific marker of articular chondrocytes. The expression of type II collagen indicates that the function of articular chondrocytes is maintained. In this study, cells cultured in all groups were positively stained with anti-collagen II antibody (Fig. 2.2c), indicating that the Col-SWCNTs did not affect the capacity for expression of chondrogenic genes. These results indicated that the Col-SWCNTs did not show any negative effects on the functions of bovine chondrocytes.

2.4.3 Cellular uptake of Col-SWCNTs

The success of many SWCNT-based applications in nanomedicine and nanotechnology largely depends on whether and how many CNTs can be taken up by cells. The major pathways for the cellular uptake of SWCNTs include passive uptake, by which SWCNTs penetrate cell membranes in a manner similar to that of nanoneedles[22,43,44] and active uptake via clathrin-mediated endocytosis[6,28,33]. The adsorption of some biocompatible molecules, such as BSA, DNA and peptides, on the surfaces of SWCNTs may induce and

facilitate receptor-mediated endocytosis of nanotubes[5,22,29]. The cellular uptake of Col-SWCNTs by bovine chondrocytes during cell culture was investigated using UV-vis-NIR spectroscopy (Fig. 2.3a). The cells were cultured with DMEM supplemented with Col-SWCNTs at a concentration of 5 μg/mL for 3 days. Next, the medium was changed to normal DMEM without Col-SWCNTs. The amount of SWCNTs in the entire cell population increased over time and then remained stable after being cultured for 6 days. The trend for the amount of cellular uptake of SWCNTs to increase was maintained even when the cell culture medium was changed to normal medium without Col-SWCNTs. To explain this phenomenon, SWCNTs in the extracellular matrix (ECM) were quantitatively investigated (Fig. 2.3b). The amount of SWCNTs in the ECM increased during the first 3 days of culture with medium containing Col-SWCNTs and decreased when the culture medium was changed to that without Col-SWCNTs. Cells are surrounded by ECM. After the culture medium was changed to DMEM without Col-SWCNTs, no new SWCNTs were absorbed in the ECM. The amount of SWCNTs in the ECM should maintain unchanged. However, the cells should continually uptake SWCNTs from the ECM that surrounds the cells. Therefore, the amount of cellular uptake of SWCNTs still increased while the amount in the ECM decreased after the cell culture medium was changed to SWCNT-free medium. From these results, we suggest that absorption of SWCNTs by the ECM could be an important step for the cellular uptake of the SWCNTs, especially for the cells with abundant ECM such as chondrocytes, which has not been previously shown.

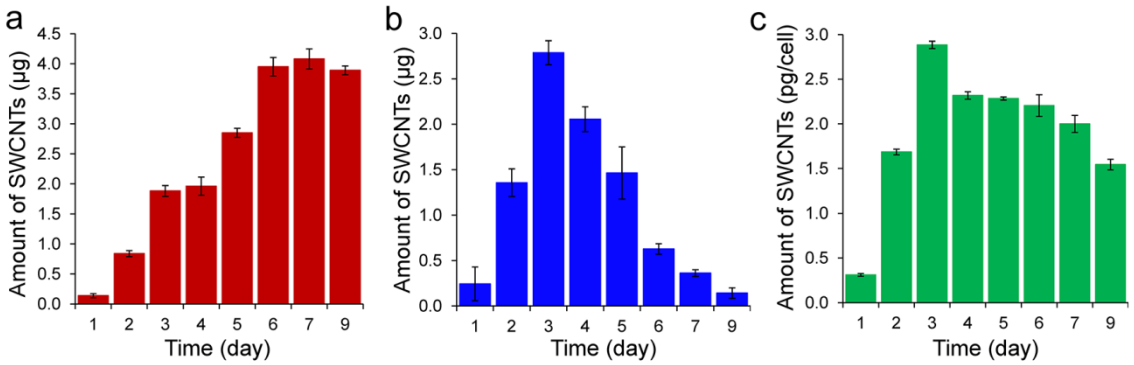

Fig. 2.3 (a) Quantification of cellular uptake of Col-SWCNTs in a BAC population after different culture time. (b) Amount of SWCNTs absorbed in the ECM during cell culture. (c) Average amount of Col-SWCNTs internalized in a single cell after different culture time.

Based on the cellular uptake of SWCNTs by the population of cells, the amount of SWCNTs uptaken by a single cell was calculated (Fig. 2.3c). The uptake amount of SWCNTs by a single cell increased to a peak at day 3 and then decreased over time. In this study, the population doubling time (PDT) of the BACs was calculated to be 2.8 ± 0.4 days. Therefore, the decrease in uptake by a single cell after 3 days may be caused by cell division, which can dilute the average amount of SWCNTs in one cell[45]. At day 3, there were up to 2.9 ± 0.1 pg of SWCNTs per cell, which was much higher than previously reported[25,33]. In other words, up to ten million (≈ 10.3 ± 0.4 × 10^6 SWCNTs/cell) SWCNTs (molecular mass ≈ 170 kDa for length ≈ 235 nm, diameter ≈ 0.9 nm) were internalized by one cell on average. The high uptake of Col-SWCNTs will facilitate their applications for SWCNT-based drug delivery, DNA transport, biological probing, intracellular imaging and cancer therapy.

It has been reported that CNTs are expelled from cells through exocytosis after internalization over hours or days[25,30]. However, in this study, Col-functionalized SWCNTs were retained in the cells for over a week, suggesting that the Col-SWCNTs were cytocompatible and appropriate for CNT-based cell imaging and cell therapy. The enhanced uptake and prolonged dwell time of Col-SWCNTs in cells should be attributed to the bioactive collagen on the surface of nanotubes.

2.4.4 Intracellular distribution of Col-SWCNTs

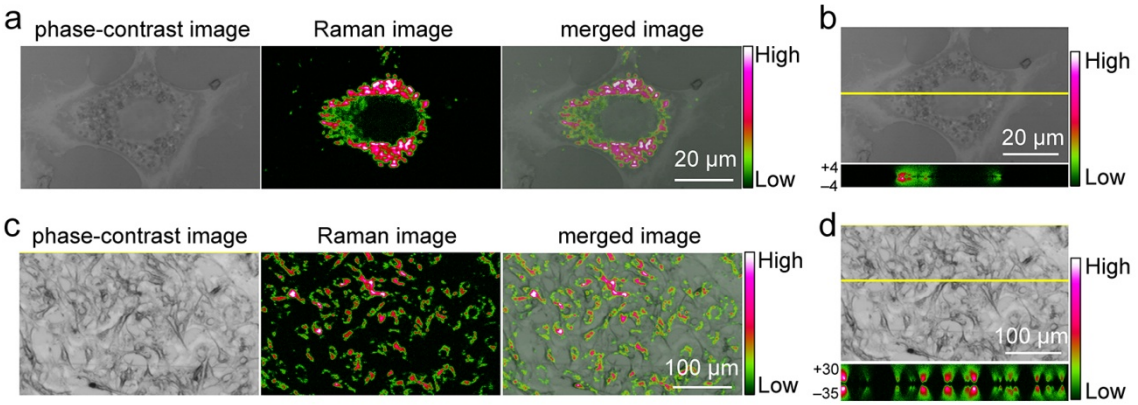

Fig. 2.4 (a) Phase-contrast, Raman and merged micrographs and (b) phase-contrast micrograph and x-z cross section confocal Raman image of a single cell after being cultured with Col-SWCNTs for 3 days. X-z cross section scanning was performed along the yellow line in the phase-contrast micrograph. (c) Phase-contrast, Raman and merged micrographs and (d) phase-contrast micrograph and x-z cross section confocal Raman image of a BAC population after being cultured with Col-SWCNTs for 3 days. The color-coded scale bar represents the G-band intensity of SWCNTs.

To visualize cellular uptake and the intracellular distribution of SWCNTs, confocal Raman imaging was performed. Fig. 2.4a shows the phase-contrast and x-y plane scanning confocal Raman images of a single cell. The phase-contrast image clearly revealed the cellular morphology of BACs, including the cell shape, nucleus position and cell extension. To confirm that the confocal Raman scanning was performed within the cell rather than outside the cell, the measured plane was focused on the nucleus of the cell. The confocal Raman image showed that SWCNTs were primarily located around the nucleus. This result was consistent with previous reports[24,26,29,31] and was supported by the x-z plane scanning confocal Raman imaging performed across the center of nucleus (Fig. 2.4b). By imaging multiple cells (Fig. 2.4c and d), cellular uptake was confirmed within the population of cells and the intensity of SWCNTs was most prevalent in the perinuclear region. Meanwhile, change of SWCNTs distribution in cells with culture time was investigated by observing the cells after being cultured with Col-SWCNTs for 4 hours, 1, 3 and 5 days (Fig. 2.5). The amount of SWCNTs internalized in cells increased with culture time and the intensity of the G-band of SWCNTs showed the highest value at the third day. The result was well consistent with the quantification data of cellular uptake of Col-SWCNTs using UV-vis-NIR as shown in Fig. 2.3.

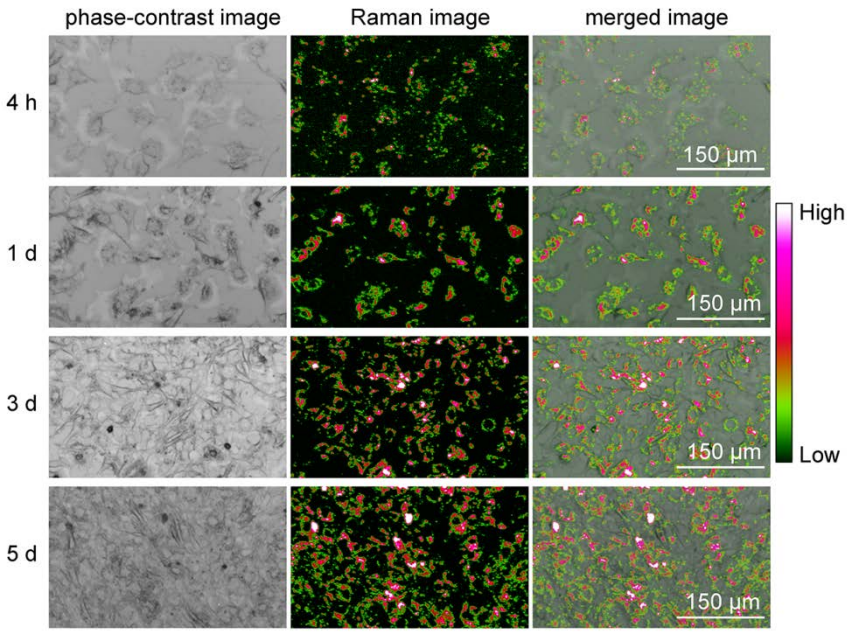

Fig. 2.5 Phase-contrast, Raman and merged micrographs of BACs after being cultured with Col-SWCNTs for different time (4 hours, 1 day, 3 days and 5 days). The color-coded scale bar represents the G-band intensity of SWCNTs.

2.5 Conclusions

In summary, well-dispersed SWCNTs in aqueous solutions were obtained through functionalization of SWCNTs with type I collagen. The inherent properties of SWCNTs were retained after collagen functionalization and the Col-SWCNT suspension solution was stable over 63 days. The Col-SWCNTs showed no obvious negative cellular effects on the BACs in this 2D cell culture system. Cellular uptake of Col-SWCNTs by BACs was confirmed and up to ten million SWCNTs were internalized in one cell on average. The distribution of Col-SWCNTs in the cells was most prevalent in the perinuclear region. Absorption of SWCNTs by the ECM could be an important step during the SWCNT uptake process. The results suggested that SWCNTs functionalized by collagen should be suitable for applications in biomedicine and biotechnology.

2.6 References

1. Liu, Z. *et al.* Drug delivery with carbon nanotubes for in vivo cancer treatment. *Cancer Res.* **68,** 6652–6660 (2008).
2. Liu, Z. *et al.* Carbon materials for drug delivery & cancer therapy. *Mater. Today* **14,** 316–323 (2011).
3. Meng, L., Zhang, X., Lu, Q., Fei, Z. & Dyson, P. J. Single walled carbon nanotubes as drug delivery vehicles: Targeting doxorubicin to tumors. *Biomaterials* **33,** 1689–1698 (2011).
4. Zhang, X., Meng, L., Lu, Q., Fei, Z. & Dyson, P. J. Targeted delivery and controlled release of doxorubicin to cancer cells using modified single wall carbon nanotubes. *Biomaterials* **30,** 6041–6047 (2009).

5. Holt, B. D., McCorry, M. C., Boyer, P. D., Dahl, K. N. & Islam, M. F. Not all protein-mediated single-wall carbon nanotube dispersions are equally bioactive. *Nanoscale* **4,** 7425–7434 (2012).
6. Kam, N. W. S., Liu, Z. & Dai, H. Carbon nanotubes as intracellular transporters for proteins and DNA: an investigation of the uptake mechanism and pathway. *Angew. Chem. Int. Ed.* **45,** 577–581 (2006).
7. Wong, N. *et al.* Nanotube Molecular Transporters : Internalization of Carbon Nanotube-Protein Conjugates into Mammalian Cells. *J. Am. Chem.Soc.* **126,** 6850–6851 (2004).
8. Pantarotto, D. *et al.* Functionalized carbon nanotubes for plasmid DNA gene delivery. *Angew. Chem. Int. Ed.* **43,** 5242–6 (2004).
9. Vehicles, G. D. Cationic Glyco-Functionalized Single-Walled Carbon Nanotubes as Efficient Gene Delivery Vehicles. *Bioconjug. Chem.* **20,** 2017–2022 (2009).
10. Zhou, F. *et al.* Antitumor immunologically modified carbon nanotubes for photothermal therapy. *Biomaterials* **33,** 3235–42 (2012).
11. Wang, L. *et al.* Synergistic anticancer effect of RNAi and photothermal therapy mediated by functionalized single-walled carbon nanotubes. *Biomaterials* **34,** 262–74 (2013).
12. Robinson, J. T. *et al.* High Performance In Vivo Near-IR (1μm) Imaging and Photothermal Cancer Therapy with Carbon Nanotubes. *Nano Res.* **3,** 779–793 (2010).
13. Harrison, B. S. *et al*. Carbon nanotube applications for tissue engineering. *Biomaterials* **28,** 344–53 (2007).
14. Hong, S. Y. *et al.* Filled and glycosylated carbon nanotubes for in vivo radioemitter localization and imaging. *Nat. Mater.* **9,** 485–490 (2010).
15. Bergstrom, D. E. & Cheng, J. X. Label-free imaging of semiconducting and metallic carbon nanotubes in cells and mice using transient absorption microscopy. *Nat. Nanotech.* **7,** 56–61 (2012).
16. Welsher, K., Sherlock, S. P. & Dai, H. Deep-tissue anatomical imaging of mice using carbon nanotube fluorophores in the second near-infrared window. *Proc. Natl. Acad. Sci. USA* **108,** 8943–8948 (2011).
17. Baughman, R. H. *et al*. Carbon nanotubes--the route toward applications. *Science.* **297,** 787–792 (2002).
18. Schnorr, J. M. *et al*. Emerging Applications of Carbon Nanotubes. *Chem. Mater.* **23,** 646–657 (2011).
19. Kostarelos, K., Bianco, A. & Prato, M. Promises, facts and challenges for carbon nanotubes in imaging and therapeutics. *Nat. Nanotech.* **4,** 627–633 (2009).
20. Bachilo, S. M. *et al.* Structure-assigned optical spectra of single-walled carbon nanotubes. *Science (80-.).* **298,** 2361–2366 (2002).
21. Cheng, J. *et al.* Reversible accumulation of PEGylated single-walled carbon nanotubes in the mammalian nucleus. *ACS Nano* **2,** 2085–2094 (2008).
22. Pantarotto, D., Briand, J.-P., Prato, M. & Bianco, A. Translocation of bioactive peptides across cell membranes by carbon nanotubes. *Chem. Commun.* 16–17 (2004).
23. Mu, Q., Broughton, D. L. & Yan, B. Endosomal leakage and nuclear translocation of multiwalled carbon nanotubes: developing a model for cell uptake. *Nano Lett.* **9,** 4370–4375 (2009).
24. Porter, A. E. *et al.* Uptake of noncytotoxic acid-treated single-walled carbon nanotubes into the cytoplasm of human macrophage cells. *ACS Nano* **3,** 1485–1492 (2009).
25. Neves, V. *et al.* Uptake and Release of Double-Walled Carbon Nanotubes by Mammalian Cells. *Adv. Funct. Mater.* **20,** 3272–3279 (2010).

26. Lacerda, L. *et al.* Intracellular Trafficking of Carbon Nanotubes by Confocal Laser Scanning Microscopy. *Adv. Mater.* **19,** 1480–1484 (2007).
27. Becker, M. L. *et al.* Length-Dependent Uptake of DNA-Wrapped Single-Walled Carbon Nanotubes. *Adv. Mater.* **19,** 939–945 (2007).
28. Hong, G. *et al.* Three-dimensional imaging of single nanotube molecule endocytosis on plasmonic substrates. *Nat. Commun.* **3,** 1–9 (2012).
29. Kostarelos, K. *et al.* Cellular uptake of functionalized carbon nanotubes is independent of functional group and cell type. *Nat. Nanotech.* **2,** 108–113 (2007).
30. Kang, B., Chang, S., Dai, Y., Yu, D. & Chen, D. Cell response to carbon nanotubes: size-dependent intracellular uptake mechanism and subcellular fate. *Small* **6,** 2362–2366 (2010).
31. Holt, B. D. *et al.* Quantification of Uptake and Localization of Bovine Serum Albumin-Stabilized Single-Wall Carbon Nanotubes in Different Human Cell Types. *Small* **7,** 2348–2355 (2011).
32. Liu, D., Yi, C., Zhang, D., Zhang, J. & Yang, M. Inhibition of proliferation and differentiation of mesenchymal stem cells by carboxylated carbon nanotubes. *ACS Nano* **4,** 2185–2195 (2010).
33. Cherukuri, P., Bachilo, S. M., Litovsky, S. H. & Weisman, R. B. Near-infrared fluorescence microscopy of single-walled carbon nanotubes in phagocytic cells. *J. Am. Chem.Soc.* **126,** 15638–15639 (2004).
34. Islam, M. F., Rojas, E., Bergey, D. M., Johnson, a. T. & Yodh, a. G. High Weight Fraction Surfactant Solubilization of Single-Wall Carbon Nanotubes in Water. *Nano Lett.* **3,** 269–273 (2003).
35. Nish, A., Hwang, J.-Y., Doig, J. & Nicholas, R. J. Highly selective dispersion of single-walled carbon nanotubes using aromatic polymers. *Nat. Nanotech.* **2,** 640–646 (2007).
36. Tsyboulski, D. A. *et al.* Self-assembling peptide coatings designed for highly luminescent suspension of single-walled carbon nanotubes. *J. Am. Chem.Soc.* **130,** 17134–17140 (2008).
37. Zheng, M. *et al.* DNA-assisted dispersion and separation of carbon nanotubes. *Nat. Mater.* **2,** 338–342 (2003).
38. Hirata, E. *et al.* Multiwalled carbon nanotube-coating of 3D collagen scaffolds for bone tissue engineering. *Carbon N. Y.* **49,** 3284–3291 (2011).
39. Alarcon, E. I. *et al.* The biocompatibility and antibacterial properties of collagen-stabilized, photochemically prepared silver nanoparticles. *Biomaterials* **33,** 4947–56 (2012).
40. Magrez, A. *et al.* Cellular toxicity of carbon-based nanomaterials. *Nano Lett.* **6,** 1121–1125 (2006).
41. Cheng, C. *et al.* Toxicity and imaging of multi-walled carbon nanotubes in human macrophage cells. *Biomaterials* **30,** 4152–4160 (2009).
42. Sachar, S. & Saxena, R. K. Cytotoxic effect of poly-dispersed single walled carbon nanotubes on erythrocytes in vitro and in vivo. *PLoS One* **6,** e22032 (2011).
43. Bianco, A. *et al.* Cationic carbon nanotubes bind to CpG oligodeoxynucleotides and enhance their immunostimulatory properties. *J. Am. Chem.Soc.* **127,** 58–59 (2005).
44. Lu, Q. *et al.* RNA Polymer Translocation with Single-Walled Carbon Nanotubes. *Nano Lett.* **4,** 2473–2477 (2004).
45. Kim, J. A., Åberg, C., Salvati, A. & Dawson, K. A. Role of cell cycle on the cellular uptake and dilution of nanoparticles in a cell population. *Nat. Nanotech.* **7,** 62–68 (2012).

Chapter 3

Investigation of nanomaterials-mediated cell effects using atomic force microscopy

3.1 Summary

Besides the traditional investigation methods, feasible techniques that permit real-time, accurate and effective detection of the subtle changes of cells when they were exposed to nanomaterials are also highly needed. Atomic force microscopy (AFM) has been developed as a powerful tool in the imaging of cells and probing their mechanical properties under physiological conditions. In this part, AFM was employed to investigate the effects of nanomaterials on cells. Two different types of nanomaterials (SWCNTs and Fe-FeO core-shell magnetic nanoparticles) and three types of cells (BACs, hMSCs and HeLa cells) were used. WST-1 assay and live/dead staining showed that the cells had almost the same levels of viability. However, AFM measurement showed that the cells changed their Young's modulus when different types of nanomaterials with different diameters were applied in the cell culture medium for different time. The results indicated that the effects of nanomaterials on the mechanical properties of cells were dependent on nanoparticles size, concentration and cell type as well as exposure time. More importantly, AFM was demonstrated to useful to identify the subtle changes of the mechanical properties of cells when they were exposed to nanomaterials even for very short time.

3.2 Introduction

Because of their small size, large specific surface area and high surface atomic slot insufficiency, nanomaterials exhibit fascinating and novel properties that are often vastly different from their bulk counterparts[1,2]. The unique properties of nanomaterials offer excellent platforms for different applications, including healthcare, electronics, cosmetics, textiles, information technology and environmental protection[3–8]. For biomedical usage, the interaction of nanomaterials with biological systems, especially with cells is the focus of current investigations[9,10]. The success of nanomaterials-based applications in disease diagnosis and

therapy largely depends on whether the designated nanomaterials can be easily internalized by cells[11–13]. However, the internalized nanomaterials may produce some negative effects on cells. For example, when nanomaterials enter the biological system and accumulate within cells, they may disrupt the organelle integrity, alter gene expression and lead to other intracellular changes[14–17]. Therefore, one of the crucial issues regarding nanomaterials-based applications that have to be addressed is to understand how nanomaterials interact with cells and to uncover their potential risks. Meanwhile, feasible techniques are needed to detect the subtle changes of cells when they are exposed to nanomaterials.

Atomic force microscopy (AFM) has been developed as a powerful technique to study the topography and mechanics of materials under both air and liquid conditions[18–26]. Generally, AFM has four major parts of compositions: piezoelectric scanner, cantilever and tip, optical deflection system and electrical feedback system[27,28]. The basic principle of AFM is to sense and record the interaction between the tip and the specimen while the tip is scanning over the surface of the specimen. The tip is fixed to a soft cantilever that will be deflected from a very small force (in the piconewton range, 10^{-12} N) of interaction between the specimen and the tip. The deflection of the cantilever is detected by movement of a laser beam reflected from the tip and digitally transformed to a topographic image or an interaction force file of the specimen. The major advantages of AFM include the ability to perform measurement in aqueous, nonaqueous or dry conditions and the lack of a requirement for any special sample pretreatment. AFM imaging the topography and probing the mechanics of live cells under physiological conditions allows obtaining real information about cells in their natural environment.

In this part, AFM was applied to study the effects of nanomaterials on cells. The mechanical properties of three types of cells (BACs, hMSCs and HeLa cells) exposed to two different types of nanomaterials (SWCNTs and Fe-FeO core-shell magnetic nanoparticles) were measered. The results showed that cells changed their Young's modulus when different types of nanomaterials at different concentrations were applied in the cell culture medium for different time. The effects of nanomaterials on the mechanical properties of cells were dependent on nanoparticles size, concentration and cell type as well as exposure time. More importantly, AFM was demonstrated to be useful to identify the subtle changes of the mechanical properties of cells when they were exposed to nanomaterials even for very short time.

3.3 Materials and methods

3.3.1 Materials

Two different types of nanomaterials (SWCNTs and Fe-FeO core-shell magnetic nanoparticles) were used in this part of study. SWCNTs (purity > 90%, 0.7-1.3 nm in diameter, Sigma-Aldrich, USA) were functionalized with collagen using a simple non-covalent approach to improve the dispersibility in water[29]. Briefly, 1,000 μg SWCNTs were sterilized using ultraviolet light for 2 hours and put in 10 mL 0.1 wt% collagen solution that was prepared by diluting 1.0 wt% collagen aqueous solution (type I collagen in pH = 3.0 acetic acid aqueous solution, Nippon Meat Packers Inc., Japan) with pH = 3.0 acetic acid aqueous solution. The mixture was sonicated (135 W, Bransonic, Japan) in an ice bath for 2 hours. The dispersion

solution was then centrifuged (Tomy MX-301, Japan) at 20,000× g for 30 minutes to remove aggregated and bundled SWCNTs. Finally, the supernatant was collected and underwent an additional centrifugation round. Fe-FeO core-shell magnetic nanoparticles were bought from Boutiq, Wellington, New Zealand in aqueous solution and used as they were.

3.3.2 Cell culture with nanoparticles

Bovine articular chondrocytes (BACs, isolated from the articular cartilage derived from a 9-week old female calf, passage 2), HeLa cells (human cervical cancer, ATCC, Manassas, VA) and human bone marrow-derived mesenchymal stem cells (hMSCs, obtained from Osiris Therapeutics, Columbia, MD, passage 4) were used. The culture medium for BACs and hMSCs was Dulbecco's modified Eagle's medium (DMEM, Sigma, USA) supplemented with 10% fetal bovine serum. The culture medium for HeLa cells was Eagle's Minimum Essential Medium (EMEM, ATCC, Manassas, VA) supplemented with 10% fetal bovine serum.

For WST-1 assay, cells were cultured in 96-well plates (BD Falcon, USA) with culture medium. After 4 hours of pre-culture, culture medium was changed to nanoparticle-containing medium with definite concentrations and cultured at 37 °C in humidified air containing 5% CO_2. At a designated time point, cell culture medium was replaced with 110 μL of WST-1 solution (Roche, Germany, 10 μL of WST-1 stock solution diluted with 100 μL of complete medium) or 110 μL complete medium and the cells were cultured for an additional 3 hours. The absorbance of each well of the 96-well plates was measured at 440 nm using a plate reader (Benchmark Plus, USA). The cells cultured with 110 μL complete medium without supplement of WST-1 were used as nanoparticles sample blank to eliminate the effect of nanoparticles on the absorbance. The cells cultured in normal medium without nanoparticles were used as control. The relative viability of cells exposed to nanoparticles were expressed as percentage of $(OD_{sample} - OD_{blank}) / (OD_{control} - OD_{blank}) \times 100$.

For live/dead staining, cells were cultured in 24-well plates. After 4 hours of pre-culture, culture medium was changed to nanoparticle-containing medium with definite concentrations and cultured at 37 °C in humidified air containing 5% CO_2. At a designated time point, cells were washed with warm PBS three times and stained with a Cellstain Live-Dead Double Staining kit (Sigma-Aldrich, USA) according to the manufacturer's instructions. The live/dead images were observed using an inverted fluorescence microscope (Olympus, Japan).

To investigate the cellular uptake of Fe-FeO core-shell magnetic nanoparticles, cells were cultured in 24-well plates with iron nanoparticle-containing medium for 3 days and stained with an Iron Stain kit (Dojindo, Japan) according to the manufacturer's instructions. The images of the stained cells were observed using an optical microscope microscope (Olympus, Japan).

For AFM measurements, cells were cultured in 60 mm cell culture dishes (BD Falcon, USA). After 4 hours of pre-culture, culture medium was changed to nanoparticle-containing medium with designed concentrations and cultured at 37 °C in humidified air containing 5% CO_2. After cultivation for definite times, cells were washed with warm PBS three times and 1 mL warm culture medium was added in the cell culture dishes for AFM measurements.

3.3.3 AFM measurements

Measurement of the mechanical property of cells was performed using a commercially available MFP-3D-Bio AFM microscope (Asylum Research, Santa Barbara, USA). To control the position of the AFM probe and to locate a cell, an optical microscope was used. Silicon nitride V-shaped cantilever (nominal spring constant, k = 0.06 N/m) with 600 nm-diameter glass ball as a probe (Novascan, Ames, USA) was used. The exact spring constant of the cantilever was measured before every set of experiment using the thermal tuning method[30]. Force distance curves were collected per cells at an indentation velocity of 4 μm per second. The measurement was performed in polystyrene culture Petri dishes filled with DMEM serum medium at room temperature. Determination of the Young's modulus was based on the force curve that reflects the cell stiffness[31]. Force curve experiments were performed at the same loading rate equal to 5 nN and force curves were obtained through a standard approach. Force-volume height imaging (FVH) was performed before stiffness measurement (Fig. 3.1a). The scan size was set to a square from 20 pixel × 20 line to 50 pixel × 50 line (map area of 80 × 80 μm) to collect the force curves. The FVH imaging was recorded at an indentation velocity of 8 μm per second and a maximum applied force 3 nN. The FVH imaging is a powerful technique, which can be used to choose the appropriate area on the cell surface where the force curves will be collected. Regions around cell center were chosen for the measurement. At each chosen region, a grid of 5 × 5 points was created and each point was measured. Therefore, twenty five force distance curves were collected per cell.

3.3.4 Young's modulus determination based on AFM measurements

In AFM measurement, a probing tip indents the cells causing a deflection of the sensitive cantilever. To achieve the mechanical property of cells, calculation is based on the force curve which is obtained by monitoring the cantilever deflection. When the same load force is applied to indent control cells and cells treated with collagen-SWCNTs, the deflections should reflect the elastic property of the cells. In practice, it is important to convert force curves into force-versus-indentation curves by subtraction of two force curves, the one collected on a cell and the other one collected on a hard substrate (glass slide) (Fig. 3.1b). The force-versus-indentation curve describes the mechanical response to the applied load. The relative Young's modulus value can be calculated based on Hertz-Sneddon model[32]. This model is described for configuration of a spherical probe over a flat homogeneous surface. The formula used to describe the relationship between the loading force F and the indentation depth is:

$$F(\delta) = \frac{4}{3} \cdot \sqrt{R} \cdot E_{\text{eff}} \cdot \delta^{3/2}$$

where F is the loading force, R is the radius of the ball (AFM probe), E_{eff} is the reduced Young's modulus and δ is the indentation depth. The reduced Young's modulus is given by:

$$\frac{1}{E_{\text{eff}}} = \left(\frac{1 - \nu_{\text{tip}}^2}{E_{\text{tip}}} + \frac{1 - \nu_{\text{sample}}^2}{E_{\text{sample}}} \right)$$

When Esample << Etip (as is true for living cells), Eeff can be calculated as:

$$E_{\text{eff}} = \frac{E_{\text{sample}}}{1 - \nu^2_{\text{sample}}}$$

where sample and tip are the Poisson ratio. The Poisson ratio of cells is unknown, but for the majority of biological materials it is equal to 0.5[33]. The important factors influencing the Young's modulus values are (i) depth of probe penetration and (ii) appropriate area on the cell surface where the force curves are collected. In this study, the relative Young's modulus was calculated for 200 nm indentation depth. 200 nm was chosen because the Hertz model is valid for small indentations where the substrate does not influence the calculations. In the case of the second factor influencing Young's modulus, force curves were collected only at the topologically highest parts of the cells. By doing so, variability in Young's modulus derived from probing different cellular structures could be minimized. A previous report[34] demonstrates that each cell has at least three areas of different rigidity: area over nucleus, cytoplasm and cell edge. The optimal area on the cell surface for the measurement could be decided from the FVH imaging. This mode imaging combines force measurements with topographic imaging. The force curve was recorded and the sample was also translated in the x–y plane. The FVH image is an array of scanner positions at the points of the maximal deflection of the force curves. An example of Young's modulus distribution is shown in Fig. 3.1c. The final Young's modulus value was determined by fitting the Gaussian function to the histogram created from all the obtained data for each cell population. The center of the distribution corresponded to a mean value of the Young's modulus, and the half width taken at the half height (HWHH) was regarded as a standard deviation (SD).

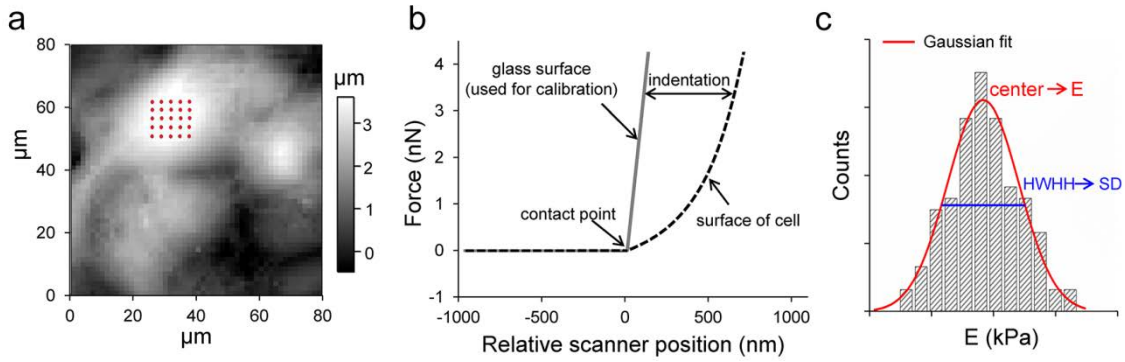

Fig. 3.1 (a) Cell height map obtained in Force Map mode. Inset shows an illustration of the force spectroscopy mode: a grid has been set in the middle of living cell. (b) Representative force curves collected on a hard non-deformable surface of glass coverslip and a soft deformable surface of cell. (c) Representative Young's modulus distributions obtained for cells. The center of the distribution corresponded to a mean value of the Young's modulus, and the half width taken at the half height (HWHH) was regarded as a standard deviation (SD).

3.3.5 Statistical analysis

All data were reported as mean ± standard deviation (SD). One-way analysis of variance was performed to reveal statistical differences followed by Tukey's post hoc test for pairwise comparison. All statistical analyses were executed using Kyplot 2.0 beta 15.

3.4 Results and discussion

3.4.1 Young's modulus of cells versus concentration of SWCNTs

Cell Viability: Fig. 3.2a shows the results of WST-1 assays on the relative viability BACs cultured with Col-SWCNTs at different concentrations for 12, 48 and 96 hours. No obvious difference was observed between the experimental and the control groups even cells were cultured with Col-SWCNTs at a high concentration of ≈ 15 μg/mL over time. This result was well consistent with the results in former part.

Cell Young's Modulus: Fig. 3.2b shows the Young's modulus of BACs cultured with Col-SWCNTs at different concentrations. The Young's modulus of cells cultured in medium without SWCNTs was used as a control. BACs exposed to SWCNTs showed significant higher stiffness than did the control BACs. The average Young's modulus value (E value) of control BACs was 2.04 ± 1.31 kPa. The average E value of BACs exposed to 5, 10 and 20 μg/mL SWCNTs was 3.64 ± 1.73, 3.48 ± 2.35 and 4.56 ± 2.11 kPa, respectively. Although the average E value of BACs treated with 5 and 10 μg/mL SWCNTs was almost the same, it increased after treatment with 20 μg/mL SWCNTs. The results indicated SWCNTs concentration-dependent increase in cell stiffness. The big increase of stiffness of BACs treated with 20 μg/mL Col-SWCNTs might be due to the accumulation of SWCNTs inside the cells. The Col-SWCNTs at a concentration of 5 μg/mL could change the mechanical property of the cells and might avoid excess accumulation. Therefore, concentration of 5 μg/mL of SWCNTs was chosen for the following AFM measurements to investigate the nanomechanical profiles of cells.

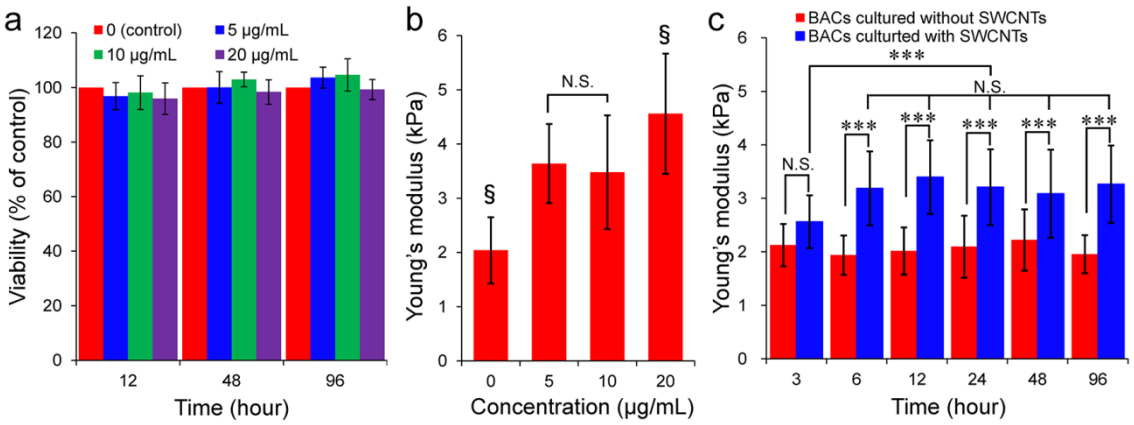

Fig. 3.2 (a) Relative viability of BACs cultured with Col-SWCNTs at different concentrations for 12, 48 and 96 hours through WST-1 assay. The viability of BACs cultured without Col-SWCNTs at each time point was used as a control. (b) Young's modulus of BACs cultured with Col-SWCNTs at different concentrations for 3 days. (c) Young's modulus of BACs cultured without or with Col-SWCNTs at a concentration of 5 μg/mL for different time. §, significant difference compared to all other groups, $P < 0.001$. ***, significant difference, $P < 0.001$. *, significant difference, $P < 0.05$. N.S., no significant difference.

3.4.2 Young's modulus of cells versus cultivation time with SWCNTs

Fig. 3.2c shows the Young's modulus of the cells after being cultured without or with SWCNTs (5

μg/mL) for 0, 3, 6, 12, 24, 48 and 96 hours. The Young's modulus of cells cultured with SWCNTs was higher than that of cells cultured without SWCNTs. The difference was not significant after cells cultured for 3 hours. However the difference increased and became significant after cells cultured for more than 6 hours. When cells were cultured without SWCNTs, there was some difference among the different culture time, while the difference was not significant. When cells were cultured with SWCNTs, the Young's modulus increased with culture time until 6 hours. After 6 hours, the change was not significant. These results indicated that the internalized SWCNTs had some effect on cellular mechanical property. Cells became stiffer after exposed to SWCNTs. And the changes became significant when cultivation time increased. One of the reasons is the amount of internalized SWCNTs. For short time period exposed to SWCNTs the amount of internalized SWCNTs was small and did not induce significant change. After culture for longer period, more SWCNTs were internalized by the cells and the influence of SWCNTs was also accumulated. Another reason may be due to the lag of cell response to SWCNTs which should be further studied in the future work. More importantly, through the traditional investigation methods, such as WST-1 assay and live/dead staining, no significant difference was detected (Fig. 3.2a, Fig. 2.2a and b in Chapter 2) even cells were cultured with SWCNTs at higher concentration and for longer time. But AFM was able to identify the subtle changes of the mechanical properties of cells when they were exposed to SWCNTs even for very short time, suggesting AFM could be a useful tool to investigate cellular effects of nanomaterials.

3.4.3 Young's modulus of cells versus cell type

Cell Viability: The viability of cells was measured after the BACs, hMSCs and HeLa cells were cultured with SWCNT at a concentration of 20 μg/mL for 3 days. Fig. 3.3a shows that exposure to Col-SWCNTs at a concentration of 20 g/mL did not have any significant effect on cell viability, compared to the cells culture without SWCNTs.

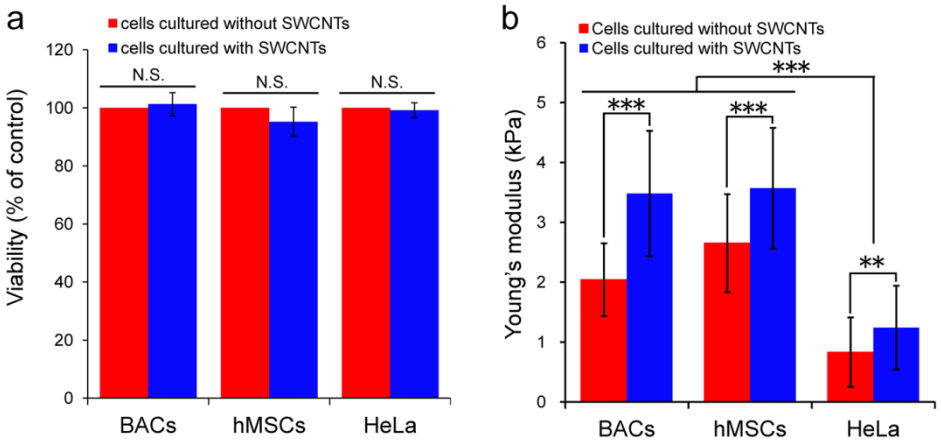

Fig. 3.3 (a) Relative viability of BACs, hMSCs and HeLa cells cultured with Col-SWCNTs at a concentration of 20 μg/mL for 3 days through WST-1 assay. The viability of cells cultured without Col-SWCNTs was used as a control. (b) Young's modulus of BACs, hMSCs and HeLa cells cultured without or with Col-SWCNTs at a concentration of 20 μg/mL for 3 days. ***, significant difference, $P < 0.001$. **, significant difference, $P < 0.01$. N.S., no significant difference.

Cell Young's Modulus: Fig. 3.3b shows histograms with distinct character of Young's modulus of cells treated with or without SWCNTs. The smallest change of Young's modulus value between treatment with or without SWCNTs was observed for hMSCs. It is important to note that the cancer cells are softer compared to the other, as reported in the literature[35]. The Young's modulus of HeLa cells in this study was lower than that of BACs and hMSC and, which was in agreement with the previous report. The difference between E value of HeLa cells treated with or without Col-SWCNTs was also significant ($P < 0.01$). Mechanical property reflects the organization of cell cytoskeleton, in particular the actin cytoskeleton. Our results showed that the three different cell types showed different mechanical property when being exposed to SWCNTs although their viabilities were not affected by SWCNTs. The change of mechanical property was significant before and after the treatment with Col-SWCNTs. Although the change level was dependent on the cell type, stem cells, normal cells and cancer cells showed similar variation. The results conformed that observation by AFM may be a useful tool to investigate cellular effect of nanomaterials in addition to the conventional analysis and this method does not dependent on the types of cell.

3.4.4 Young's modulus of cells exposed to Fe-FeO core-shell magnetic nanoparticles

Cellular Uptake: Fig. 3.4 shows the results of iron staining of BACs cultured with Fe-FeO core-shell nanoparticles at different concentrations for 3 days. Iron nanoparticles were stained to blue, nuclei were stained to red (Pararosaniline stain) while cytoplasm was stained to pink. The blue staining indicates that nanoparticles were internalized into the cells and the increased blue staining suggested that the amount of the internalized nanoparticles increased with the increasing of the concentration of nanoparticles.

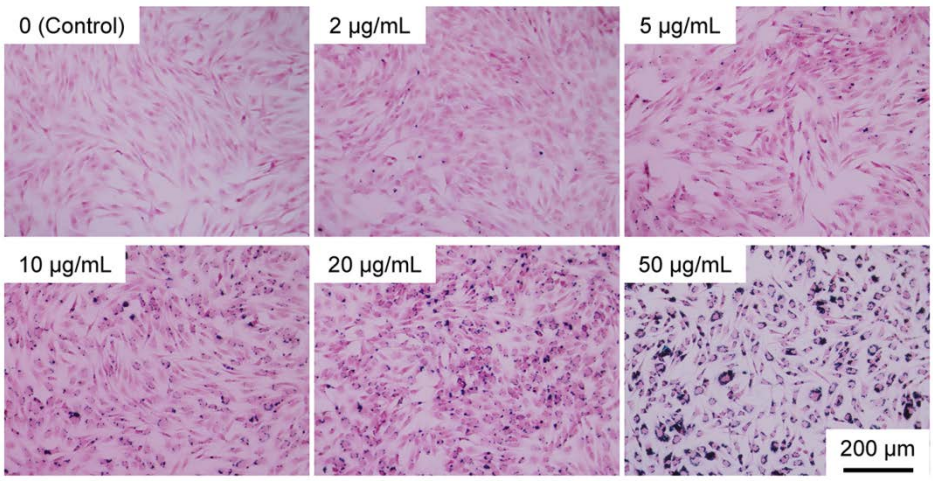

Fig. 3.4 Optical microscopy images of BACs stained for Fe, with the blue stains showing positive detection of Fe in cells treated with Fe-FeO core-shell nanoparticles at different concentrations.

Cell Viability: The results of WST-1 assays on the relative viability BACs cultured with Fe-FeO core-shell nanoparticles at different concentrations are shown in Fig. 3.5a. No obvious difference was observed between the experimental and the control groups. Fig. 3.5b shows the live/dead double staining results. Live cells were stained green while dead cells were stained red. Few or no red-stained cells were detected. These results indicated that Fe-FeO core-shell nanoparticles did not affect the viability of BACs, or

the influences were too weak to be detected by the traditional methods, even the cells were cultured with the nanoparticles at very high concentration.

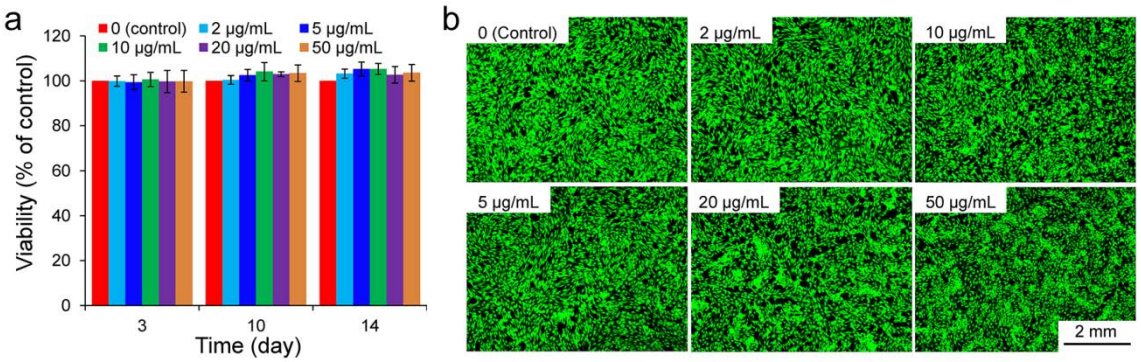

Fig. 3.5 (a) Relative viability of BACs cultured with Fe-FeO core-shell nanoparticles at different concentrations for 3, 10 and 14 days through WST-1 assay. The viability of BACs cultured without Fe-FeO core-shell nanoparticles at each time point was used as a control. (b) Live/dead double staining of BACs cultured with Fe-FeO core-shell nanoparticles at different concentrations for 3 days.

Cell Young's Modulus: Fig. 3.6 shows the Young's modulus of BACs cultured with Fe-FeO core-shell nanoparticles at different concentrations. The Young's modulus of cells cultured in medium without iron nanoparticles was used as a control. BACs exposed to iron nanoparticles showed higher stiffness than did the control BACs, even though there was no significant difference between the cells cultured with 5 μg/mL iron nanoparticles and that of the cells cultured without iron nanoparticles. Young's modulus of BACs increased with the increasing of the concentration of iron nanoparticles. The results indicated that cell stiffness increase dependent on the concentration of iron nanoparticles. The increase of stiffness of BACs can be explained by the accumulation of nanoparticles inside the cells as shown in Fig. 3.4. Through the traditional investigation methods, such as WST-1 assay and live/dead staining, no significant difference was detected (Fig. 3.5) when the cells were cultured with iron nanoparticles. AFM was able to identify the changes of the mechanical properties of cells even the concentration of iron nanoparticles was low. These results further conformed that observation by AFM may be a useful tool to investigate cellular effect of nanomaterials in addition to the conventional analysis and this method does not dependent on the types of nanoparticles.

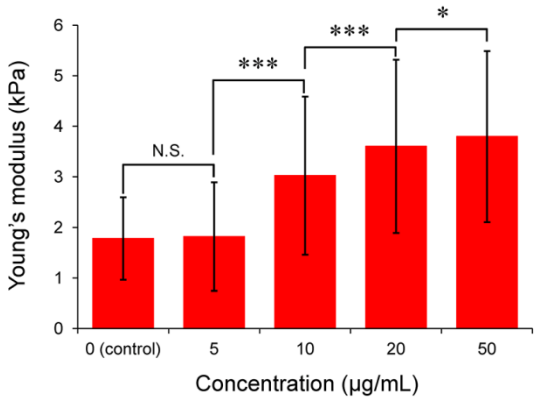

Fig. 3.6 Young's modulus of BACs cultured with Fe-FeO core-shell nanoparticles at different concentrations for 3 days. ***, significant difference, $P < 0.001$. *, significant difference, $P < 0.05$. N.S., no significant difference.

3.5 Conclusions

In summary, AFM was employed to investigate the effects of nanomaterials on cells. The cells showed almost the same levels of viability through WST-1 assay and live/dead staining. However, AFM was able to identify the subtle changes of the mechanical properties of cells when they were exposed to different types of nanomaterials at different concentrations for different time. The effects of nanomaterials on the mechanical properties of cells were dependent on nanoparticles size, concentration and cell type as well as exposure time. More importantly, AFM was demonstrated to be useful to investigate cellular effects of nanomaterials.

3.6 References

1. Buzea, C., Pacheco, I. I. & Robbie, K. Nanomaterials and nanoparticles: Sources and toxicity. *Biointerphases* **2,** 17–71 (2007).
2. Roduner, E. Size matters: why nanomaterials are different. *Chem. Soc. Rev.* **35,** 583–92 (2006).
3. Zhang, L. & Webster, T. J. Nanotechnology and nanomaterials: Promises for improved tissue regeneration. *Nano Today* **4,** 66–80 (2009).
4. Bruce, P. G., Scrosati, B. & Tarascon, J.-M. Nanomaterials for rechargeable lithium batteries. *Angew. Chem. Int. Ed. Engl.* **47,** 2930–46 (2008).
5. Mauter, M. & Elimelech, M. Environmental applications of carbon-based nanomaterials. *Environ. Sci. Technol.* **42,** 5843–5859 (2008).
6. Savage, N. & Diallo, M. S. Nanomaterials and Water Purification: Opportunities and Challenges. *J. Nanoparticle Res.* **7,** 331–342 (2005).
7. Lei, J. & Ju, H. Signal amplification using functional nanomaterials for biosensing. *Chem. Soc. Rev.* **41,** 2122–34 (2012).
8. Barreto, J. A. *et al.* Nanomaterials: applications in cancer imaging and therapy. *Adv. Mater.* **23,** H18–40 (2011).
9. Zhao, J. & Castranova, V. Toxicology of nanomaterials used in nanomedicine. *J. Toxicol. Environ. Health. B. Crit. Rev.* **14,** 593–632 (2011).
10. Sharifi, S., Behzadi,S., Laurent, S., Forrest, M. L., Stroevee, P. & Mahmoudi, M. Toxicity of nanomaterials. *Chem. Soc. Rev.* **41,** 2323–43 (2012).
11. Mao, H., Cai, R., Kawazoe, N. & Chen, G. Long-term stem cell labeling by collagen-functionalized single-walled carbon nanotubes. *Nanoscale* **6,** 1552–1559 (2013).
12. Zhao, F. *et al.* Cellular uptake, intracellular trafficking, and cytotoxicity of nanomaterials. *Small* **7,** 1322–37 (2011).
13. Stefanick, J., Ashley, J. & Bilgicer, B. Enhanced Cellular Uptake of Peptide-Targeted Nanoparticles through Increased Peptide Hydrophilicity and Optimized Ethylene Glycol Peptide-Linker Length. *ACS Nano* **7,** 8115–8127 (2013).

14. Holt, B. D. *et al.* Carbon nanotubes reorganize actin structures in cells and *ex vivo*. *ACS Nano* **4,** 4872–8 (2010).
15. Kaiser, J.-P., Wick, P., Manser, P., Spohn, P. & Bruinink, A. Single walled carbon nanotubes (SWCNT) affect cell physiology and cell architecture. *J. Mater. Sci. Mater. Med.* **19,** 1523–7 (2008).
16. Liu, D., Yi, C., Zhang, D., Zhang, J. & Yang, M. Inhibition of proliferation and differentiation of mesenchymal stem cells by carboxylated carbon nanotubes. *ACS Nano* **4,** 2185–2195 (2010).
17. Yi, C., Liu, D., Fong, C.-C., Zhang, J. & Yang, M. Gold nanoparticles promote osteogenic differentiation of mesenchymal stem cells through p38 MAPK pathway. *ACS Nano* **4,** 6439–48 (2010).
18. Lekka, M. Atomic force microscopy: A tip for diagnosing cancer. *Nat. Nanotechnol.* **7,** 691–692 (2012).
19. Gavara, N. & Chadwick, R. S. Determination of the elastic moduli of thin samples and adherent cells using conical atomic force microscope tips. *Nat. Nanotechnol.* **7,** 733–736 (2012).
20. Wozniak, M. J., Kawazoe, N., Tateishi, T. & Chen, G. Monitoring of mechanical properties of serially passaged bovine articular chondrocytes by atomic force microscopy. *Micron* 40, 870–5 (2009).
21. Raman, A., S., Trigueros, Cartagena, A., Stevenson, A. P. Z., Susilo1, M., Nauman1, E. & Contera, S. A. Mapping nanomechanical properties of live cells using multi-harmonic atomic force microscopy. *Nat. Nanotech.* **6,** 809–814 (2011).
22. Banquy, X. *et al.* Effect of mechanical properties of hydrogel nanoparticles on macrophage cell uptake. *Soft Matter* .5, 3984 (2009).
23. Dorobantu, L. S., Goss, G. G. & Burrell, R. E. Atomic force microscopy: a nanoscopic view of microbial cell surfaces. *Micron* 43, 1312–22 (2012).
24. Kelly, G. M. *et al.* Bone cell elasticity and morphology changes during the cell cycle. *J. Biomech.* 44, 1484–90 (2011).
25. Kuznetsova, T. G., Starodubtseva, M. N., Yegorenkov, N. I., Chizhik, S. a & Zhdanov, R. I. Atomic force microscopy probing of cell elasticity. *Micron* 38, 824–33 (2007).
26. Shi, X. *et al.* Elasticity of cardiac cells on the polymer substrates with different stiffness: an atomic force microscopy study. *Phys. Chem. Chem. Phys.* 13, 7540–5 (2011).
27. Binnig, G., Quate, C. & Gerber, C. Atomic force microscope. *Phys. Rev. Lett.* **56,** 930–933 (1986).
28. Giessibl, F. Advances in atomic force microscopy. *Rev. Mod. Phys.* **75,** 949–983 (2003).
29. Mao, H., Kawazoe, N. & Chen, G. Uptake and intracellular distribution of collagen-functionalized single-walled carbon nanotubes. *Biomaterials* **34,** 2472–2479 (2013).
30. Ohler, B. Cantilever spring constant calibration using laser Doppler vibrometry. *Rev. Sci. Instrum.* **78,** 063701 (2007).
31. Weisenhorn, A. L., Khorsandi, M., Kasas, S., Gotzos, V. & Butt, H.-J. Deformation and height anomaly of soft surfaces studied with an AFM. *Nanotechnology* **4,** 106 (1993).
32. Sneddon, I. The relation between load and penetration in the axisymmetric Boussinesq problem for a punch of arbitrary profile. *Int. J. Eng. Sci.* **3,** 47–57 (1965).
33. Radmacher, M. Measuring the Elastic Properties of Living Cells by the Atomic Force Microscope. *Methods Cell Biol.* **68,** 67–90 (2002).

34. Berdyyeva, T. K., Woodworth, C. D. & Sokolov, I. Human epithelial cells increase their rigidity with ageing *in vitro* : direct measurements. *Phys. Med. Biol.* **50,** 81 (2005).
35. Cross, S. E., Jin, Y.-S., Rao, J. & Gimzewski, J. K. Nanomechanical analysis of cells from cancer patients. *Nat. Nanotechnol.* **2,** 780–3 (2007).

Chapter 4

SWCNTs-based long-term stem cell labeling and imaging

4.1 Summary

The monitoring of grafted stem cells is crucial to assess the efficiency, effectiveness and safety of such stem cell-based therapies. In this regards, a reliable and cytocompatible labeling method for stem cells is critically needed. In this part, the collagen-functionalized single-walled carbon nanotubes (Col-SWCNTs) were used as an imaging probe for labeling of human mesenchymal stem cells (hMSCs) and the inherent Raman scattering of SWCNTs was used to image the SWCNT-labeled cells. The results showed that the Col-SWCNTs exhibit efficient cellular internalization by hMSCs without affecting their proliferation and differentiation. The prolonged dwell time of Col-SWCNTs in cells ensured the long-term labeling up to 2 weeks. This work reveals the potential of Col-SWCNTs as a probe for long-term stem cell labeling.

4.2 Introduction

Stem cells have shown great potential in the field of regenerative medicine because of their capacity to self-renew and differentiate into multiple cell lineages, and stem cell implantation has been considered as a promising therapeutic strategy for various diseases and defects[1-3]. A critical aspect of stem cell-based therapies is to distinguish the implanted cells from the host cells and to monitor them in terms of their viability, migration, distribution and the relative contributions from the delivered cells versus host cells[4-6]. With this respect, a long-term and non-invasive *ex vivo* labeling method for stem cells is critically needed.

Genetically encoded luciferase and fluorescent proteins such as green fluorescent protein (GFP) are commonly used for stem cell labeling and tracking[7-9]. They can be produced via the expression of the transduced reporter genes in live cells and will be passed on to progeny cells for cell tracking in a relatively long period of time. However, this method requires complicated genetic modification of the stem cells and is hard to avoid the overlap with the autofluorescence signals. A variety of exogenous contrast agents have also been widely used for labeling and tracking of stem cells, such as radio active isotopes, magnetic

nanoparticles, organic fluorophores and inorganic quantum dots (QDs)[4,10-13]. These exogenous contrast agents are easy to use and are capable of labeling cells in culture for short time. However, some of these fluorophores show high cytotoxicity and may suffer from photobleaching and fluorescence losing and therefore are not typically used to label cells for long time.

On the other hand, carbon nanotubes (CNTs), especially single-walled carbon nanotubes (SWCNTs) have been extensively explored for biological and medical applications motivated by a consequence of their unique physical and chemical properties[14-19]. One of the most attractive advantages of SWCNTs is that they can penetrate the biological barriers and be internalized by cells effectively in an energy dependent or independent manner[20-22]. In previous part, SWCNTs functionalized with collagen (Col-SWCNTs) showed excellent internalization ability into bovine articular chondrocytes (up to ten million SWCNTs were internalized in one cell on average) without showing obvious negative cellular effects[23]. The internalized Col-SWCNTs were distributed in the perinuclear region and retained in the cells for more than one week. Meanwhile, as a kind of quasi one-dimensional (1D) nanomaterials, SWCNTs exhibit various unique optical properties which are helpful in biomedical labeling and imaging[24-27]. SWCNTs have sharp electronic density of states at the van Hove singularities, resulting in strong and distinctive resonance Raman scattering that includes the radial breathing mode (RBM) and tangential mode (G-band). These peaks are sharp and strong and can be easily distinguished from fluorescence backgrounds, which are suitable for optical imaging. Another important advantage of SWCNTs as fluorophores is the lack of photobleaching without any noticeable decay or loss of photoluminescence intensity even under extended laser excitation[28]. All of these features make SWCNTs suitable for stem cells labeling and imaging.

In this part, collagen-functionalized SWCNTs (Col-SWCNTs) were used as a probe to label and image human mesenchymal stem cells (hMSCs). Internalization of Col-SWCNTs into hMSCs was conformed. The viability and differentiation capacity of the labeled hMSCs were investigated via WST-1 assay and osteogenic and adipogenic differentiation-induction experiments, respectively. The cells could be detected by Raman microscope easily even after 2 weeks of culture post labeling, revealing the Col-SWCNTs should be an useful probe for long-term stem cells labeling.

4.3 Materials and methods

4.3.1 Preparation and characterization of Col-SWCNTs

SWCNTs (purity > 90%, Sigma-Aldrich, USA) were functionalized with collagen as mentioned in previous part to improve the dispersibility in water. Briefly, 1 mg SWCNTs were put in 10 mL 0.1 wt% collagen (type I, Nippon Meat Packers Inc., Japan) solution after being sterilized using ultraviolet light for 2 hours. The mixture was sonicated (135 W, Bransonic, Japan) in an ice bath for 2 hours. The dispersion solution was then centrifuged (Tomy MX-301, Japan) at 20,000× g for 30 minutes twice to remove aggregated and bundled SWCNTs. The supernatant was collected and mixed with normal cell culture medium to prepare the SWCNTs-containing cell culture medium. The Col-SWCNTs could be well dispersed in cell culture medium and the final concentrations of Col-SWCNTs in the dispersions were determined via

concentration-dependent ultraviolet visible near-infrared (UV-vis-NIR) spectroscopy (V-7200, JASCO, Japan).

4.3.2 Cell culture and labeling with Col-SWCNTs

Human bone marrow-derived mesenchymal stem cells (hMSCs) were obtained from LONZA (Walkersvile, MD) at passage 2 (P2). The cells were cultured in 75 cm^2 tissue culture flasks (BD Falcon, USA) with normal cell culture medium at 37 °C in humidified air containing 5% CO_2. The normal cell culture medium was Dulbecco's modified Eagle's medium (DMEM, Sigma, USA) supplemented with 10% fetal bovine serum, 4,500 mg/L glucose, 4 mM glutamine, 100 U/mL penicillin, 100 μg/mL streptomycin, 0.1 mM nonessential amino acids, 0.4 mM proline, 1 mM sodium pyruvate and 50 μg/mL ascorbic acid. The cells were subcultured once after reaching confluence and used at passage 4. To label the hMSCs, P4 cells were seeded into 60 mm cell culture dish (BD Falcon, USA) at a density of 5,000 cells/cm^2. The cell culture medium was changed to DMEM containing Col-SWCNTs at a concentration of 5 μg/mL after 4 hours of pre-culture. After being cultured for an additional 48 hours, the cells were washed with warm PBS, collected by treatment with trypsin/EDTA solution and seeded in 4-chamber culture slides with normal DMEM for 4 hours. Then the cells were washed with warm PBS and fixed with 4% paraformaldehyde solution for 15 minutes. After that, the samples were washed with PBS and the slides were mounted and hermetically sealed using nail lacquer. The labeling efficiency of hMSCs was then observed by a confocal Raman microscope. A phase-contrast image of the cells was focused, revealing cellular morphologies including the nuclei and extensions. And then, a horizontal confocal Raman image (x-y imaging mode) was acquired to investigate SWCNTs signals in the cells. The confocal Raman spectra from 779.7 to 1970.0 cm^{-1} were collected and the G-band, indicative of SWCNTs, was used to map the distribution of SWCNTs. Control of imaging parameters and processing and data analysis were performed in a Raman Data Viewer software (Nanophoton, Japan). Meanwhile, to determine the amount of Col-SWCNTs internalized in hMSCs, the cells after being exposed to Col-SWCTs for 12, 24 and 48 hours were collected by trypsin/EDTA treatment. The cells were then washed with PBS through two rounds of washing-centrifugation and ruptured via a papain (Sigma, USA) buffer solution. The amount of SWCNTs in the papain buffer solution was measured using UV-vis-NIR spectroscopy and considered to be the amount of SWCNTs internalized in cells. Before being ruptured, the cells were counted with a hemacytometer. To investigate the detection efficiency of the labeled hMSCs by Raman imaging, the labeled hMSCs were co-cultured with unlabeled hMSCs at different ratios (labeled:unlabeled = 1:1, 1:50, 1:100, 0:100). After 4 hours preculture, the samples were washed with PBS, fixed with 4% paraformaldehyde solution for 15 minutes and observed under a confocal Raman microscope.

4.3.3 Viability of the labeled hMSCs

The viability of labeled hMSCs was evaluated by WST-1 assay. Briefly, the labeled hMSCs were cultured in 96-well plates with normal cell culture medium for a designated period of time. At each time point, the medium was replaced with 110 μL of WST-1 solution (Roche, Germany, 10 μL of WST-1 stock solution diluted with 100 μL of complete medium) and the cells were cultured for an additional 3 hours. The absorbance of each well of the 96-well plates was measured at 440 nm using a plate reader (Benchmark Plus,

USA). The cells cultured with 110 μL normal medium without supplement of WST-1 were used as SWCNTs sample blank to eliminate the effect of SWCNTs on the absorbance. Cells without labeling were used as a control. The relative viability of labeled hMSCs were expressed as percentage of $(OD_{sample} - OD_{sample\ blank}) / (OD_{control} - OD_{control\ blank}) \times 100$. Live/dead staining with a Cellstain Live-Dead Double Staining kit (Dojindo, Japan) was also used to confirm live and dead cells after cell culture. The staining was conducted according to the manufacturer's instructions. Briefly, after being cultured in 24-well plates for 1 day, 2 and 3 weeks, the cells were washed with warm PBS three times and incubated in 2 mM calcein-AM and 4 mM propidium iodide (PI) in PBS for 15 minutes. The live/dead images were observed using an inverted fluorescence microscope (Olympus, Japan).

4.3.4 Differentiation capacity of the labeled hMSCs

The labeled and unlabeled hMSCs were seeded into 24-well plates at a density of 5,000 cells/cm^2 with normal cell culture medium. After 4 hours, the normal medium was replaced with osteogenic or adipogenic differentiation medium. The osteogenic differentiation medium consisted of DMEM supplemented with 1000 mg/L glucose, 584 mg/L glutamine, 100 U/mL penicillin, 100 μg/mL streptomycin, 0.1 mM nonessential amino acids, 50 mg/L ascorbic acid, 10% FBS, 10 nM dexamethasone, and 10 mM β-glycerophosphate. The adipogenic differentiation medium consisted of DMEM supplemented with 4500 mg/L glucose, 584 mg/L glutamine, 100 U/mL penicillin, 100 μg/mL streptomycin, 0.1 mM nonessential amino acids, 0.4 mM proline, 50 mg/L ascorbic acid, 10% FBS, 1 μM dexamethasone, 0.5 mM methylisobutylxanthine, 10 μg/mL insulin, and 100 μM indomethacin.

Alkaline phosphatase (ALP) staining was carried out after incubation in osteogenic differentiation medium for 1 and 3 weeks. The cells were washed with warm PBS twice and fixed with 4% paraformaldehyde for 10 minutes at room temperature. The fixed cells were washed with PBS three times and incubated with 0.1% naphthol AS-MX phosphate (Sigma, USA) and 0.1% fast blue RR salt (Sigma, USA) in 56 mM 2-amino-2-methyl-1,3-propanediol (pH 9.9, Sigma, USA) working solution at room temperature for 10 minutes, washed with PBS twice and observed by an optical microscope (Olympus, Japan). Differentiation percentage was evaluated by quantification of ALP stained areas. The stained images were analyzed by an automated image analysis software and the stained areas were converted to a percentage of the total area of cells.

Alizarin Red S staining was carried out after the labeled and unlabeled hMSCs were cultured with osteogenic medium for 3 weeks. The cells were washed with warm PBS twice, followed by fixation with 4% paraformaldehyde for 10 minutes at room temperature. After that, the cells were incubated with 0.5% Alizarin Red S (Sigma, USA) solution at room temperature for 10 minutes, washed twice with PBS and observed by an optical microscope. The percentage of Alizarin Red S positively stained areas were quantified by analyzing the images with an automated image analysis software as mentioned above.

Oil Red O staining was performed after the labeled and unlabeled hMSCs were cultured with adipogenic medium for 1 and 3 weeks. The cells were washed with warm PBS three times, fixed with with 4% paraformaldehyde for 10 minutes at room temperature. After treating with 60% 2-propanol for 5 minutes, the cells were treated with Oil Red O staining solution for 5 minutes. The Oil Red O staining solution was

prepared by mixing the stocking solution (0.3 g/mL, Sigma, USA) with MilliQ water at a volume ratio of 3:2 and filtering with a 0.2 μm filter. The stained cells were washed with 60% 2-propanol once and PBS three times to remove the background. The photo micrographs of the stained cells were captured by an optical microscope. Adipogenesis percentage was evaluated by quantification of Oil Red O stained areas using an automated image analysis software as mentioned above.

4.3.5 Long-term stem cell labeling capacity of Col-SWCNTs

To study the long-term stem cell labeling capacity and investigate whether the internalized Col-SWNTs were released from the labeled hMSCs and internalized by the nearby unlabeled hMSCs, a homemade inverse co-culture system was used. At first, the unlabeled hMSCs were seeded in a 60 mm cell culture dish (BD Falcon, USA). The Col-SWCNTs labeled hMSCs were seeded in a dish plate that was cut from the bottom part of a 35 mm cell culture dish (BD Falcon, USA). After 4 hours culture, the labeled hMSCs attached on the surface of the dish plate. Subsequently, the dish plate with labeled hMSCs was turned over and put in the 60 mm cell culture dish with unlabeled hMSCs. The labeled hMSCs at the upper side and unlabeled hMSCs at the down side were co-cultured in the same culture system with normal cell culture medium for different time. At each designated time point (1, 3, 7, 10 and 14 days), both the labeled and unlabeled cells were collected by trypsin/EDTA treatment and re-seeded in 4-chamber culture slides separately. After being cultured for 4 hours, the cells were washed with warm PBS, fixed with 4% paraformaldehyde solution and observed by a confocal Raman microscope. Meanwhile, to determine the amount of SWCNTs in the labeled hMSCs at different time point after co-culture, the cells were collected by trypsin/EDTA treatment, washed with PBS through two rounds of washing-centrifugation and ruptured via a papain buffer solution. The amount of SWCNTs in the papain buffer solution was measured using UV-vis-NIR spectroscopy and considered to be the amount of SWCNTs in the labeled cells. Before being ruptured, the cells were counted with a hemacytometer.

4.3.6 Statistical analysis

All data were reported as mean ± standard deviation (SD). A one-way analysis of variance (ANOVA) with Tukey's post hoc test for multiple comparisons was used for statistical analysis. A value of $P < 0.05$ was considered to be a statistically significant difference.

4.4 Results and discussion

4.4.1 Stem cells labeling and detection efficiency with Col-SWCNTs

A key premise for extraneous agents based cell labeling is that the agents can be efficiently internalized by the cells. It has been reported that functionalization of SWCNTs with some biocompatible molecules, such as BSA, DNA and peptides on their surfaces may induce and facilitate receptor-mediated endocytosis of nanotubes[29-31]. We have found that the Col-SWCNTs showed enhanced cellular uptake by bovine articular chondrocytes in previous part. Fig. 4.1a shows a photo of the labeled and unlabeled hMSCs pellets after

centrifugation. The labeled cells showed black color due to the color of the carbon nanotubes. Fig. 4.1b shows the amount of SWCNTs internalized by hMSCs, which was divided by the number of cells. The average amount of internalized SWCNTs in each cell was 2.17 ± 0.34 pg after the cells were cultured with Col-SWCNTs for 48 hours. In other words, the average number of internalized SWCNTs in each cell was $7.68 \pm 1.20 \times 10^6$. A high amount of Col-SWCNTs were internalized by cells, which should suffice to label and image the hMSCs efficiently. The internalized Col-SWCNTs were further confirmed by confocal Raman imaging (Fig. 4.1c, d and e). The morphology of hMSC including the cell shape, nucleus position and cell extension was revealed through the phase-contrast image and the measured plane was focused on the nucleus of the cell. The labeled hMSC showed strong Raman signals around the nucleus, suggesting the internalized Col-SWCNTs were primarily located around the nucleus. This result was well consistent with previous reports[30-33] and further conformed by the vertical scanning Raman imaging performed across the centre of nucleus (Fig. 4.1d). By imaging multiple cells (Fig. 4.1e), cellular labeling was confirmed within the population of cells. The three spectra in Fig. 1f corresponded to different positions in or out the cell on the mapping area. Absence of the indicative G-band Raman peak of SWCNTs at 1590 cm^{-1} in Raman spectrum, which was obtained from the position out the cell (no cell region) revealed no SWCNTs were detected at the outside of cells.

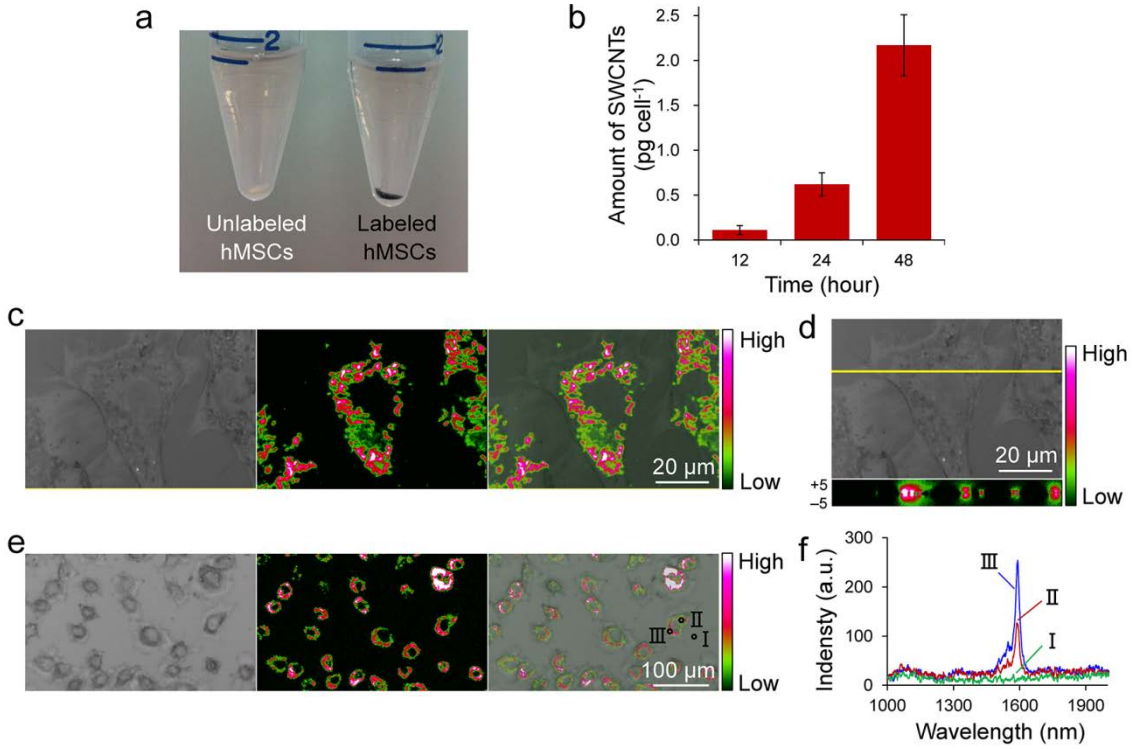

Fig. 4.1 (a) A photo of the labeled and unlabeled hMSCs pellets. (b) Quantification of the internalized Col-SWCNTs in hMSCs after different culture time. (c) Phase-contrast, confocal Raman and merged micrographs and (d) phase-contrast micrograph and x-z cross section confocal Raman image of a single hMSC labeled by Col-SWCNTs. The x-z cross section scanning was performed along the yellow line in the phase-contrast micrograph. The color-coded scale bar represents the G-band intensity of SWCNTs. (e) Phase-contrast, confocal Raman and merged micrographs of a hMSC population labeled by Col-SWCNTs. (f) Raman spectra (G-band) performed at position (I) outside the cell boundary and positions (II and III) within the cell as shown in Fig. 1e.

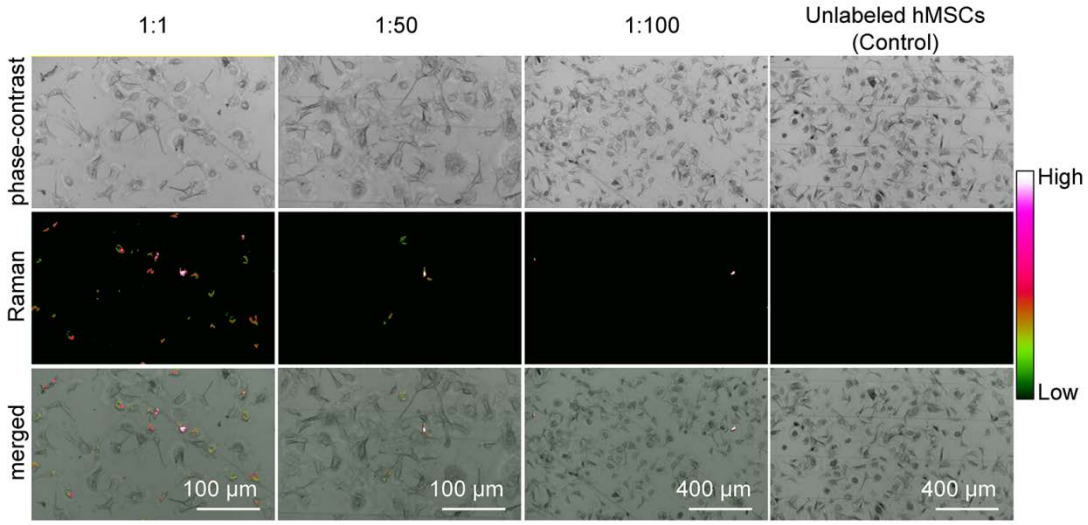

Fig. 4.2 Phase-contrast, confocal Raman and merged micrographs of the labeled hMSCs after being cultured with unlabeled hMSCs at different ratios (labeled:unlabeled = 1:1, 1:50, 1:100, 0:100). The color-coded scale bar represents the G-band intensity of SWCNTs.

Fig. 4.2 shows the detection efficiency of the labeled hMSCs from the unlabeled hMSCs by using confocal Raman imaging. The ratio of the cells showed positive and negative signals for SWCNTs were consistent with the initio mixing ratio of labeld and unlabeld hMSCs. What's more, the labeled cells could be detected easily even there were only one or two labeled hMSCs in the entire visual field.

4.4.2 Viability of the labeled hMSCs

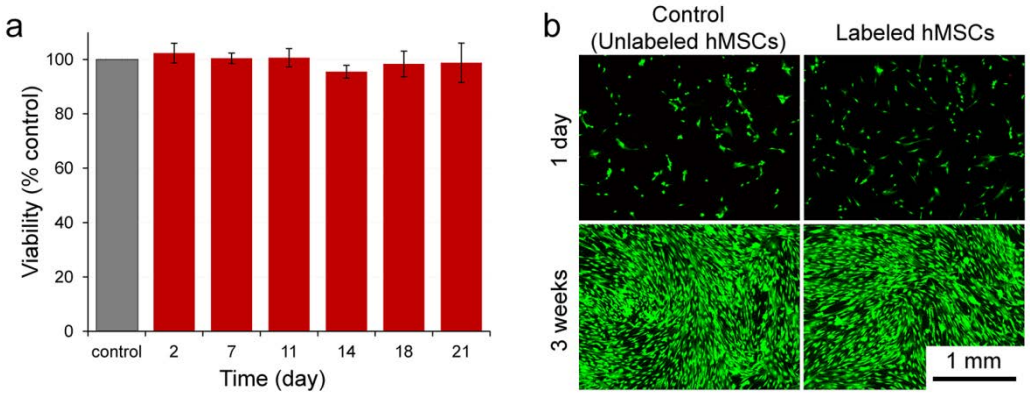

Fig. 4.3 (a) Relative viability of SWCNTs-labeled hMSCs through WST-1 assay. The viability of unlabeled hMSCs was used as a control. (b) Live/dead double staining of the labeled and unlabeled hMSCs after being cultured for 1 day and 3 weeks.

The results of WST-1 assays on the metabolic activity (cell viability) of the Col-SWCNTs labeled hMSCs are shown in Fig. 4.3a. No obvious difference was observed between the experimental and the control groups, indicating that Col-SWCNTs exhibited no obvious cytotoxicity on hMSCs. This result was further confirmed by live/dead double staining (Fig. 4.3b). Live cells were stained green while dead cells

were stained red. Few red-stained cells were detected, suggesting that most of the cells were viable no matter being labeled with Col-SWCNTs or not. This result should be attributed to the good dispersibility of Col-SWCNTs and the bioactive collagen on the surface of nanotubes.

4.4.3 Differentiation capacity of the labeled hMSCs

One of the most attractive characters that hMSCs possess is their multiple differentiation potentiality. It is generally known that cells maintain their homeostasis through a comprehensive signalling network and any perturbation of this system by nanomaterials will affect cell function and behavior. Therefore, the effect of SWCNTs on the differentiation potential of hMSCs is a critical concern for stem cell labeling. In osteogenesis, differentiation of stem cells into osteoblasts is a key step and ALP is an important early marker for cells undergoing differentiation to form preosteoblasts and osteoblasts. ALP staining was performed to investigate the osteogenic differentiation potential of the Col-SWCNTs labeled hMSCs. Fig. 4.4a shows the ALP staining of the labeled and unlabeled hMSCs after being cultured with or without osteogenic induction factors for 1 and 3 weeks. When hMSCs were cultured without osteogenic induction factors, ALP was only slightly stained even after being cultured for 3 weeks. In contrast, the cells no matter being labeled with Col-SWCNTs or not were positively stained after 1 and 3 weeks of osteogenic induction culture. And no significant difference was detected through the quantitative analysis of the positively stained areas between the control and experimental groups (Fig. 4.4b), revealing that the labeling with Col-SWCNTs did not affect the osteogenic differentiation of hMSCs.

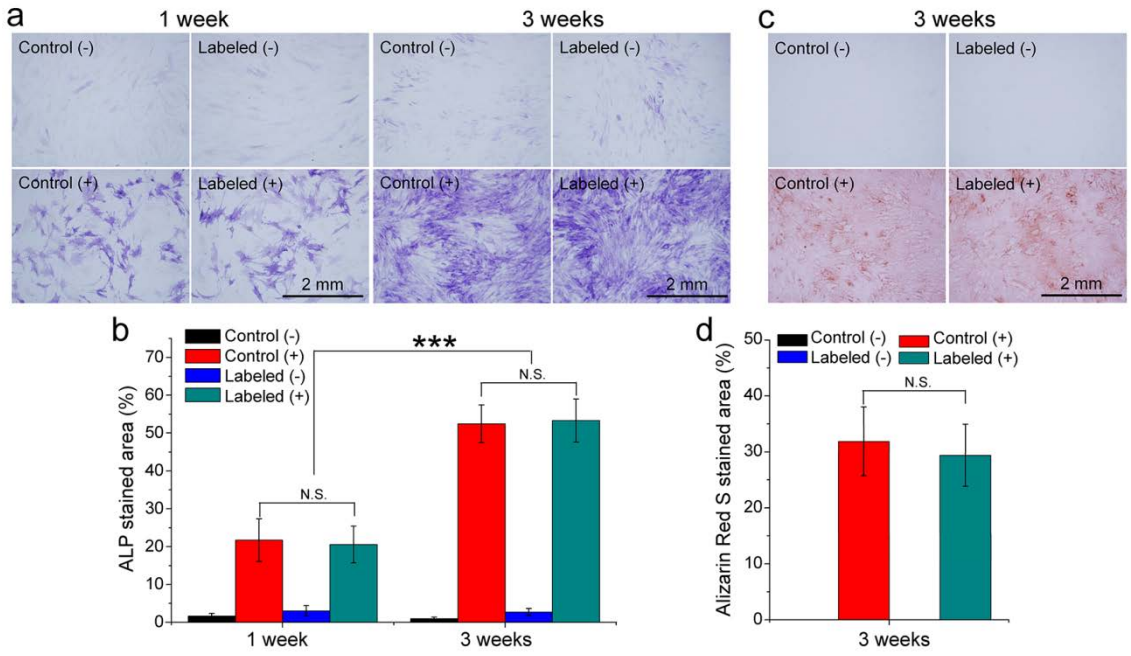

Fig. 4.4 (a) ALP staining and (b) the relative stained area of the labeled and unlabeled hMSCs after being cultured with (+) or without (-) osteogenic induction factors for 1 and 3 weeks. (c) Alizarin Red S staining and (d) the relative stained area of the labeled and unlabeled hMSCs after being cultured with (+) or without (-) osteogenic induction factors for 3 weeks. ***, significant difference, $P < 0.001$. N.S., no significant difference.

Calcium deposition which is an important late indicator of osteogenic differentiation was assessed by

Alizarin Red S staining (Fig. 4.4c). Since mineralization usually happens at a late stage of osteogenic differentiation, Alizarin Red S staining was performed after 3 weeks of culture. Alizarin Red S staining was positive in both control and experimental groups and there was no notable difference between them (Fig. 4.4d), indicating that the labeling of hMSCs with Col-SWCNTs did not affect the calcium deposition.

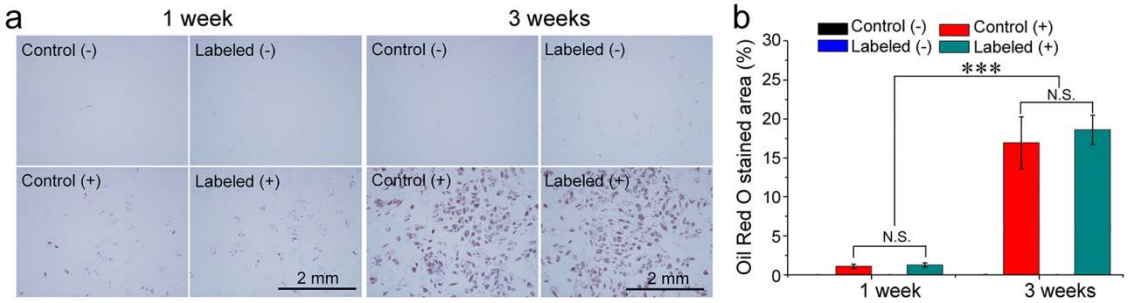

Fig. 4.5 (a) Oil Red O staining and (b) the relative stained area of the labeled and unlabeled hMSCs after being cultured with (+) or without (-) adipogenic induction factors for 1 and 3 weeks. ***, significant difference, $P < 0.001$. N.S., no significant difference.

Adipogenic differentiation capacity of the labeled hMSCs was analyzed by specifically staining intracytoplasmic lipids with Oil Red O. Representative optical photographs of the labeled and unlabeled cells after being stained with Oil Red O are shown in Fig. 4.5a. Because lipid vacuoles are specific markers for adipogenic differentiation of hMSCs, these results suggest that both the labeled and unlabeled hMSCs cultured with adipogenic introduction factors could become adipocytes. Quantification of the positively stained areas of the cells after 1 and 3 weeks of adipogenic induction culture demonstrated the similar levels of adipogenic differentiation between the labeled and unlabeled hMSCs (Fig. 4.5b), revealing the labeling with Col-SWCNTs did not affect the adipogenic differentiation of hMSCs.

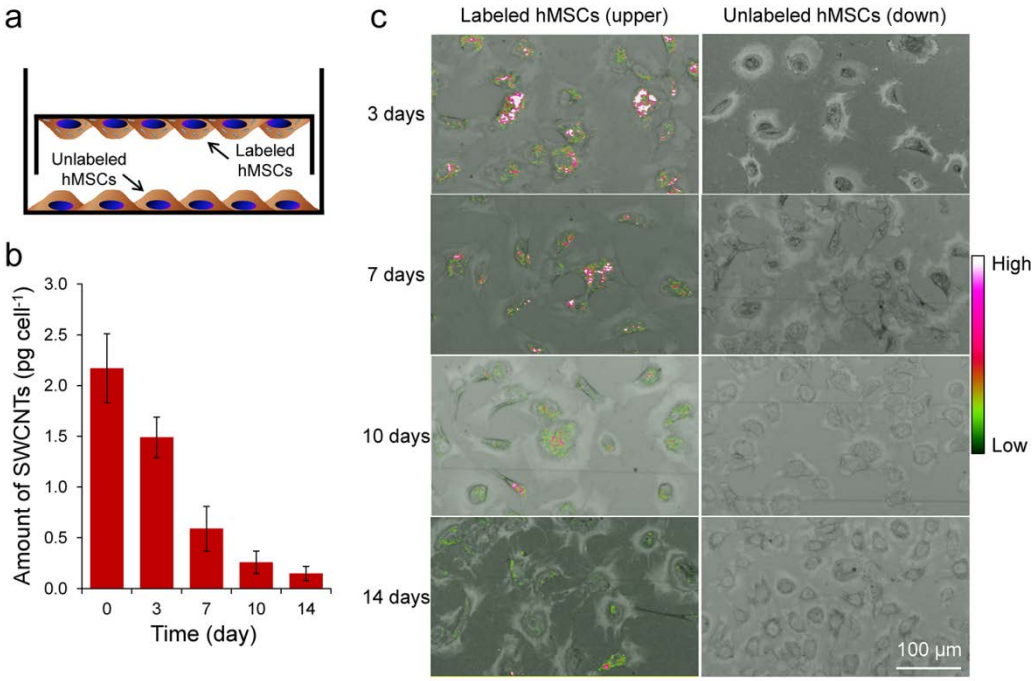

Fig. 4.6 (a) Schematic of the homemade inverse culture system used for co-culture of the labeled and unlabeled hMSCs.

The labeled hMSCs were cultured at the upper side of this system while the unlabeled cells were cultured at the down side. (b) Quantification of SWCNTs in the labeled hMSCs after being cultured in this system for 3-14 days. (c) Merged Raman images of the labeled and unlabeled hMSCs after being cultured in this system for different time. The color-coded scale bar represents the G-band intensity of SWCNTs.

4.4.4 Long-term stem cell labeling capacity of Col-SWCNTs

Another problem in stem cell labeling and imaging is that the ectogenous labeling agents may be released from the labeled cells and internalized by other nearby cells, which can cause a false-positive result. It has been reported that CNTs can be expelled from cells through exocytosis after internalization over hours or days[22,34]. However, in our previous part, we found that Col-SWCNTs were retained in bovine articular chondrocytes for over a week and the prolonged dwell time of Col-SWCNTs in cells should be attributed to the bioactive collagen on the surface of nanotubes.

To conform whether the Col-SWCNTs were released from the labeled hMSCs and internalized by the nearby unlabeled hMSCs, a homemade inverse co-culture system was used (Fig. 4.6a). The unlabeled hMSCs were cultured at the down side of this system, while the Col-SWCNTs labeled hMSCs were cultured at the upper side. Fig. 4.6b shows the amount of SWCNTs in one cell on average of the labeled hMSC over time. The amount of the SWCNTs per cell decreased over time and the decrease was supposed to be caused by cell division, which can dilute the average amount of the internalized nanomaterials in one cell[35]. At day 14, there were 0.15 ± 0.07 pg of SWCNTs per cell ($0.53 \pm 0.25 \times 10^6$ SWCNTs/cell), which was still valid for cell imaging. However, no SWCNTs were detected from the lysates of unlabeled hMSCs. To further visualize SWCNTs in cells, both the labeled (from the upper side) and unlabeled (from the down side) hMSCs were harvested and imaged by the confocal Raman microscope at different time point (Fig. 4.6c). The signals of SWCNTs from the labeled hMSCs through Raman imaging decreased over time, which was consistent with the quantitative data. But, no obvious Raman signals were detected in the unlabeled hMSCs cultured at the down side of the co-culture system, indicating that almost all of the internalized Col-SWCNTs could dwell in hMSCs for a long period of time. These results suggest the potential of collagen functionalized SWCNTs as a probe for long-term stem cell labeling and imaging.

4.5 Conclusions

In summary, SWCNTs were functionalized with collagen and used as a probe for labeling of hMSCs. The Col-SWCNTs showed efficient cellular internalization by hMSCs, without affecting their proliferation and differentiation capacity. The internalized Col-SWCNTs by hMSCs could dwell in cells for 2 weeks and did not come out from the cells. The good cytocompatibility and long dwell time of Col-SWCNTs reveal the potential of SWCNTs-based long-term stem cell labeling.

4.6 References

1. Pittenger, M. F. Multilineage Potential of Adult Human Mesenchymal Stem Cells. *Science* **284,** 143–147 (1999).
2. Weissman, I. L. Translating Stem and Progenitor Cell Biology to the Clinic: Barriers and Opportunities. *Science* **287,** 1442–1446 (2000).
3. Reya, T., Morrison, S. J., Clarke, M. F. & Weissman, I. L. Stem cells, cancer, and cancer stem cells. *Nature* **414,** 105–11 (2001).
4. Yukawa, H. *et al.* Quantum dots labeling using octa-arginine peptides for imaging of adipose tissue-derived stem cells. *Biomaterials* **31,** 4094–103 (2010).
5. Wang, L., Neoh, K.-G., Kang, E.-T., Shuter, B. & Wang, S.-C. Biodegradable magnetic-fluorescent magnetite/poly(dl-lactic acid-co-alpha,beta-malic acid) composite nanoparticles for stem cell labeling. *Biomaterials* **31,** 3502–11 (2010).
6. Quintavalla, J. *et al.* Fluorescently labeled mesenchymal stem cells (MSCs) maintain multilineage potential and can be detected following implantation into articular cartilage defects. *Biomaterials* **23,** 109–19 (2002).
7. Tolar, J. *et al.* Sarcoma derived from cultured mesenchymal stem cells. *Stem Cells* **25,** 371–9 (2007).
8. Meyerrose, T. E. *et al. In Vivo* Distribution of Human Adipose-Derived Mesenchymal Stem Cells in Novel Xenotransplantation Models. *Stem Cells* **25,** 220–227 (2007).
9. Yuste, R. Fluorescence microscopy today. *Nat. Methods* **2,** 902–4 (2005).
10. Yi, P. *et al.* Magnetic resonance imaging of Fe(3)O(4)@SiO(2)-labeled human mesenchymal stem cells in mice at 11.7 T. *Biomaterials* **34,** 3010–9 (2013).
11. Andreas, K. *et al.* Highly efficient magnetic stem cell labeling with citrate-coated superparamagnetic iron oxide nanoparticles for MRI tracking. *Biomaterials* **33,** 4515–25 (2012).
12. Neoh, K. G. & Kang, E. T. Surface modification of magnetic nanoparticles for stem cell labeling. *Soft Matter.* **8,** 2057–2069 (2012).
13. Bhirde, A., Xie, J., Swierczewska, M. & Chen, X. Nanoparticles for cell labeling. *Nanoscale* **3,** 142–53 (2011).
14. Kostarelos, K., Bianco, A. & Prato, M. Promises, facts and challenges for carbon nanotubes in imaging and therapeutics. *Nat. Nanotech.* **4,** 627–633 (2009).
15. Di Crescenzo, A., Velluto, D., Hubbell, J. A. & Fontana, A. Biocompatible dispersions of carbon nanotubes: a potential tool for intracellular transport of anticancer drugs. *Nanoscale* **3,** 925–928 (2011).
16. Liu, Z., Robinson, J. T., Tabakman, S. M., Yang, K. & Dai, H. Carbon materials for drug delivery & cancer therapy. *Mater. Today* **14,** 316–323 (2011).
17. Meng, L., Zhang, X., Lu, Q., Fei, Z. & Dyson, P. J. Single walled carbon nanotubes as drug delivery vehicles: Targeting doxorubicin to tumors. *Biomaterials* **33,** 1689–1698 (2011).
18. Antaris, A. L. *et al.* Ultra-Low Doses of Chirality Sorted （6,5） Simultaneous Tumor Imaging and Photothermal Therapy. *ACS Nano* **7,** 3644–3652 (2013).
19. Wang, L. *et al.* Synergistic anticancer effect of RNAi and photothermal therapy mediated by functionalized single-walled carbon nanotubes. *Biomaterials* **34,** 262–74 (2013).

20. Al-Jamal, K. T. *et al.* Cellular uptake mechanisms of functionalised multi-walled carbon nanotubes by 3D electron tomography imaging. *Nanoscale* **3,** 2627–2635 (2011).
21. Mu, Q., Broughton, D. L. & Yan, B. Endosomal leakage and nuclear translocation of multiwalled carbon nanotubes: developing a model for cell uptake. *Nano Lett.* **9,** 4370–4375 (2009).
22. Neves, V. *et al.* Uptake and Release of Double-Walled Carbon Nanotubes by Mammalian Cells. *Adv. Funct. Mater.* **20,** 3272–3279 (2010).
23. Mao, H., Kawazoe, N. & Chen, G. Uptake and intracellular distribution of collagen-functionalized single-walled carbon nanotubes. *Biomaterials* **34,** 2472–2479 (2013).
24. Chen, Z. *et al.* Single-walled carbon nanotubes as optical materials for biosensing. *Nanoscale* **3,** 1949–56 (2011).
25. Bachilo, S. M. *et al.* Structure-assigned optical spectra of single-walled carbon nanotubes. *Science* **298,** 2361–2366 (2002).
26. Lamanna, G. *et al.* Endowing carbon nanotubes with superparamagnetic properties: applications for cell labeling, MRI cell tracking and magnetic manipulations. *Nanoscale* **5,** 4412–4421 (2013).
27. Liu, Z., Tabakman, S. M., Chen, Z. & Dai, H. Preparation of carbon nanotube bioconjugates for biomedical applications. *Nat. Protoc.* **4,** 1372–1381 (2009).
28. Arnold, M. S., Sharping, J. E., Stupp, S. I., Kumar, P. & Hersam, M. C. Band Gap Photobleaching in Isolated Single-Walled Carbon Nanotubes. *Nano Lett.* **3,** 1549–1554 (2003).
29. Fujigaya, T., Yamamoto, Y., Kano, A., Maruyama, A. & Nakashima, N. Enhanced cell uptake via non-covalent decollation of a single-walled carbon nanotube-DNA hybrid with polyethylene glycol-grafted poly(l-lysine) labeled with an Alexa-dye and its efficient uptake in a cancer cell. *Nanoscale* **3,** 4352–4358 (2011).
30. Holt, B. D., Dahl, K. N. & Islam, M. F. Quantification of Uptake and Localization of Bovine Serum Albumin-Stabilized Single-Wall Carbon Nanotubes in Different Human Cell Types. *Small* **7,** 2348–2355 (2011).
31. Kostarelos, K. *et al.* Cellular uptake of functionalized carbon nanotubes is independent of functional group and cell type. *Nat. Nanotech.* **2,** 108–113 (2007).
32. Porter, A. E. *et al.* Uptake of noncytotoxic acid-treated single-walled carbon nanotubes into the cytoplasm of human macrophage cells. *ACS Nano* **3,** 1485–1492 (2009).
33. Lacerda, L. *et al.* Intracellular Trafficking of Carbon Nanotubes by Confocal Laser Scanning Microscopy. *Adv. Mater.* **19,** 1480–1484 (2007).
34. Kang, B., Chang, S., Dai, Y., Yu, D. & Chen, D. Cell response to carbon nanotubes: size-dependent intracellular uptake mechanism and subcellular fate. *Small* **6,** 2362–2366 (2010).
35. Kim, J. A., Åberg, C., Salvati, A. & Dawson, K. A. Role of cell cycle on the cellular uptake and dilution of nanoparticles in a cell population. *Nat. Nanotech.* **7,** 62–68 (2012).

Chapter 5

Cellular response to collagen-functionalized SWCNTs in composite collagen hydrogels

5.1 Summary

Single-walled carbon nanotubes (SWCNTs) exhibit intrinsic unique physical and chemical properties that make them attractive candidates for biological and biomedicine applications. Cellular interaction of nanomaterials is a focus of current research on the nanomaterials-based applications. A proper 3D cell culture system that can mimic the microenvironment *in vivo* is quite necessary to investigate the interaction of SWCNTs with cells. In this part, SWCNTs/collagen composite hygrogels (SWCNTs/Col hydrogels) were prepared. Cellular uptake and effects of SWCNTs was investigated by culturing of bovine articular chondrocytes (BACs) in these 3D cell culture systems. The results showed that SWCNTs incorporated in the composite hygrogels could be internalized by BACs. BACs cultured in SWCNTs/Col hydrogels maintained their proliferation capacity when compared to the culture in collagen hydrogels (Col hydrogels). Due to the composite 3D scaffolds can mimic the microenvironment *in vivo*, these results may reflect the responses of cells to the nanomaterials in nature biological system more realistically and will facilitate the nanomaterials-based applications in tissue engineering.

5.2 Introduction

One of the most important characteristics of carbon nanotubes (CNTs) is that they can effectively cross biological barriers[1,2] and therefore can be used as targeted and multi-delivery vehicles for diagnostically and therapeutically active molecules[3,4]. Meanwhile, their inherent optical, electrical and thermal properties make CNTs attractive candidates for biological imaging, detection and therapy[3,5,6]. Nevertheless, the main intrinsic drawback of CNTs is their extremely poor dispersibility in most of the common solvents due to their super-hydrophobicity and significant van der Waal's forces[7,8]. These features are associated with cytotoxicity and other negative cellular effects[9], whereas well dispersed CNTs have no apparent cytotoxicity[10,11].

Furthermore, the success of many CNTs-based applications largely depends on how many CNTs can be internalized by cells. An efficient cellular uptake can greatly facilitate such applications in biomedicine and biotechnology. Two major pathways for the cellular uptake of CNTs have been confirmed. One describes CNTs as nanoneedles that can penetrate cell membranes in an energy-independent manner[12,13] and another one suggests that cellular uptake of CNTs performed via the clathrin-mediated endocytosis[14,15] which is an energy-dependent manner. In addition, adsorption of some biocompatible molecules, such as BSA, DNA and peptides, on the surfaces of CNTs may induce and facilitate receptor-mediated endocytosis of CNTs[16-18]. However, most of the cellular uptake studies *in vitro* have been performed with a two-dimensional (2D) cell culture system. 2D cell culture conditions are different from the microenvironment surrounding cells *in vivo*. As a result, the response of cells to CNTs, including cellular uptake, can not completely reflect the virtual behavior in their native tissue. One potential strategy to overcome the problem is to culture cells with a three-dimensional (3D) culture system which can mimic the natural extracellular matrix (ECM) and provide a functional support for cell growth, proliferation, differentiation and metabolism[19-21].

Hydrogels with their beneficial characteristics, such as high water content, controllable biodegradability and excellent mass transfer properties, have been extensively explored for applications in 3D cell culture and regenerative medicine[22,23]. Compared with other materials, collagen-based hydrogles are of particular interest because collagen is the most abundant protein in mammals, shows regular helical structure, excellent biocompatibility and moderate immunogenicity[24]. Furthermore, collagen fibrils can physically assemble with each other to form a collagen network (fibrillogenesis) in aqueous solution. The resulting collagen hydrogels show a highly porous structure and can offer a three-dimensional biomimetic microenviroment for cells.

In this study, collagen hydrogels (Col hydrogels) were used to investigate the cellular uptake of single-walled carbon nanotubes (SWCNTs) in a biomimetic 3D culture system. SWCNTs were modified by coating their surfaces with collagen and incorporated in Col hydrogels to form the composite hydrogels (SWCNTs/Col hydrogels). Bovine articular chondrocytes were cultured in the SWCNTs/Col composite hydrogels and cellular effects of SWCNTs were investigated.

5.3 Materials and methods

5.3.1 Preparation of SWCNTs/Col composite hydrogels

Prior to the preparation of SWCNTs/Col composite hydrogels, SWCNTs (purity > 90%, 0.7-1.3 nm in diameter, Sigma-Aldrich, USA) were coated with collagen to improve the dispersibility in water as reported before[25]. Briefly, 1,000 μg SWCNTs were sterilized using ultraviolet light for 2 hours and put in 10 mL 0.1 wt% collagen solution that was prepared by diluting 1.0 wt% collagen aqueous solution (type I collagen in pH = 3.0 acetic acid aqueous solution, Nippon Meat Packers Inc., Japan) with pH = 3.0 acetic acid aqueous solution. The mixture was sonicated (135 W, Bransonic, Japan) in an ice bath for 2 hours. The dispersion solution was then centrifuged (Tomy MX-301, Japan) at 20,000× g for 30 minutes to remove aggregated and bundled SWCNTs. To prepare SWCNTs/Col composite hydrogels, the supernatant was mixed with 1.0 wt% collagen aqueous solution at a designated ratio. The SWCNTs-containing collagen solution was mixed with

10 times concentrated DMEM (Dulbecco's modified Eagle's medium, Sigma, USA) and HEPES buffer solution (50 mM NaOH, 260 mM $NaHCO_3$ and 200 mM HEPES) at a volume ratio of 8:1:1. All the solutions were pre-cooled at 4 °C before mixing and all the operations were performed in an ice bath. The mixtures were placed at 37 °C for gelation to form SWCNTs/Col composite hydrogels.

5.3.2 Characterization of hydrogels

The microstructures of the freeze-dried Col and SWCNTs/Col hydrogels were observed and imaged with a JSM-5610 scanning electron microscope (SEM, JEOL, Japan). Briefly, hydrogel samples were frozen at -80 °C and freeze-dried for 24 hours in a freeze-dryer (VirTis AdVantage Benchtop Freeze Dryer, SP Industries Inc.). The freeze-dried specimens were plunged into liquid nitrogen and cut using a cold scalpel. The cross sections were then coated with platinum and observed by SEM at 10 kV accelerating voltage.

5.3.3 Cell culture in hydrogels

Bovine articular chondrocytes (BACs) were isolated from the articular cartilage derived from a 9-week old female calf. Freshly isolated chondrocytes were defined as P0. BACs that were subcultured twice (P2) were used in this study. The BACs were cultured in 75 cm^2 tissue culture flasks (BD Falcon, USA) at 37 °C in humidified air containing 5% CO_2. The culture medium was DMEM supplemented with 10% fetal bovine serum, 4,500 mg/L glucose, 4 mM glutamine, 100 U/mL penicillin, 100 μg/mL streptomycin, 0.1 mM nonessential amino acids, 0.4 mM proline, 1 mM sodium pyruvate and 50 μg/mL ascorbic acid (serum DMEM). P2 cells were seeded into the composite hydrogels during hydrogel preparation. P2 cells were suspended in 10 times concentrated serum DMEM to prepare cell suspension solution at a density of 1.0×10^8 cells/cm^3. The SWCNTs-containing collagen solution, cell suspension solution and HEPES buffer solution were mixed at a volume ratio of 8:1:1. The cells-containing mixture solution was placed in 12-well plates and incubated at 37 °C in humidified air containing 5% CO_2 for 4 hours for formation of hydrogels. After hydrogel formation, 1.5 mL serum DMEM was added in each well. Cells cultured in SWCNTs-free Col hydrogels, which were used as control, were prepared by the same method as described above by using collagen solution without SWCNTs. Cell culture medium was changed every 3 days.

5.3.4 Cell viability assay

The proliferation of cells was evaluated by WST-1 assay. Firstly, the cell culture medium was replaced with 550 μL of WST-1 solution (Roche, Germany, 50 μL of WST-1 stock solution diluted with 500 μL of serum DMEM). After incubation for 3 hour, 100 μL of supernatant solution was collected and placed into a 96-well plate. The absorbance was measured at 440 nm using a plate reader (Benchmark Plus, USA).

5.3.5 Cellular uptake of SWCNTs in the composite hydrogels

To determine the amount of SWCNTs internalized in the BACs, the cells were harvested by digesting the hydrogels with type I collagenase/trypsin-EDTA solution and washed with warm PBS for 3 times. Then the washed cells were ruptured via a papain (Sigma, USA) buffer solution and the amount of SWCNTs in the buffer solution was measured by using UV-vis-NIR spectroscopy. The value was considered to be the amount

of SWCNTs internalized in cells. Before being ruptured, the cells were counted with a cytometer.

5.3.6 Analysis of intracellular distribution of SWCNTs

An inverted confocal Raman microscope (AMANplus, Nanophoton, Japan) with a 532 nm laser (500 mW) and phase objectives (Nikon Microsystems, Japan) was used for both Raman and phase-contrast imaging. Briefly, the cells cultured in the hydrogels with or without SWCNTs for 7 days were harvested and re-cultured in a 4-chamber culture slide. And then the cells were fixed with 4% paraformaldehyde solution to prevent morphological and chemical changes during image acquisition. After that, the samples were washed with PBS and the slides were mounted and sealed using nail lacquer. A phase-contrast image of the cells was focused, revealing cellular morphologies including the nuclei and extensions. A horizontal confocal Raman image (x-y imaging mode) and an entire vertical section image (x-z imaging mode) were acquired to investigate the distribution of SWCNTs in cells. The confocal Raman spectra from 779.7 to 1970.0 cm^{-1} were collected and the G-band, indicative of SWCNTs, was used to map the distribution of SWCNTs. Control of imaging parameters, processing and data analysis were performed in a Raman Data Viewer software (Nanophoton, Japan).

5.3.7 Statistical analysis

All data were reported as mean ± standard deviation (SD). One-way analysis of variance was performed to reveal statistical differences followed by Tukey's post hoc test for pairwise comparison. All statistical analyses were executed using Kyplot 2.0 beta 15.

5.4 Results and discussion

5.4.1 Characterization of hydrogels

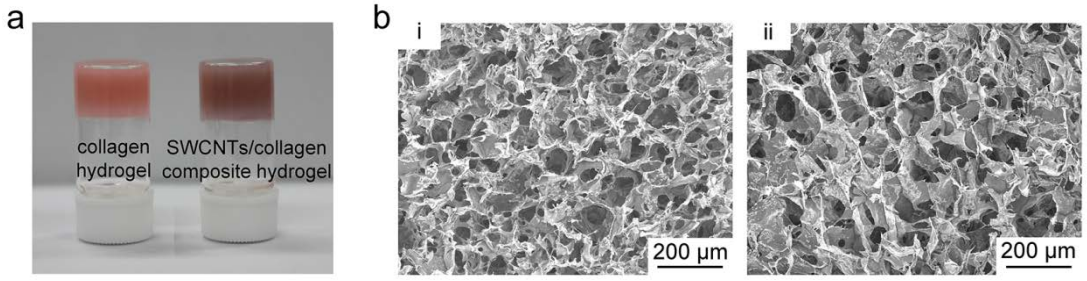

Fig. 5.1 (a) Photographs of Col hydrogel and SWCNTs/Col composite hydrogel. (b) SEM images of freeze-dried (i) Col hydrogel and (ii) SWCNTs/Col composite hydrogel.

Fig. 5.1a shows photographs of Col hydrogel and SWCNTs/Col composite hydrogel gelated at neutral pH and 37 °C. The hydrogels were sticky and became static even when vessels were put upside down. The pink color was due to the color of the cell culture medium. The SWCNTs/Col composite hydrogels were slightly black because of the incorporation of SWCNTs. The microstructure of Col hydrogels and SWCNTs/Col composite hydrogels were observed by SEM after freeze-drying. The Col hydrogels and SWCNTs/Col composite hydrogels showed the same microstructures (Fig. 5.1b). There were many

micropores in both hydrogels. The size of the micropores was around 100 μm. The micropore structure in the hydrogels should support cell movement and benefit diffusion of nutrients and metabolic substances.

5.4.2 Cell viability in hydrogels

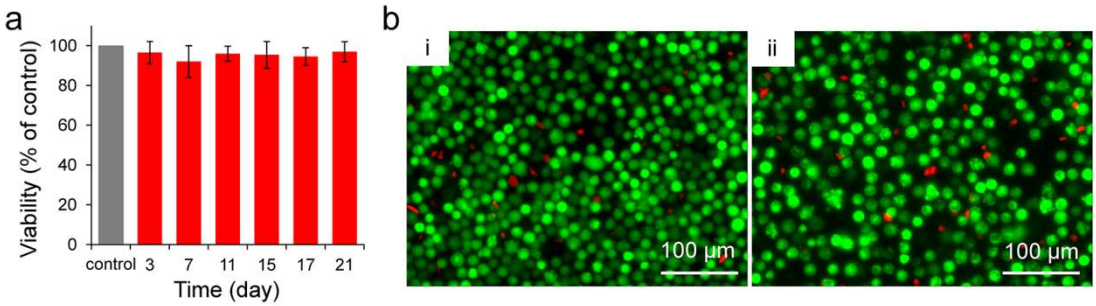

Fig. 5.2 (a) Relative viability of BACs cultured in SWCNTs/Col composite hydrogels through WST-1 assay. The viability of BACs cultured in Col hydrogels was used as a control. (b) Live/dead double staining of BACs cultured in (i) Col hydrogels and (ii) SWCNTs/Col composite hydrogels for 7 days.

The effect of SWCNTs on cell viability has been investigated *in vitro* by culturing cells with SWCNTs-containing culture medium. However, the published data are fiercely debated and extremely inconsistent[9,10,11,26]. Fig. 5.2a shows the results of WST-1 assays on cell viability cultured in Col hydrogels and SWCNTs/Col composite hydrogels over time. There was no significant difference between the two hydrogels, suggesting that the SWCNTs in the hydrogels did not affect cell viability. The viability of the cells was further confirmed by live/dead staining (Fig. 5.2b). Few red-stained cells were detected. Most of the cells were alive in both Col hydrogels and SWCNTs/Col composite hydrogels.

5.4.3 Cellular uptake of SWCNTs in composite hydrogels

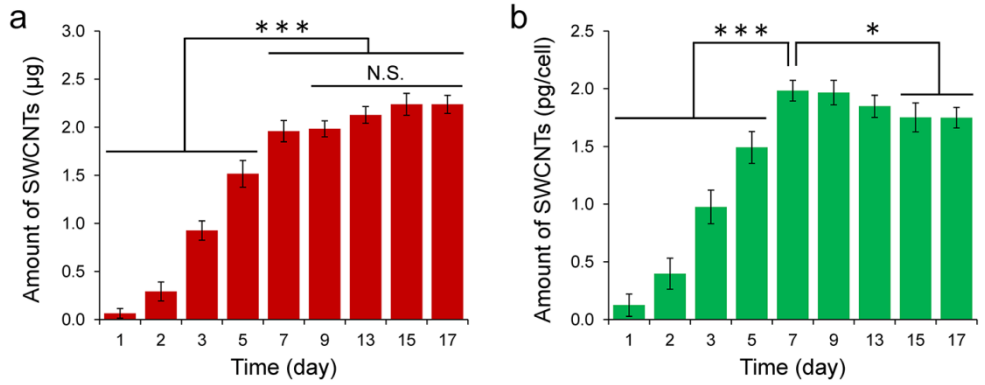

Fig. 5.3 (a) Quantification of cellular uptake of SWCNTs in a BAC population after culture for 1 to 17 days. (b) Average amount of SWCNTs internalized in one cell on average after culture for 1 to 17 days. (N.S. indicates no significant difference, *, significant difference, $P < 0.05$, ***, significant difference, $P < 0.001$).

There are many reports on the cellular uptake of SWCNTs. The effects of size, shape and surface functionalization of SWCNTs on internalization have been reported[17,27,28]. The results suggest that all of these parameters affect cellular uptake and surface adsorption of some biocompatible molecules, such as

BSA, DNA and peptides, can be an important factor to affect cellular uptake of SWCNTs[16,17]. In this part, SWCNTs were detected in the cells when the cells were cultured in SWCNTs/Col composite hydrogels. The amount of SWCNTs in the entire cell population increased with culture time until day 7 and remained unchanged since then (Fig. 5.3a). By dividing the total amount of internalized SWCNTs by cell number, the amount of SWCNTs internalized per cell was calculated (Fig. 5.3b). The uptake amount of SWCNTs per cell increased until day 7 and decreased slightly since day 7. Significant decrease was detected after culture for 15 and 17 days. At day 7, the amount of SWCNTs per cell was 1.98 ± 0.09 pg. In other words, up to 7.01 ± 0.32 × 10^6 SWCNTs (molecular mass ≈ 170 kDa for length ≈ 235 nm, diameter ≈ 0.9 nm) were internalized by one cell on average. The high internalization amount of SWCNTs should benefit their applications for delivery of therapeutic and diagnostic biomolecules.

5.4.4 Intracellular distribution of internalized SWCNTs

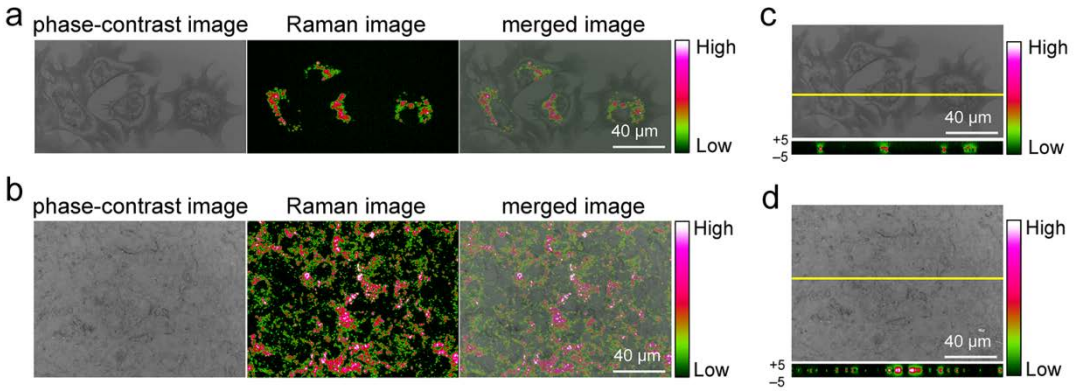

Fig. 5.4 Phase-contrast, Raman and merged micrographs and of (a) a few cells and a BAC population after being cultured in SWCNTs/Col composite hydrogels for 7 days. The x-z cross section confocal Raman image of (c) a few cells and (d) a BAC population after being cultured in SWCNTs/Col composite hydrogels for 7 days. The x–z cross section scanning was performed along the yellow line in the phase-contrast micrograph. The color-coded scale bar represents the G-band intensity of SWCNTs.

Raman spectroscopy as a label-free technique is a useful tool to visualize the SWCNTs in living cells[16,25,29]. Confocal Raman imaging was performed to investigate intracellular distribution of SWCNTs. Fig. 5.4 shows the phase-contrast and confocal Raman images of cells using different scanning modes. The phase-contrast image clearly revealed the cellular morphology of BACs, including the cell shape, nucleus position and cell extension. In x-y scanning mode, the confocal Raman image showed that SWCNTs were primarily located around the nucleus (Fig. 5.4a). The result was consistent with previous reports[16,29,30] and supported by the x-z plane scanning confocal Raman imaging performed across the center of nucleus (Fig. 5.4c). By imaging a cell population (Fig. 5.4b and d), cellular uptake was confirmed within the population of cells and the intensity of SWCNTs was most prevalent in the perinuclear region. The results indicated that SWCNTs could be internalized in cells when hydrogels were used for 3D cell culture. The internalized SWCNTs were predominantly distributed around the nuclei of cells. The results suggest SWCNTs/Col composite hydrogels may be useful for the delivery of proteins, drugs and genes for biomedical applications.

5.5 Conclusions

Cellular uptake of SWCNTs in a 3D culture condition was investigated by culturing chondrocytes in SWCNTs/Col composite hydrogels. The SWCNTs/Col hydrogels showed no negative effects on the viability of chondrocytes. Uptake of SWCNTs by chondrocytes during 3D culture was confirmed by using UV-vis-NIR spectroscopy and $7.01 \pm 0.32 \times 10^6$ SWCNTs were internalized in one cell on average. The internalized SWCNTs were prevalently accumulated in the perinuclear region. The results indicated that SWCNTs could be internalized by cells when being cultured in the 3D biomimetic Col hydrogels.

5.6 References

1. Pogodin, S. & Baulin, V. A. Can a carbon nanotube pierce through a phospholipid bilayer? *ACS Nano* **4,** 5293–5300 (2010).
2. Höfinger, S. *et al.* A computational analysis of the insertion of carbon nanotubes into cellular membranes. *Biomaterials* **32,** 7079–85 (2011).
3. Liu, Z., Robinson, J. T., Tabakman, S. M., Yang, K. & Dai, H. Carbon materials for drug delivery & cancer therapy. *Mater. Today* **14,** 316–323 (2011).
4. Ren, J. *et al.* The targeted delivery of anticancer drugs to brain glioma by PEGylated oxidized multi-walled carbon nanotubes modified with angiopep-2. *Biomaterials* **33,** 3324–33 (2012).
5. Porter, A. E. *et al.* Direct imaging of single-walled carbon nanotubes in cells. *Nat. Nanotech.* **2,** 713–717 (2007).
6. Yi, H. *et al.* M13 phage-functionalized single-walled carbon nanotubes as nanoprobes for second near-infrared window fluorescence imaging of targeted tumors. *Nano Lett.* **12,** 1176–1183 (2012).
7. Geckeler, K. E. & Premkumar, T. Carbon nanotubes: are they dispersed or dissolved in liquids? *Nanoscale Res. Lett.* **6,** 136 (2011).
8. Bandyopadhyaya, R., Nativ-Roth, E., Regev, O. & Yerushalmi-Rozen, R. Stabilization of individual carbon nanotubes in aqueous solutions. *Nano Lett.* **2,** 25–28 (2002).
9. Liu, D., Yi, C., Zhang, D., Zhang, J. & Yang, M. Inhibition of proliferation and differentiation of mesenchymal stem cells by carboxylated carbon nanotubes. *ACS Nano* **4,** 2185–2195 (2010).
10. Kam, N. W. S., Liu, Z. & Dai, H. Carbon nanotubes as intracellular transporters for proteins and DNA: an investigation of the uptake mechanism and pathway. *Angew. Chem. Int. Ed.* **45,** 577–581 (2006).
11. Wong, N., Kam, S., Jessop, T. C., Wender, P. A. & Dai, H. Nanotube Molecular Transporters : Internalization of Carbon Nanotube-Protein Conjugates into Mammalian Cells. *J. Am. Chem.Soc.* **126,** 6850–6851 (2004).
12. Pantarotto, D., Briand, J.-P., Prato, M. & Bianco, A. Translocation of bioactive peptides across cell membranes by carbon nanotubes. *Chem. Commun.* 16–17 (2004).
13. Lu, Q. *et al.* RNA Polymer Translocation with Single-Walled Carbon Nanotubes. *Nano Lett.* **4,** 2473–2477 (2004).

14. Hong, G. *et al.* Three-dimensional imaging of single nanotube molecule endocytosis on plasmonic substrates. *Nat. Commun.* **3,** 1–9 (2012).
15. Al-Jamal, K. T. *et al.* Cellular uptake mechanisms of functionalised multi-walled carbon nanotubes by 3D electron tomography imaging. *Nanoscale* **3,** 2627–2635 (2011).
16. Holt, B. D., Dahl, K. N. & Islam, M. F. Quantification of Uptake and Localization of Bovine Serum Albumin-Stabilized Single-Wall Carbon Nanotubes in Different Human Cell Types. *Small* **7,** 2348–2355 (2011).
17. Becker, M. L. *et al.* Length-Dependent Uptake of DNA-Wrapped Single-Walled Carbon Nanotubes. *Adv. Mater.* **19,** 939–945 (2007).
18. Tsyboulski, D. A. *et al.* Self-assembling peptide coatings designed for highly luminescent suspension of single-walled carbon nanotubes. *J. Am. Chem.Soc.* **130,** 17134–17140 (2008).
19. Haines-Butterick, L. *et al.* Controlling hydrogelation kinetics by peptide design for three-dimensional encapsulation and injectable delivery of cells. *Proc. Natl. Acad. Sci. USA* **104,** 7791–6 (2007).
20. Kisiday, J., Jin, M. & Kurz, B. Self-assembling peptide hydrogel fosters chondrocyte extracellular matrix production and cell division: implications for cartilage tissue repair. *Proc. Natl. Acad. Sci. USA* **99,** 9996–10001 (2002).
21. Zhang, S. Fabrication of novel biomaterials through molecular self-assembly. *Nat. Biotechnol.* **21,** 1171–8 (2003).
22. Lee, K. Y. & Mooney, D. J. Hydrogels for Tissue Engineering. *Chem. Rev.* **101,** 1869–1880 (2001).
23. Nicodemus, G. D. & Bryant, S. J. Cell encapsulation in biodegradable hydrogels for tissue engineering applications. *Tissue Eng. Part B. Rev.* **14,** 149–65 (2008).
24. Parenteau-Bareil, R., Gauvin, R. & Berthod, F. Collagen-Based Biomaterials for Tissue Engineering Applications. *Materials.* **3,** 1863–1887 (2010).
25. Peng, Y. Y. *et al.* A Streptococcus pyogenes derived collagen-like protein as a non-cytotoxic and non-immunogenic cross-linkable biomaterial. *Biomaterials* **31,** 2755–61 (2010).
26. Mao, H., Kawazoe, N. & Chen, G. Uptake and intracellular distribution of collagen-functionalized single-walled carbon nanotubes. *Biomaterials* **34,** 2472–2479 (2013).
27. Zhang, Y. *et al.* Mechanistic toxicity evaluation of uncoated and PEGylated single-walled carbon nanotubes in neuronal PC12 cells. *ACS Nano* **5,** 7020–33 (2011).
28. Kang, B., Chang, S., Dai, Y., Yu, D. & Chen, D. Cell response to carbon nanotubes: size-dependent intracellular uptake mechanism and subcellular fate. *Small* **6,** 2362–2366 (2010).
29. Jin, H., Heller, D. A., Sharma, R. & Strano, M. S. Size-dependent cellular uptake and expulsion of single-walled carbon nanotubes: single particle tracking and a generic uptake model for nanoparticles. *ACS Nano* **3,** 149–158 (2009).
30. Porter, A. E. *et al.* Uptake of noncytotoxic acid-treated single-walled carbon nanotubes into the cytoplasm of human macrophage cells. *ACS Nano* **3,** 1485–1492 (2009).
31. Lacerda, L. *et al.* Intracellular Trafficking of Carbon Nanotubes by Confocal Laser Scanning Microscopy. *Adv. Mater.* **19,** 1480–1484 (2007).

Chapter 6

Cellular response to collagen-functionalized SWCNTs in composite collagen porous sponges

6.1 Summary

Three-dimensional (3D) porous collagen sponges incorporated with single-walled carbon nanotubes (SWCNTs) were prepared and used for 3D culture of bovine articular chondrocytes (BACs). The pore structures of the sponges were controlled by using ice particulates as a porogen material. The responses of cells to SWCNTs were investigated in this 3D cell culture system by evaluation of cell functions and cellular uptake of SWCNTs. The results showed that cells adhered and spatially distributed in the porous sponges. The incorporation of SWCNTs in the porous sponges promoted cell proliferation and production of sulfated glycosaminoglycans (sGAG). Confocal Raman imaging revealed that SWCNTs could be internalized by cells. The hybrid porous sponges not only provided nanostructured pore surfaces to facilitate cell proliferation and extracellular matrix (ECM) secretion also supplied nanomaterials for cellular uptake which may be useful for delivery of bioactive molecules and genes into cells.

6.2 Introduction

Tissue engineering has been developed as a promising approach to improve or replace biological functions by the combination of cells, scaffolds and growth factors[1,2]. Among these three key factors, the scaffolds play a crucial role by furnishing a biomimetic microenvironment to control cell functions and guiding new tissue formation[3,4]. Scaffolds with ideal properties, such as good biocompatibility, appropriate mechanical property and inner pore structures are highly demanded for successful tissue regeneration. Thus far, a variety of scaffolds have been fabricated either from natural polymers or synthetic polymers[5,6]. Compared with other biodegradable polymers, collagen-based scaffolds are particularly attractive because

collagen is one of the most abundant proteins in mammals, shows regular helical structure, high hydrophilicity, excellent biocompatibility and moderate immunogenicity[7–9].

Except the microstructures of scaffolds, creation of nanostructures to mimic the native cellular microenvironments has been a great challenge. The extracellular matrix (ECM), as the main components of *in vivo* cellular microenvironments, is a hierarchically organized nanocomposite that provides structural and biochemical supports to the surrounding cells[10]. To address this challenge, researchers have made efforts on the design of advanced nanocomposite scaffolds that can better mimic the ECM by using existing nanotechnological tools[11,12]. One of the effective methods is to incorporate nanomaterials into porous scaffolds[13–15]. Nanomaterials may affect the functions of the cells not only through the interaction between their nanoscaled structures and cells, but also through the internalization. However, the effects of incorporated nanomaterials in porous scaffolds have not been well elucidated. Therefore, detailed interaction of nanomaterials with cells needs to be thoroughly investigated for their extensive application in tissue engineering.

In this study, 3D collagen porous sponges (Col sponges) with controlled pore structures were prepared by using ice particulates as a porogen material. Single-walled carbon nanotubes (SWCNTs), as one of the most attractive nanomaterials, were incorporated in Col sponges to prepare SWCNTs/Col hybrid sponges by immersion of Col sponges in SWCNTs-containing aqueous solution. The interaction of SWCNTs with cells was investigated by culturing bovine articular chondrocytes in the hybrid porous scaffolds.

6.3 Materials and methods

6.3.1 Preparation of Col and SWCNTs/Col porous sponges

3D collagen porous sponges (Col sponges) with controlled pore structure were prepared by using ice particulates as a porogen material as previously reported[16–19]. Ice particulates were prepared by spaying Milli Q water into liquid nitrogen using a sprayer. The ice particulates were sieved by sieves with 355 and 425 μm mesh pores to obtain ice particulates having a diameter from 355 and 425 μm. The sieving process was conducted in a -15 °C low-temperature chamber (Espec, Osaka, Japan). The sieved ice particulates were stored in closed glass bottles in a -80 °C freezer until use. Collagen solution with a concentration of 2% (w/v) was prepared by dissolving freeze-dried porcine type I collagen (Nitta Gelatin, Osaka, Japan) in a mixture solution of 0.1 M acetic acid (pH = 3.0) and ethanol at a ratio of 80:20 (v/v). The collagen solution and the sieved ice particulates were kept in the low-temperature chamber at -4 °C for 6 hours for temperature balance. The temperature-balanced ice particulates and collagen solution were mixed homogeneously at a ratio of 50:50 (w/v) at the low-temperature chamber. The mixture was frozen in a deep freezer (-80 °C) for 6 hours and freeze-dried in a freeze-dryer under a vacuum of 20 Pa (VirTis AdVantage Benchtop Freeze Dryer, SP Industries Inc.). After freeze-drying, Col sponges were cross-linked with glutaraldehyde vapor for 6 hours, treated with 0.1 M glycine aqueous solution to block any unreacted aldehyde groups, washed with pure water for 6 times, frozen in the deep freezer (-80 °C) for 6 hours and freeze-dried again as described above to obtain the cross-linked Col sponges.

Prior to the preparation of SWCNTs/Col porous sponges (SWCNTs/Col sponges), SWCNTs (purity > 90%, 0.7-1.3 nm in diameter, Sigma-Aldrich, USA) were coated with collagen using a simple non-covalent approach to improve the dispersibility in water as previously reported[20–22]. Briefly, 1,000 μg SWCNTs were sterilized using ultraviolet light for 2 hours and put in 10 mL 0.1 wt% collagen solution. The mixture was sonicated (135 W, Bransonic, Japan) in an ice bath for 2 hours. The dispersion solution was then centrifuged (Tomy MX-301, Japan) at 20,000× g for 30 minutes to remove aggregated and bundled SWCNTs. To prepare SWCNTs/Col sponges, pure cross-linked Col sponges was immersed in the collagen-treated SWCNTs aqueous solution over night, frozen in the deep freezer (-80 °C) for 6 hours and freeze-dried again as described above.

6.3.2 Characterization of porous sponges

The inner structures of the Col and SWCNTs/Col sponges were observed and imaged with a high resolution scanning electron microscope (SEM, S-4800, Hitachi, Japan). The freeze-dried specimens were plunged into liquid nitrogen and cut using a cold scalpel. The cross sections were taken out from liquid nitrogen and air-dried. They were then coated with platinum and observed by SEM at a 10 kV accelerating voltage. The mean pore size of the porous sponges was measured from the SEM images by a MetaVue Image System (Universal Imaging Corp., Buckinghamshire, UK). Six images were taken from each scaffold and used for the mean pore size calculation.

6.3.3 Cell culture in the porous sponges

For cell culture use, the Col and SWCNTs/Col sponges were punched into cylindrical samples (Ø8 mm × H3 mm). The samples were sterilized with 70% ethanol, washed 3 times with sterile Milli Q water and conditioned with cell culture medium at 37 °C for 30 min. Bovine articular chondrocytes (BACs) were isolated from the articular cartilage derived from a 9-week old female calf. Freshly isolated chondrocytes were defined as P0. BACs that were subcultured twice (P2) were used in this study. Cells were suspended in culture medium at a density of 5.0×10^7 cells/ mL. The cell suspension was seeded into the cylindrical sponges (100 μL/sponge) that were placed in 24-well cell culture plates (non-treated). After 4 hours, the sponges were transferred into 25 cm^2 flasks and cultured under an atmosphere of 5% CO_2 at 37 °C with shaking at 60 rpm for a designated time. The medium was changed twice per week. The cells in the medium and the cells adhered to each well of the cell culture plates after 4 hours culture after cell seeding were collected, counted and taken as the number of cells leaked from the sponges during cells seeding. The number of adhered cells to each sponge was obtained by subtracting the leaked cell number from the initial cell seeding number. The seeding efficiency of each sponge was calculated by dividing the number of adhered cells by the number of seeded cells. Six samples were used for these measurements in order to obtain averages and standard deviations (SD). The culture medium was Dulbecco's Modified Eagle Medium (DMEM) supplemented with 10% fetal bovine serum, 4,500 mg/L glucose, 4 mM glutamine, 100 U/mL penicillin, 100 μg/mL streptomycin, 0.1 mM nonessential amino acids, 0.4 mM proline, 1 mM sodium pyruvate and 50 μg/mL ascorbic acid (serum DMEM).

After being cultured for another 2 hours, the cell/sponge constructs were washed with PBS for 3 times and fixed with 0.25% glutaraldehyde solution at room temperature for 1 hour. The cell/sponge constructs were washed with pure water for 3 times and freeze-dried in a freeze-dryer under a vacuum of 20 Pa. The freeze-dried specimens were sliced using a scalpel. The cross sections were coated with platinum and the cell adhesion in the sponges was observed by an SEM at a 10 kV accelerating voltage. To visualize the cell distribution in the sponges, the cell/sponge constructs after 24 hours cell culture were collected, washed with PBS for 3 times and sectioned (around 1 μm in thickness) with a scalpel. The as-prepared cross-sections were stained with 4',6-diamidino-2-phenylindole (DAPI, Vector Laboratories, Inc.) and observed under a fluorescence microscope (Olympus, Tokyo, Japan).

6.3.4 Cell proliferation and sulfated glycosaminoglycans (sGAG) production

Cell proliferation in the porous sponges was investigated by the DNA content measurement after 6 hours, 1 and 2 weeks of cell culture. The cell/sponge constructs after culture for 6 hours, 1 and 2 weeks were washed with warm PBS, freeze-dried and digested with papain solution (400 μg/mL, with 5 mM L-cysteine and 5 mM EDTA in 0.1 M phosphate buffer at a pH of 6.0). An aliquot of the papain-digested solution was dyed with Hoechst 33258 dye (Sigma-Aldrich, St. Louis, MO, USA) and the DNA amount (n = 3) was measured under a spectrofluorometer (FP-6500, JASCO, Japan). The sGAG content was measured with the above papain digestion solution by a dimethylmethylene blue dye binding method (Biocolor, Newtonabbey, UK) and a microplate spectrophotometer (Benchmark Plus; Bio-Rad Laboratories, Tokyo, Japan) at 656 nm. The sGAG content (n = 3) was calculated based on a standard curve obtained with the standard sGAG supplied with the kits.

6.3.5 Cellular uptake of SWCNTs in the porous sponges

An inverted confocal Raman microscope (AMANplus, Nanophoton, Japan) with a 532 nm laser (500 mW) and phase objectives (Nikon Microsystems, Japan) was used for both Raman and phase-contrast imaging. Cells cultured in the Col and SWCNTs/Col sponges for 2 weeks were released from the sponges by treatment with trypsin/collagenase mixed solution for 4 hours and re-cultured in a 4-chamber culture slide. After culture for 4 hours, the cells were fixed with 4% paraformaldehyde solution to prevent morphological change during image acquisition. After that, the samples were washed with PBS and the slides were mounted and sealed using nail lacquer. A phase-contrast image of the cells was focused, revealing cellular morphologies including the nuclei and extensions. A horizontal confocal Raman image (x-y imaging mode) was acquired to investigate the cellular uptake and intracellular distribution of SWCNTs. The confocal Raman spectra from 779.7 to 1970.0 cm^{-1} were collected and the G-band, indicative of SWCNTs, was used to map the distribution of SWCNTs. Control of imaging parameters, processing and data analysis were performed in a Raman Data Viewer software (Nanophoton, Japan).

6.3.6 Statistical analysis

All data were reported as mean ± standard deviation (SD). One-way analysis of variance was performed to reveal statistical differences followed by Tukey's post hoc test for pairwise comparison. All statistical analyses were executed using Kyplot 2.0 beta 15.

6.4 Results and discussion

6.4.1 Characterization of porous sponges

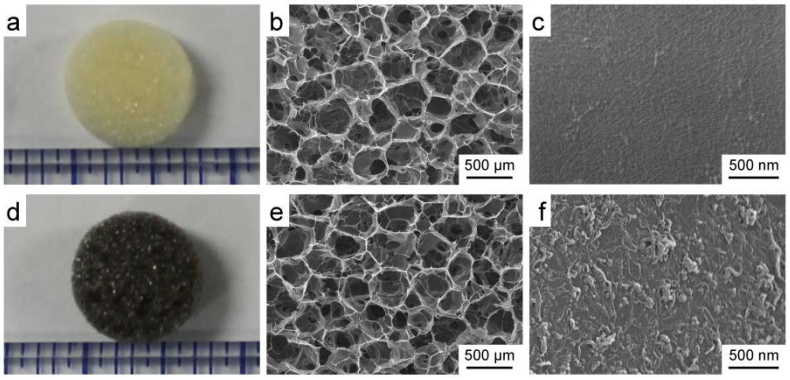

Fig. 6.1 Gross appearances (a, e) and SEM images (b, c, d, f, g, h) of Col sponge (a, b, c, d) and SWCNTs/Col hybrid sponge (e, f, g, h). The images are shown in low (b, c, f, g) and high (d, h) magnifications.

Fig. 6.1 shows the gross appearances (Fig. 6.1a and e) and the inner structures (Fig. 6.1b, c, e and f) of Col (Fig. 6.1a, b and c) and SWCNTs/Col (Fig. 6.1d, e and f) sponges. The SWCNTs/Col sponges were slightly black because of the incorporation of SWCNTs. The Col and SWCNTs/Col sponges showed similar microstructure and the large pores in all the sponges were homogeneously distributed and interconnected with each other through the surrounded small pores. The size of the large spherical pores in Col and SWCNTs/Col sponges was 359 ± 53 and 356 ± 49 μm in diameter (Table 6.1), respectively. The large pore size was well consistent with the size of the ice particulates. Observation under a high magnification showed that tube-like nanostructure was found on the surface of the walls of the SWCNTs/Col sponges (Fig. 6.1f), while the surface of the walls of Col sponges was smooth (Fig. 6.1c).

Table 6.1 Size of the large spherical pores in Col and SWCNTs/Col sponges.

Scaffold type	Pore size (μm)
Col sponge	359 ± 53
SWCNTs/Col sponge	356 ± 49

The data are represented as the mean ± SD, n = 6.

No significant difference was detected between Col and SWCNTs/Col sponges.

Pore architecture has been reported to have a markedly effect on the properties of the porous scaffolds and behaviors of the seeded cells, as well as the formation of new tissues[19,23]. Therefore, a scaffold with

appropriate pore structures, such as high porosity, optimal pore size and good interconnectivity, is highly demanded for tissue engineering. In this study, spherical ice particulates with a diameter range from 425 μm to 500 μm were used as a porogen material to control the pore structure of Col and SWCNTs/Col sponges. Observation by SEM showed that the Col and SWCNTs/Col sponges had similar pore structures, indicating that the introduction of SWCNTs did not affect the porous structures of the sponges. The large spherical pores in both scaffolds were homogeneously distributed throughout the sponges and interconnected with each other through the surrounded small pores. The size of the large pores was well consistent with the size of the ice particulates, indicating the large pores were the negative replicas of the ice particulates. The small pores were induced by the ice crystals that were formed at the freezing step during sponge preparation.

6.4.2 Cell seeding and spatial distribution in porous sponges

Table 6.2 Cell seeding efficiency of BACs in Col and SWCNTs/Col sponges.

Scaffold type	Cell seeding efficiency
Col sponge	94.9 ± 1.8%
SWCNTs/Col sponge	95.1 ± 2.2%

The data are represented as the mean ± SD, n = 6.

No significant difference was detected between Col and SWCNTs/Col sponges.

The seeding efficiency of BACs in Col and SWCNTs/Col sponges was 94.9 ± 1.8% and 95.1 ± 2.2%, respectively (Table 6.2). No significant difference was observed between them. The process of cell seeding did not affect the porous structure of the sponges (Fig. 6.2a and c). The cells adhered and spread on the surfaces of the large pores in both Col and SWCNTs/Col sponges (Fig. 6.2 b and d).

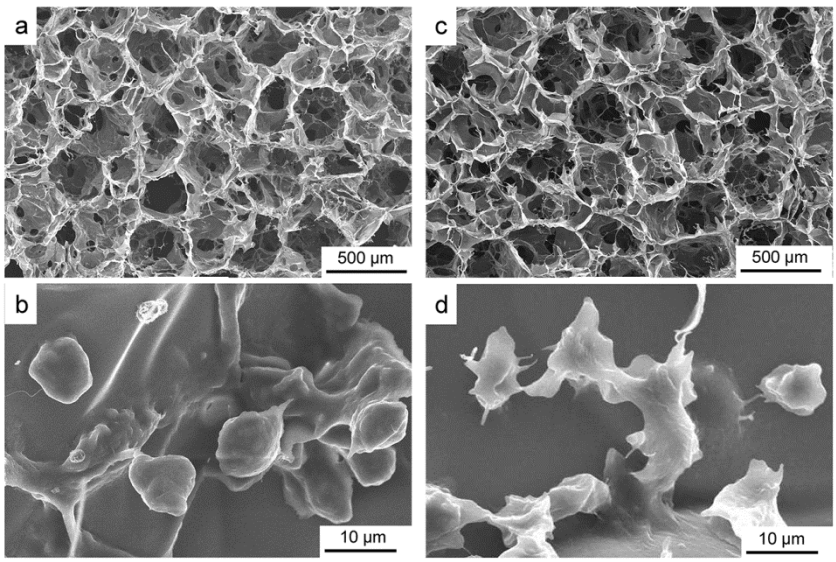

Fig. 6.2 Adhesion of BACs in Col sponge (a, b) and SWCNTs/Col hybrid sponge (c, d) after being cultured for 6 hours. The images are shown in low (a, c) and high (b, d) magnifications.

The spatial cell distribution in the porous sponges was investigated by observing cell nuclei that were stained with DAPI after the cells were cultured in the sponges for 24 hours. Cell nuclei were observed in the

whole specimen although slightly more cells were located on the surface layer of the sponges (Fig. 6.3a and b). Col and SWCNTs/Col sponges showed similar cell distribution.

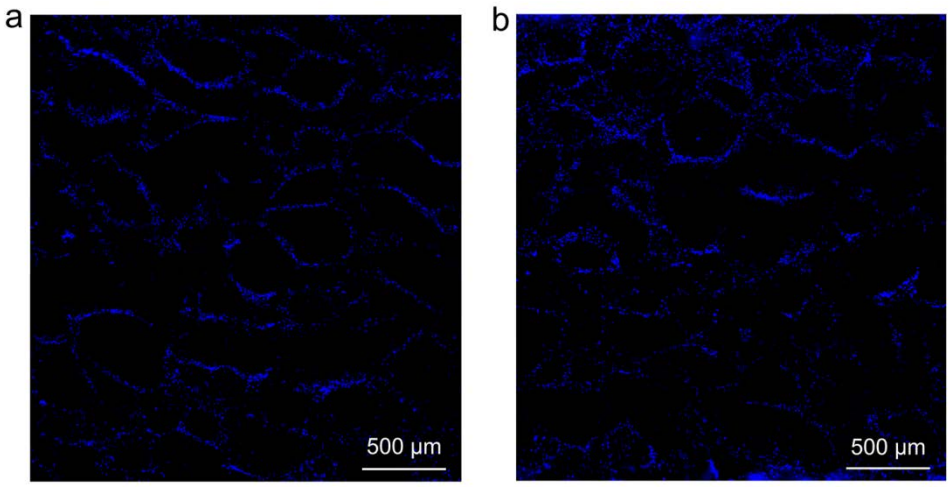

Fig. 6.3 Spatial cell distribution of BACs in Col sponge (a) and SWCNTs/Col hybrid sponge (b). Cell nuclei were stained by DAPI and observed under a fluorescence microscope.

In tissue engineering, an universal issue is that a thin cell-layer may be formed rapidly on the exterior surface of the porous scaffolds which is caused by the heterogeneous cell seeding and distribution and will subsequently result in a failure of the functional tissue regeneration[24,25]. Therefore, a spatial distribution of cells throughout porous scaffolds is desirable to avoid the problems for even ECM deposition and uniform tissue regeneration. In this study, cells adhered and distributed both on the surface and in the inner pores of the sponges. The spatial cell distribution should be due to the high homogeneity of the spherical large pores and good interconnectivity of the sponges, which facilitated the smooth delivery of cells throughout the sponges.

6.4.3 Cell proliferation and sGAG production

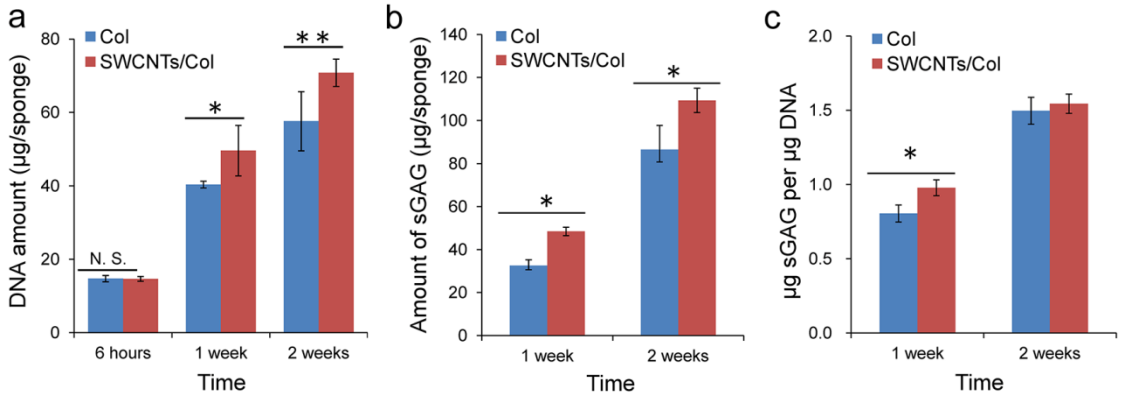

Fig. 6.4 DNA amount of BACs cultured in Col and SWCNTs/Col hybrid sponges for 6 hours, 1 and 2 weeks (a). sGAG amount (b) and the ratio of sGAG/DNA (c) of BACs cultured in Col and SWCNTs/Col hybrid sponges for 1 and 2 weeks. The data are represented as the mean ± SD, n = 3. **, significant difference, $P < 0.01$; *, significant difference, $P < 0.05$.

DNA quantification was performed to evaluate the proliferation of cells in the porous sponges. Fig. 6.4a shows that the DNA amount increased over time, indicating that the cells proliferated in both sponges. The DNA amount in SWCNTs/Col sponges was significantly higher than that in the Col sponges when the cells were cultured for 1 and 2 weeks, suggesting that cells proliferated more quickly in SWCNTs/Col sponges than did in Col sponges during cell culture.

The total amount of sGAG secreted by the whole cell population in each sponge was measured and the amount of sGAG/DNA ratio was calculated from the sGAG and DNA contents of each sample. Both the total amount of sGAG (Fig. 6.4b) and the sGAG/DNA ratio (Fig. 6.4c) increased significantly over time in both sponges, indicateing that the chondrocytes produced extracellular matrices continually during the whole culture period. The sGAG content in the SWCNTs/Col sponges was significantly higher than that in the Col sponges. The sGAG/DNA ratio in the SWCNTs/Col sponges was higher than that in the Col sponges. These results indicated that the SWCNTs/Col sponge were more favorable to the production of cartilaginous ECM than the Col sponges.

It has been reported that cells can sense and respond differently to the substrates under various conditions, including the changing of the geometry and topography[26–28]. And the interaction of cells with surface topology has been proved to be a significant signaling modality in regulating cell functions, such as cell adhesion, alignment, migration, proliferation and cytoskeleton organization. In native microenvironment, cells interact with ECM components in the nanometer scale[10,29]. Nanoscaled surface topology has been shown to have positive effect on the cell behaviors[30–32]. In this study, the cell proliferation and sGAG production were improved by the incorporation of nanoscaled topography provided by SWCNTs in the SWCNTs/Col sponges. Since SWCNTs have high surface energy and high ability to adsorb proteins, they can adsorb various proteins from the culture medium and these proteins may affect cell functions such as proliferation and ECM secretion. Meanwhile, cells secrete soluble factors which can benefit cell functions during cell culture. Such secreted factors may also be adsorbed and concentrated by SWCNTs and provide continuous stimulation to cells. In contrast, the soluble factors secreted by cells cultured in collagen sponges were remained in the medium and removed during medium replacement every time.

6.4.4 Cellular uptake of SWCNTs in sponges

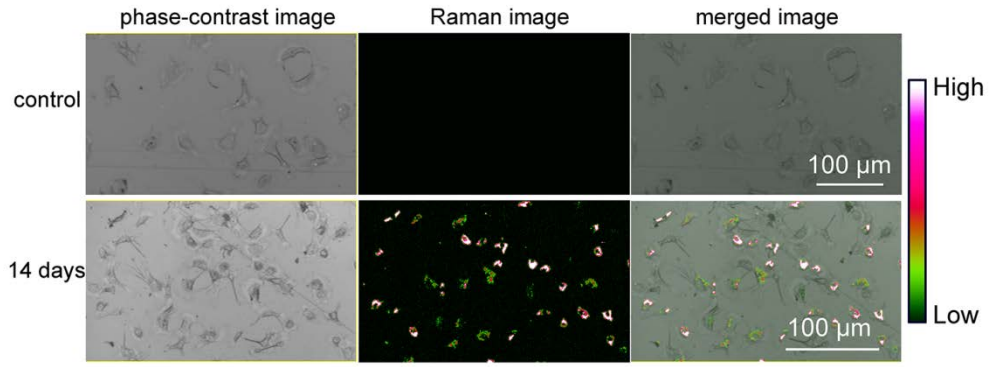

Fig. 6.5 Phase-contrast, Raman and merged micrographs of BAC population after being cultured in Col and SWCNTs/Col hybrid sponges for 2 weeks. The color-coded scale bar represents the G-band intensity of SWCNTs.

Confocal Raman imaging was performed to visualize the cellular uptake of SWCNTs. Fig. 6.5 shows the phase-contrast and confocal Raman images of cells after being cultured in the Col and SWCNTs/Col sponges for 2 weeks. The phase-contrast image clearly revealed the cellular morphology of BACs, including the cell shape, nucleus position and cell extension. The signals of SWCNTs were only detected from the cells cultured in the SWCNTs/Col sponges. The intensity of SWCNTs signals was most prevalent in the perinuclear region, indicating that SWCNTs could be internalized by BACs and predominantly distributed around the nuclei of cells, which was well consistent with previous reports[20,33,34]. Merged images indicated that most of the cells showed uptake of SWCNTs although a small amount of cells showed negative signal for SWCNTs uptake.

As a unique quasi one-dimensional material, SWCNTs have been widely explored for the delivery of various biomolecules, including drugs, proteins and genes[35–37]. Achieving spatially and temporally controlled delivery of biomolecules represents another key factor in tissue regeneration. In this study, Raman imaging results revealed that SWCNTs in the hybrid sponges could be internalized by the cells. Our previous studies showed that the internalization of collagen-functionalized SWCNTs did not affect the cell viability and proliferation[20,21]. Furthermore, due to the ability of implantation into designated location, the hybrid sponges may achieve controlled and localized delivery of biological factors which will benefit tissue developing. Therefore, incorporation of nanomaterials in macroporous sponges highlights the importance of combining physicochemical and biological cues at different scales to improve cell functions in scaffolds and should be an attractive strategy for preparation of functional scaffolds for tissue engineering.

6.5 Conclusions

Hybrid 3D porous collagen sponges with controlled pore structures were prepared by using ice particulates as a porogen material and coating with SWCNTs. Incorporation of SWCNTs in the sponges improved cell proliferation and sGAG production through offering nanoscaled topography. The SWCNTs in the hybrid sponges could be internalized by cells, which may benefit the controlled and localized delivery of biological factors. Due to similarity of 3D culture in the hybrid porous sponges to the *in vivo* microenvironment, the results reflected the responses of cells to the SWCNTs more realistically than 2D culture. The hybrid scaffolds will be useful for tissue engineering.

6.6 References

1. Langer, R. & Vacanti, J. P. Tissue Engineering. *Science.* **260,** 920–926 (1993).
2. Griffith, L. G. & Naughton, G. Tissue engineering--current challenges and expanding opportunities. *Science.* **295,** 1009–14 (2002).
3. Chen, G., Ushida, T. & Tateishi, T. Scaffold Design for Tissue Engineering. *Macromol. Biosci.* **2,** 67–77 (2002).
4. Hollister, S. J. Porous scaffold design for tissue engineering. *Nat. Mater.* **4,** 518–24 (2005).

5. Rice, J. J. *et al.* Engineering the regenerative microenvironment with biomaterials. *Adv. Healthc. Mater.* **2,** 57–71 (2013).
6. Hench, L. L. Biomaterials: a forecast for the future. *Biomaterials* **19,** 1419–23 (1998).
7. Schneider, R. K. *et al.* The osteogenic differentiation of adult bone marrow and perinatal umbilical mesenchymal stem cells and matrix remodelling in three-dimensional collagen scaffolds. *Biomaterials* **31,** 467–80 (2010).
8. Glowacki, J. & Mizuno, S. Collagen scaffolds for tissue engineering. *Biopolymers* **89,** 338–44 (2008).
9. Mao, H., Kawazoe, N. & Chen, G. Cellular Uptake of Single-Walled Carbon Nanotubes in 3D Extracellular Matrix-Mimetic Composite Collagen Hydrogels. *J. Nanosci. Nanotechnol.* **14,** 2487–2492 (2014).
10. Tsang, K. Y., Cheung, M. C., Chan, D. & Cheah, K. S. The developmental roles of the extracellular matrix: beyond structure to regulation. *Cell Tissue. Res.* **339,** 93–110 (2010).
11. Dvir, T., Timko, B. P., Kohane, D. S. & Langer, R. Nanotechnological strategies for engineering complex tissues. *Nat. Nanotech.* **6,** 13–22 (2011).
12. Shi, J., Votruba, A. R., Farokhzad, O. C. & Langer, R. Nanotechnology in drug delivery and tissue engineering: from discovery to applications. *Nano Lett.* **10,** 3223–3230 (2010).
13. Wei, G. & Ma, P. X. Structure and properties of nano-hydroxyapatite/polymer composite scaffolds for bone tissue engineering. *Biomaterials* **25,** 4749–57 (2004).
14. Kim, K., Dean, D., Lu, A., Mikos, A. G. & Fisher, J. P. Early osteogenic signal expression of rat bone marrow stromal cells is influenced by both hydroxyapatite nanoparticle content and initial cell seeding density in biodegradable nanocomposite scaffolds. *Acta Biomater.* **7,** 1249–64 (2011).
15. Pathi, S. P., Lin, D. D. W., Dorvee, J. R., Estroff, L. a & Fischbach, C. Hydroxyapatite nanoparticle-containing scaffolds for the study of breast cancer bone metastasis. *Biomaterials* **32,** 5112–22 (2011).
16. Chen, G., Ushida, T. & Tateishi, T. Preparation of poly(L-lactic acid) and poly(DL-lactic-co-glycolic acid) foams by use of ice microparticulates. *Biomaterials* **22,** 2563–7 (2001).
17. Lu, H., Ko, Y.-G., Kawazoe, N. & Chen, G. Cartilage tissue engineering using funnel-like collagen sponges prepared with embossing ice particulate templates. *Biomaterials* **31,** 5825–35 (2010).
18. Zhang, Q., Lu, H., Kawazoe, N. & Chen, G. Preparation of collagen scaffolds with controlled pore structures and improved mechanical property for cartilage tissue engineering. *J. Bioact. Compat. Polym.* **28,** 426–438 (2013).
19. Zhang, Q., Lu, H., Kawazoe, N. & Chen, G. Pore size effect of collagen scaffolds on cartilage regeneration. *Acta Biomater.* **10,** 2005–2013 (2013).
20. Mao, H., Kawazoe, N. & Chen, G. Uptake and intracellular distribution of collagen-functionalized single-walled carbon nanotubes. *Biomaterials* **34,** 2472–2479 (2013).
21. Mao, H., Cai, R., Kawazoe, N. & Chen, G. Long-term stem cell labeling by collagen-functionalized single-walled carbon nanotubes. *Nanoscale* **6,** 1552–1559 (2013).

22. Dulínska-Molak, I., Mao, H., Kawazoe, N. & Chen, G. Variation of Mechanical Property of Single-Walled Carbon Nanotubes-Treated Cells Explored by Atomic Force Microscopy. *J. Biomed. Nanotechnol.* **10,** 651–659 (2014).
23. Murphy, C. M., Haugh, M. G. & O'Brien, F. J. The effect of mean pore size on cell attachment, proliferation and migration in collagen-glycosaminoglycan scaffolds for bone tissue engineering. *Biomaterials* **31,** 461–6 (2010).
24. Ishaug, S. L., Crane, G. M., Miller, M. J., Yasko, A. W., Yaszemski, M. J. & Mikos, A. G. Bone formation by three-dimensional stromal osteoblast culture in biodegradable polymer scaffolds. *J. Biomed. Mater. Res.* **36,** 17–28 (1997).
25. Silva, M. M. C. G., Cyster, L. A., Barry, J. J. A. Yang, X. B., Oreffo, R. O. C, Grant, D. M., Scotchford, C. A., Howdle, S. M., Shakesheff, K. M. & Rose,F. R. A. J. The effect of anisotropic architecture on cell and tissue infiltration into tissue engineering scaffolds. *Biomaterials* **27,** 5909–17 (2006).
26. Nikkhah, M., Edalat, F., Manoucheri, S. & Khademhosseini, A. Engineering microscale topographies to control the cell-substrate interface. *Biomaterials* **32,** 5230–46 (2012).
27. Lee, H., Jang, Y., Seo, J., Nam, J.-M. & Char, K. Nanoparticle-functionalized polymer platform for controlling metastatic cancer cell adhesion, shape, and motility. *ACS Nano* **5,** 5444–56 (2011).
28. Seo, C. H., Seo, C. H., Jeong, H., Feng, Y., Montagne, K., Ushida, T., Suzuki, Y. & Furukawa, K. S. Micropit surfaces designed for accelerating osteogenic differentiation of murine mesenchymal stem cells via enhancing focal adhesion and actin polymerization. *Biomaterials* **35,** 2245–52 (2014).
29. Hynes, R. O. The extracellular matrix: not just pretty fibrils. *Science.* **326,** 1216–1219 (2009).
30. Li, X., Liu, H., Niu, X., Yu, B., Fan, Y., Feng, Q., Cui, F.-Z. & Watari, F. The use of carbon nanotubes to induce osteogenic differentiation of human adipose-derived MSCs in vitro and ectopic bone formation in vivo. *Biomaterials* **33,** 4818–27 (2012).
31. Chen, Y.-S. & Hsiue, G.-H. Directing neural differentiation of mesenchymal stem cells by carboxylated multiwalled carbon nanotubes. *Biomaterials* **34,** 4936–4944 (2013).
32. Solanki, A., Solanki, A., Chueng, S.-T. D., Yin, P. T., Kappera, R., Chhowalla, M. & Lee, K.-B. Axonal alignment and enhanced neuronal differentiation of neural stem cells on graphene-nanoparticle hybrid structures. *Adv. Mater.* **25,** 5477–82 (2013).
33. Lacerda, L., Pastorin, G., Gathercole, D., Buddle, J., Prato, M., Bianco, A. & Kostarelos, K. Intracellular Trafficking of Carbon Nanotubes by Confocal Laser Scanning Microscopy. *Adv. Mater.* **19,** 1480–1484 (2007).
34. Holt, B. D., Dahl, K. N. & Islam, M. F. Quantification of Uptake and Localization of Bovine Serum Albumin-Stabilized Single-Wall Carbon Nanotubes in Different Human Cell Types. *Small* **7,** 2348–2355 (2011).
35. Meng, L., Zhang, X., Lu, Q., Fei, Z. & Dyson, P. J. Single walled carbon nanotubes as drug delivery vehicles: Targeting doxorubicin to tumors. *Biomaterials* **33,** 1689–1698 (2011).
36. Kam, N. W. S., Liu, Z. & Dai, H. Carbon nanotubes as intracellular transporters for proteins and DNA: an investigation of the uptake mechanism and pathway. *Angew. Chem. Int. Ed.* **45,** 577–581 (2006).

37. Vehicles, G. D. Cationic Glyco-Functionalized Single-Walled Carbon Nanotubes as Efficient Gene Delivery Vehicles. *Bioconjug. Chem.* **20,** 2017–2022 (2009).

Chapter 7

Concluding remarks and future prospects

7.1 Concluding remarks

This research focused on the interaction of SWCNTs with cells and their biomedical applications in stem cell research and tissue engineering. Firstly, SWCNTs were functionalized with collagen (Col-SWCNTs) to improve their dispersibility in water and the interaction of Col-SWCNTs with cells was investigated in 2D cell culture system. Subsequently, AFM was used to investigate the changes of mechanical properties of cells when they were exposed to nanomaterials. Furthermore, Col-SWCNTs were explored for long-term stem cell labeling and imaging. Finally, SWCNTs/Col composite hydrogels and porous sponges were prepared. The interaction of SWCNTs with cells was investigated in the 3D cell culture systems to explore the application possibility of these composite scaffolds for tissue engineering.

Chapter 1 introduces the background on nanomaterials. Representative nanomaterials and their applications in nanomedicine and tissue engineering were reviewed. Potential risks of nanomaterials-based applications were summarized. Investigation of the interaction of nanomaterials with cells was motivated.

Chapter 2 describes the functionalization of SWCNTs with collagen (Col-SWCNTs) and the interaction of Col-SWCNTs with cells in 2D cell culture system. The Col-SWCNTs retained the inherent properties of SWCNTs and the suspension solution was stable for months. The cellular effects, uptake and intracellular distribution of Col-SWCNTs were investigated by using them for culture of bovine articular chondrocytes (BACs). High amount of Col-SWCNTs were internalized by cells without obvious negative cellular effects. The internalized Col-SWCNTs were distributed in the perinuclear region and retained in the cells for more than one week. The high stability, easy cellular uptake and long retention time in cells of the Col-SWCNTs will facilitate the biomedical applications of SWCNTs.

Chapter 3 describes the investigation of the changes of cell mechanical properties induced by nanomaterials using AFM. Two different types of nanomaterials (SWCNTs and Fe-FeO core-shell magnetic

nanoparticles) and three types of cells (BACs, hMSCs and HeLa cells) were used. The results indicated that the effects of nanomaterials on the mechanical properties of cells were dependent on nanoparticles size, concentration and cell type as well as exposure time. More importantly, AFM was demonstrated to be useful to identify the subtle changes of the mechanical properties of cells when they were exposed to nanomaterials even for very short time.

Chapter 4 describes the Col-SWCNTs-based long-term stem cell labeling and imaging. The results showed that Col-SWCNTs exhibited efficient cellular internalization by hMSCs without affecting their proliferation and differentiation. The prolonged dwell time of Col-SWCNTs in cells ensured the long-term labeling for up to 2 weeks. This part of work revealed the potential of Col-SWCNTs as a probe for long-term stem cell labeling and imaging.

Chapter 5 describes the preparation of SWCNTs/Col composite hydrogels and the interaction of SWCNTs with cells in the hydrogels. The SWCNTs/Col hydrogels showed no negative effects on the viability of BACs. Uptake of SWCNTs by BACs was confirmed by using UV-vis-NIR spectroscopy and confocal Raman imaging. The internalized SWCNTs were prevalently accumulated in the perinuclear region. The results indicated that SWCNTs could be internalized by cells when being cultured in the 3D biomimetic collagen hydrogels.

Chapter 6 describes the preparation of SWCNTs/Col composite porous sponges and the interaction of SWCNTs with cells in the sponges. Incorporation of SWCNTs in the sponges improved cell proliferation and sGAG production through offering nanoscaled topography. The SWCNTs in the composite sponges could be internalized by cells, which may benefit the controlled and localized delivery of biological factors. Due to similarity of 3D culture in the composite porous sponges to the *in vivo* environment, the results reflected the responses of cells to the SWCNTs more realistically than 2D culture. The composite scaffolds will be useful for tissue engineering.

In conclusion, SWCNTs were functionalized with collagen and the interaction of SWCNTs with cells was investigated in 2D and 3D cell culture systems. The Col-SWCNTs showed high stability, easy cellular uptake and good cytocompatibility, which will facilitate the SWCNTs-based biomedical applications, such as drug/gene delivery, biological imaging and cancer therapy. Meanwhile, AFM was employed to investigate the effects of nanomaterials on cells. The results showed that AFM was able to identify the subtle changes of the mechanical properties of cells when they were exposed to nanomaterials and could be a useful tool to investigate cellular effects of nanomaterials. Furthermore, the Col-SWCNTs were used as an imaging probe for labeling of hMSCs. The results showed that the Col-SWCNTs exhibit efficient cellular internalization by hMSCs without affecting their proliferation and differentiation and Col-SWCNTs should be a good candidate for long-term stem cell labeling. Finally, SWCNTs were incorporated in collagen hydrogels and porous sponges to construct 3D cell culture system to investigate 3D interaction between SWCNTs and cells. The results of cells cultured in SWCNTs/Col composite scaffolds should reflect the responses of cells to the nanomaterials in nature biological system more realistically and the composite scaffolds will facilitate the nanomaterials-based applications in tissue engineering.

7.2 Future prospects

Application of nanomaterials in cancer diagnosis and therapy: Cancer, as a leading cause of death worldwide, accounting for 8.2 million deaths and 14.1 million new cancer cases in 2012 and those numbers are predicted to rise to 13 million deaths and 22 million cases annually within the next two decades, according to the World Health Organization. Current treatments based on surgery, radiation therapy and chemotherapy are often associated with severe side effects. Therefore, new approaches to treat cancer that do not rely on traditional therapeutic regimes are very important. The development of nanomedicine provides a novel approach to treat cancers. The critical issue in nanomedicine is the creation of innovative functional nanomaterials. Among various nanomaterials, carbon nanotubes (CNTs) have attracted intense interest and shown great potential in cancer treatment due to their unique inherent properties. In this study, SWCNTs were functionalized with collagen (Col-SWCNTs) and the Col-SWCNTs showed high stability, easy cellular uptake and long dwell time in cells, all of these results suggested the possibility of SWCNTs-based cancer imaging and destruction.

Multifunctionalization of nanomaterials: Each of the nanomaterials has its limitation. The limited features provided by one single type of nanomaterials can not meet the complex requirements of disease diagnosis and therapy. The elegant multifunctional materials in biological systems inspire scientists to design analogous hierarchical structures with multifunctional capabilities by hybridization or combination of different types of nanomaterials for diagnosis, imaging and therapy of disease. For example, depositing a thin layer of gold around the carbon nanotubes (gold-plated CNTs) can be expected to be used as photoacoustic and photothermal contrast agents with enhanced near-infrared contrast even using low laser fluence levels. Endowing carbon nanotubes with superparamagnetic properties by coating them with magnetic nanoparticles can achieve simultaneous biological isolation, MRI/NIR dual imaging and NIR photodynamic/magnetic hyperthermia dual therapy. In addition, nanomaterials can be engineered with targeting ligands such as antibodies, peptides and aptamers for targeted drug delivery or cancer therapy.

The fate of nanomaterials *in vivo*: Despite the many proposed advantages of nanomaterials, increasing concerns have been expressed on their biocompatibility, biodistribution and long term fate *in vivo* in biomedical applications. It is known that most nanomaterials tend to exhibit high uptake in the reticuloendothelial system (RES) (liver, spleen, etc.) once injected into animals and are not rapidly excreted. Whether or not and how these materials are cleared from the body is unknown in many cases, because of the difficulties in long term *in vivo* tracking and monitoring of the materials. Currently used radio labels or fluorescent labels for nanomaterials are useful for *in vivo* tracking over short periods of time (a few hours to a few days), but these labels may gradually dissociate from the materials or decay and lose activity over time. It is thus highly desirable to detect nanomaterials based on their intrinsic physical properties rather than relying on radiolabels or spectroscopic tags for indirect detection/measurement. The direct detection method may lead to a more accurate assessment of how nanomaterials behave *in vivo* in both short and long terms, i.e., during the blood circulation stage and during time periods lasting several months.

List of publications

[1] **H. Mao**, N. Kawazoe and G. Chen. Uptake and Intracellular Distribution of Collagen-functionalized Single-walled Carbon Nanotubes. Biomaterials 2013, 34: 2472-79.

[2] **H. Mao**, R. Cai, N. Kawazoe and G. Chen. Long-term Stem Cell Labeling by Collagen-functionalized Single-walled Carbon Nanotubes. Nanoscale 2014, 6: 1552-59.

[3] **H. Mao**, N. Kawazoe and G. Chen. Cellular Uptake of Single-Walled Carbon Nanotubes in 3D Extracellular Matrix-Mimetic Composite Collagen Hydrogels. J. Nanosci. Nanotechnol. 2014, 14: 2487-92.

[4] I. Dulińska-Molak, **H. Mao**, N. Kawazoe and G. Chen. Variation of Mechanical Property of Single-Walled Carbon Nanotubes-Treated Cells Explored by Atomic Force Microscopy. J. Biomed. Nanotechnol. 2014, 10: 651-59.

[5] I. Dulińska-Molak, **H. Mao**, N. Kawazoe and G. Chen. Effect of Single-Wall Carbon Nanotubes on Mechanical Property of Chondrocytes. J. Nanosci. Nanotechnol. 2014, 14: 2459-65.

[6] **H. Mao**, N. Kawazoe and G. Chen. Cell Response to Single-walled Carbon Nanotubes in Hybrid Porous Collagen Sponges. Colloids Surf. B. Biointerfaces, submitted.

[7] **H. Mao**, I. Dulińska-Molak, N. Kawazoe, Y. Takeda, H. Mamiya and G. Chen. Investigation of Magnetic Nanoparticle-mediated Cell Effects Using Atomic Force Microscopy. to be submitted.

Acknowledgements

At the end of my thesis, I would like to express the deepest appreciation to all those who made this thesis possible and gave me unforgettable experience.

First, I would like to gratefully and sincerely thank my supervisor Professor Guoping Chen, not only for his meticulous guidance on this thesis, but also for his generous concerns and supports on my life in Japan. During these three years PhD program, Professor Chen helped me to garner not only the necessary knowledge and skills in science, but also, even more importantly, the behavior of living in the society. The generosity, sincerity and rigorous research attitude radiates from him has and will continue to affect my future career and life.

I would also like to express my gratitude to the thesis committee members: Professor Takao Aoyagi, Professor Seiya Tsujimura and Professor Tetsushi Taguchi. Time, support and expertise from them are highly appreciated.

I would like to give my special gratitude to Dr. Naoki Kawazoe for his kind support. He always help me with any difficult in my research patiently. His modest character, positive work attitude and excellent team ethic deeply infected me.

I really appreciate the warm assistance from Mrs. Harue Nagata, Ms. Nobue Kobayashi and Mrs. Akemi Tateno. Their great efforts made my life in Japan much easier and more enjoyable.

I am thankful to all the current and former members of this group. They are Dr. Hongxu Lu, Dr. Tomoko Nakamoto, Dr. Ida Dulińska-Molak, Dr. Jasmine Li, Dr. Lingfeng Guo, Dr. Wei Song, Dr. Hwan Hee Oh, Dr. Qin Zhang, Mr. Koki Hagiwara, Mr. Himansu Nandasekhar, Ms. Rong Cai, Mr. Shangwu Chen, Mr. Xinlong Wang, Ms. Xiaohong Hu, Mr. Jingchao Li, Ms Jing Zhang, Mr.Yuichi Hirayama, Mr. Radyum Ikono, Ms. Megumi Nozato and Ms. Jia Hui NG. The years we went through together will be an integral part of my wonderful memory in Japan.

I would like to acknowledge the financial support from the Doctoral Program in Materials Science and Engineering of Graduate School of Pure and Applied Science, National Institute for Materials Science and University of Tsukuba, Japan.

Finally, and importantly, I would like to thank my wife and my family. Their selfless support, encouragement and unwavering love made my life meaningful and whole.

Thank you all and may the continued blessings to all of you.